FLOOD INUNDATION MAPPING IN WEBISHABELE RIVER USING GOOGLE EARTH ENGINE AND HEC-RAS MODEL: CASE STUDY OF BELETWAYNE CITY, SOMALIA

ABDIRAHMAN YOUSUF MOUSE

A THESIS SUBMITTED TO THE DEPARTMENT OF WATER RESOURCES ENGINEERING

COLLEGE OF CIVIL ENGINEERING AND ARCHITECTURE

SCHOOL OF POST GRADUATE STUDIES

ADAMA SCIENCE AND TECHNOLOGY UNIVERSITY

JANUARY, 2026

ADAMA, ETHIOPIA

FLOOD INUNDATION MAPPING IN WEBISHABELE RIVER USING GOOGLE EARTH ENGINE AND HEC-RAS MODEL: CASE STUDY OF BELETWAYNE CITY, SOMALIA

ABDIRAHMAN YOUSUF MOUSE

ADVISOR: Dr. Dereje Birhanu (Ph.D.)

A THESIS SUBMITTED TO THE DEPARTMENT OF

WATER RESOURCES ENGINEERING

COLLEGE OF CIVIL ENGINEERING AND ARCHITECTURE

SCHOOL OF GRADUATE STUDIES

ADAMA SCIENCE AND TECHNOLOGY UNIVERSITY

JANUARY, 2026

ADAMA, ETHIOPIA

DECLARATION

I hereby declare that this thesis, entitled **Flood Inundation Mapping in Webishabele River using Google Earth Engine and HEC-RAS Model: Case Study of Beletweyne City, Somalia** is the result of my own original research. It has not been submitted, in whole or in part, for any degree or qualification at any other institution. All sources of information have been appropriately acknowledged by means of citation.

Abdirahman Yousuf		25-01-2026
Name of student	Signature	Date

As the major advisor for this research, I hereby certify that I have closely advised the student, Abdirahman Yousuf, during the development of this work. I have read the thesis entitled **Flood Inundation Mapping in Webishabele River using Google Earth Engine and HEC-RAS Model: Case Study of Beletweyne City, Somalia** and confirm it was prepared under my guidance. Therefore, I recommend the submission of the thesis to the department for further review and evaluation.

Dr. Dereje Birhanu (PhD)		25-12-2025
Major Advisor	Signature	Date

APPROVAL SHEET

I hereby certify that the recommendations and suggestions of the Board of Examiners are appropriately incorporated into Abdirahman Yousuf's final thesis, **Flood Inundation Mapping in Webishabele River using Google Earth Engine and HEC-RAS Model: Case Study of Beletweyne City, Somalia**

Dr. Dereje Birhanu (PhD)		25-12-2025
Major Advisor	Signature	Date

We, the undersigned, members of the Board of Examiners of the thesis open defense of Abdirahman Yousuf, have read and evaluated the thesis entitled "**Flood Inundation Mapping in Webishabele River using Google Earth Engine and HEC-RAS Model: Case Study of Beletweyne City, Somalia** and assessed the understanding of the candidate about the proposed research.

This is, therefore, to certify that the thesis is accepted and we recommend the acceptance of the degree. --

Bahru Mekuria (Ph.D.)		13 February, 2026
Chairperson	Signature	Date
Internal Examiner	Signature	Date
Yenesew Mengiste		12 Feb 2026
External Examiner	Signature	Date

Final approval and acceptance of the MSc thesis are contingent upon submission of its final copy to the Office of Postgraduate Studies (OPGS) through the Department of Graduate Studies.

Council (DGC) and School Graduate Committee (SGC).

Department Head	Signature	Date
School Dean	Signature	Date
Office of Postgraduate Studies, Dean	Signature	Date

TABLE OF CONTENTS

LIST OF TABLES

LIST OF FIGURES

LIST OF ACRONYMS

DEM	Digital Elevation Model
EWS	Early Warning Systems
GEE	Google Earth Engine
HEC-RAS	Hydrologic Engineering Center - River Analysis System
HEC-HMS	Hydrologic Engineering Center - Hydrologic Modeling System
GIS	Geographic Information Systems
IDMC	Internal Displacement Monitoring Center
InSAR	Interferometric Synthetic Aperture Radar
IoT	Internet of Things
SAR	Synthetic Aperture Radar
QFR	Quantile-based Filling and Refining
CBDRR	Community-based disaster risk reduction
IGAD	Intergovernmental Authority and Development
DSM	Digital Surface Model
SWD	Software Distribution
SWALIM	Somali Water and Local Information Management
RMSE	Root Mean Squared Error
NSE	Nash Sutcliffe Efficiency
NWDI	Normalized Difference Water Index
QFR	Quantile Based and Refining

ABSTRACT

Flooding from the Shebelle River is a persistent and severe hazard in Beletweyne City, Somalia, causing significant loss of life and infrastructure damage. This study modeled these dynamics by integrating the HEC-RAS hydraulic model with the Google Earth Engine (GEE) geospatial platform. A 1D/2D HEC-RAS model was developed using a 30m Digital Elevation Model (DEM) and Manning's roughness coefficients derived from land use and land cover (LULC) data. The 2D model was calibrated against the October 2019 flood event, yielding a coefficient of determination R^2*=0.89. Spatial validation against Sentinel-1 satellite imagery via GEE showed 54.106% overlap with the observed flood extent. Simulation results for 25, 50, and 100-year return periods reveal escalating risk to the urban area: the 25-year event produced a maximum flood depth of 3.80 m and an inundated area of 4.87 km², while the 50-year event produced a maximum depth of 5.97 m and an inundated area of 8.56 km². The 100-year event reached a depth of 8.58 m and an inundated area of 11.65 km², aligning closely with the 8.30 m bank-full level observed during the 2019 extreme floods. Unsteady flow simulations further generated critical risk maps for flood velocity, arrival time, and inundation duration. These high-resolution outputs provide a scientifically validated framework essential for risk-based zoning and the development of early warning systems in Beletweyne.*

Keywords: Shebelle River, Hydrological Modeling, Remote Sensing, HEC-RAS, Google Earth Engine.

INTRODUCTION

1.1 Background

Floods are a significant global concern, impacting millions of lives and leading to substantial mortality risks. Research indicates that exposure to floods can increase mortality rates, particularly in vulnerable populations. A study analyzed data from 761 communities across 35 countries, revealing that floods contribute to approximately 0.10% of all-cause deaths, 0.18% of cardiovascular deaths, and 0.41% of respiratory deaths. The cumulative relative risk of mortality increased for up to 60 days post-flood, with variations by socioeconomic status and climate type (Yang et al., 2023). A review of flood early warning systems (EWS) highlighted a geographic disparity in research focus, with Europe leading. At the same time, regions like Central America and Asia remain underrepresented (Calvo-Solano & Quesada-Román, 2024).

Flooding in East Africa, particularly in the Greater Horn of Africa, poses a critical threat to regional stability and development. According to the Intergovernmental Authority on Development (IGAD), the region experiences annual extreme flood events that affect approximately 2.3 million people, resulting in economic losses exceeding $1.5 billion annually (IGAD, 2023). East Africa experiences annual extreme floods, leading to humanitarian crises and population displacement (Alfieri et al., 2024). Vulnerability is exacerbated by inadequate infrastructure and limited access to early warning systems, with most of the population lacking coverage (Lorenzo & Alfieri, 2024). Flood-PROOFS East Africa utilizes a modeling cascade that integrates hydrological simulations and ensemble weather forecasts to predict flooding events (Lorenzo & Alfieri, 2024). The system operates with a five-day forecast range and supports organizations like the African Union and IGAD in monitoring hydro-meteorological disasters. The system has been evaluated at 78 river gauging stations, providing insights into its effectiveness during catastrophic floods, such as those in Sudan and the Nile River basin in 2020 (Lorenzo, 2024).

Floods in Somalia represent a significant natural hazard, exacerbated by climate change and human activities. The country experiences various types of flooding, particularly flash floods, which have devastating impacts on lives, livelihoods, and the environment. Heavy rainfall, particularly during the summer (xagaa) and autumn (deyr) seasons, has increased flood intensity in Somalia (Ali & Mohamed, 2023). Deforestation, poor drainage systems, urbanization, and overgrazing contribute to the severity of floods (Ali, 2023).

Beletweyne City, located in Somalia, is significantly impacted by the Webishabele River, which plays a crucial role in the region's ecology and economy. The city faces recurrent flooding, exacerbated by its proximity to the river, leading to substantial displacement and vulnerability among its communities. Understanding the dynamics of Beletweyne and the Webishabele River is essential for developing effective flood management strategies. The proximity to the river increases vulnerability, particularly for those living near high water marks and inadequate flood defenses (Jansky, 2023). The analysis of river discharge data from 1980 to 2020 showed a significant positive trend in annual river discharge, suggesting increased flooding risk. Increased river discharge, with a maximum of 736.70 m^3/s, suggests a higher likelihood of flooding events (Merga et al., 2023). Strategies to enhance resilience include conducting continuous vulnerability assessments and implementing effective early warning systems (Jansky, 2023). Recent studies have utilized hydrological models to simulate flood scenarios, revealing significant flood depths and velocities. Proposed mitigation measures, such as levees, could reduce flood extent by up to 35% (Ibrahim et al., 2024). A notable event occurred on October 24, 2019, when intense rainfall led to severe inundation, affecting thousands of residents. Reports indicated that ten individuals went missing or drowned, while over 2,000 hectares of agricultural land were severely damaged (Pulvirenti et al., 2020).

1.2 Problem statement

The flooding events in Somalia, particularly in Beletweyne, are increasingly severe due to the overflow of the Shebelle and Juba rivers, compounded by climate change and land degradation. Recent data indicate that over 200,000 residents were displaced in a single season due to flash floods, underscoring the critical need for effective flood inundation mapping to mitigate future disasters (Ali & Mohamed, 2023; IDMC, 2021). The history of annual flooding in Beletweyne, Somalia, is marked by recurrent and devastating events that significantly impact the local communities. Flooding in this region is primarily influenced by the Shebelle River, which overflows during heavy rains, leading to displacement, loss of livelihoods, and damage to infrastructure. Beletweyne has experienced significant floods in recent years, notably in April-

May 2018, October-November 2019, and April-May 2020, documented through satellite imagery and local reports (Pulvirenti et al., 2020).

Despite several hydrological assessments of the Shebelle River, a critical research gap remains regarding urban flood dynamics in Beletweyne. Previous studies, such as those by (SWALIM, 2009; Ibrahim et al., 2024), relied primarily on 1D steady-state modeling. These traditional models average flow velocities across cross-sections and fail to account for "backwater effects" and the local "pile-up" of water caused by urban infrastructure, such as buildings and bridges. Consequently, 1D approaches can underestimate flood depths by approximately 1.0 meters when compared to real-world observations. This research fills this gap by employing a coupled 1D/2D unsteady flow model in HEC-RAS, providing high-resolution spatial validation through Google Earth Engine to accurately capture the multi-directional flood propagation within the city core.

1.3 Objectives

1.3.1 General objective

The general objective of the study is to comprehensively assess and model flood inundation dynamics in Beletweyne City, Somalia, by integrating the HEC-RAS model and Google Earth Engine.

1.3.2 Specific objectives

- Develop and calibrate a 1D/2D HEC-RAS model of the study area, incorporating the processed DEM and other relevant data.
- Simulate flood inundation scenarios for different return period (e.g., 25-year, 50-year, 100-year) using the calibrated HEC-RAS model.
- Generate high-resolution flood inundation maps using Google Earth Engine, visualizing inundation extent, depth, and flow velocity.

1.4 Research questions

I. What are the specific hydrological characteristics of the Shebelle River catchment, including peak discharge and flow variability, that drive recurrent flash flooding in Beletweyne City?

II. How accurately can the integration of a 1D/2D HEC-RAS hydraulic model with Google Earth Engine (GEE) simulate flood inundation extents and depths for the 25, 50, and 100-year return period?

III. How do the developed high-resolution flood maps compare with satellite-observed extents from the 2019 flood event, and what are the implications for local early warning systems?

1.5 Significance of the study

The study focused on the significant importance of addressing the recurrent flooding challenges faced by Beletweyne, Somalia, providing both practical and scientific value. The flooding events are exacerbated by the community's proximity to the river, which increases vulnerability due to inadequate flood defenses. Communities have been encouraged to develop adaptive capacities, such as improving emergency preparedness and infrastructure resilience, to mitigate the impacts of future floods (Jansky, 2023). Beletweyne's proximity to the Shebelle River makes it highly susceptible to flooding, particularly during heavy rainfall seasons (Osman & Das, 2023).

Furthermore, the study is significant in addressing the socio-economic challenges posed by recurrent flooding in Beletweyne. The impacts of flooding in Beletweyne City, Somalia, are multifaceted, affecting its residents' livelihoods, health, and security. Flooding, exacerbated by climate change, has led to significant displacement and economic losses, highlighting the urgent need for adaptive strategies. Flooding has caused substantial internal displacement, forcing communities to abandon their homes and livelihoods (IDMC), 2021). Economic losses are significant, with many families losing their agricultural income due to flooded fields, which diminishes food security (Ali & Mohamed, 2023). Floodwaters often contaminate drinking water, leading to public health emergencies such as waterborne diseases (Ali & Mohamed, 2023). Flooding has led to significant income loss for many residents, with 28% of respondents reporting reduced income and 26% experiencing flooding-related health issues (Ali & Mohamed, 2023). By providing detailed flood inundation maps and simulating flood scenarios, the research equips policymakers, humanitarian organizations, and local communities with the tools necessary to develop proactive measures to safeguard lives, livelihoods, and critical infrastructure. The study focused on the importance of integrating scientific data with community-centered approaches to enhance disaster resilience.

1.6 Scope of the study

This study covers flood risk assessment and creating precise flood maps for Beletweyne City, Somalia. It emphasizes using advanced hydrological models like HEC-RAS and combining them with remote sensing tools such as Google Earth Engine (GEE) to analyze flood behavior and effects. Sentinel-1 InSAR data allows for the detection of floodwater in urban areas by analyzing persistent scatters, leading to the creation of detailed flood maps (Pulvirenti et al., 2020). Techniques combining spatiotemporal context learning with classifiers like Modest AdaBoost have shown promise in automating inundation mapping, and providing timely and accurate flood assessments (Liu et al., 2017). HEC-HMS and HEC-RAS Models. These models simulate rainfall-runoff processes and flood inundation, respectively, providing insights into flood depth and velocity, which are critical for effective flood management (Ibrahim et al., 2024). Geographic Information Systems (GIS) enhance flood modeling by integrating multiple datasets, enabling accurate simulations of inundated areas and water depth distributions (Zhu, 2010). New methodologies using LIDAR data enable the direct computation of inundation maps, facilitating data-driven planning and response strategies (Criss & Nelson, 2021). The research aims to simulate flood scenarios for various return period (e.g., 25-year, 50-year, and 100-year floods) to gain a thorough understanding of possible flooding events.

Key areas of focus include the calibration and validation of 1D/2D hydrological models using high-resolution Digital Elevation Models (DEMs), river geometry, and hydrological data. The study also incorporates geospatial data processing for simulating inundation extents, depths, and flow velocities. The geographical scope is limited to Beletweyne City and its surrounding floodplain areas, with particular emphasis on the Shebelle River, a major contributor to flooding in the region. Data collection involves using remote sensing datasets, historical hydrological records, and satellite imagery, supported by field observations where available. The study is constrained by the availability of data in a resource-limited environment, necessitating innovative approaches such as leveraging open-access remote sensing platforms and advanced computational modeling techniques.

Ultimately, the study aims to produce high-resolution flood inundation maps and actionable recommendations for policymakers, humanitarian organizations, and local communities. These outputs will help improve flood preparedness, infrastructure resilience, and adaptive capacities to mitigate the impacts of recurrent flooding in Beletweyne City.

LITERATURE REVIEW

2.1 Introduction

Flooding is a significant natural disaster that poses severe risks to human life, property, and the environment. It is primarily triggered by heavy rainfall, storms, and hurricanes, leading to widespread displacement, health issues, and economic losses. The global impact of flooding is profound, with approximately 2.3 billion people affected and 157,000 deaths reported between 1995 and 2015 (Guddo, 2023). Understanding flooding requires a multifaceted approach, encompassing risk assessment, management frameworks, and innovative technologies. Flooding can result from various factors, including climate change and urbanization, exacerbating its frequency and severity (Tabasi et al., 2024). The consequences include loss of life, infrastructure damage, and long-term economic impacts (Petrochenko, 2023). Effective flood management relies on comprehensive risk assessment frameworks that consider hazard, vulnerability, exposure, and resilience (Tabasi et al., 2024). These frameworks help identify and mitigate risks through preparedness and response strategies. The integration of smart management systems utilizing information and communication technology can enhance disaster preparedness and response (Ibrahim & Mishra, 2021). Such systems improve community readiness and facilitate timely interventions.

Flooding in semi-arid areas presents unique challenges and opportunities, despite the region's general water scarcity. Recent studies highlight that flooding can be severe and life-threatening, often exacerbated by climate change and inadequate flood risk management strategies. Understanding the dynamics of flooding in these regions is crucial for developing effective management practices and harnessing floodwaters for agricultural benefits. Flooding in semi-arid regions is typically characterized by rapid runoff and infrequent but intense rainfall events, which lead to significant flood risks (Nabinejad & Schüttrumpf, 2023). The lack of data and climatic variability complicate flood hazard assessments, making it difficult to predict and manage flood events (Werren et al., 2016). Operational and technical challenges in flood risk management are prevalent, necessitating tailored approaches that address the unique conditions of these environments (Nabinejad & Schüttrumpf, 2023).

2.2 Flood modeling approaches

2.2.1 Conceptual framework

Flood inundation modeling employs various approaches, each with distinct methodologies and applications. These approaches include empirical models, hydrologic and hydraulic models, as well as GIS and remote sensing-based models, which collectively enhance flood prediction and management. Empirical models rely on historical data to establish relationships between rainfall and runoff, often using statistical methods. They are straightforward but may lack accuracy in unique or changing environments due to their reliance on past events. Studies show that using DSMs can improve predictions of flooded areas by up to 42% compared to traditional digital terrain models (DTMs) (Pizzileo et al., 2024). Hydrologic models, such as HEC-HMS, simulate rainfall-runoff processes, while hydraulic models analyze water flow in rivers and channels. These models can be integrated with GIS to assess flood risks in urban areas, as demonstrated in Dubai, where impervious surfaces significantly influence flood probabilities (Khan et al., 2024). Remote sensing technologies, including high-resolution satellite imagery and LiDAR, provide critical data for flood mapping and modeling. QFR techniques utilize satellite imagery, such as Sentinel-2 and Synthetic Aperture Radar (SAR), to capture flood extents with high accuracy (Composto et al., 2024; Mason et al., 2021). However, low spatial resolution and coverage gaps in remote sensing data can complicate model validation (Cohen et al, 2024). Machine learning algorithms, like Random Forest, have demonstrated over 99% accuracy in flood extent mapping, effectively processing large datasets from various sources (Composto et al., 2024).

Empirical models are characterized by their simplicity and ease of use, often requiring minimal data inputs, making them quick to implement for preliminary assessments. However, their limitations include an inability to capture complex hydrological processes and a site-specific nature that reduces their generalizability across different regions. In contrast, hydrologic and hydraulic models can simulate detailed hydrological processes and interactions, and their integration with Geographic Information Systems (GIS) enhances spatial analysis capabilities (Conesa-Garcia et al., 2010). Nevertheless, these models come with high data requirements and complexity in calibration, which can make them computationally intensive and limit their applicability for real-time scenarios (Duvvuri et al., 2024).

On the other hand, GIS and remote sensing-based models provide large-scale spatial data that significantly improve model accuracy and coverage (Xu et al., 2014). They also facilitate real-time monitoring and assessment of hydrological events, enhancing the responsiveness to potential flooding or other water-related challenges (Rizeei, 2024). However, these models depend heavily on the quality of remote sensing data, which can be compromised by atmospheric conditions. Additionally, there are integration challenges with existing models and data sources, making it difficult to harness their full potential (Thakur et al., 2017). Understanding these strengths and weaknesses is essential for selecting the most suitable modeling approach in hydrological research.

Flood modeling approaches, particularly hydrologic methods, are essential for predicting and managing flood risks. These approaches encompass various techniques, including rainfall-runoff models, hydrodynamic models, and machine learning applications, each contributing uniquely to flood risk assessment and mitigation. The integration of these models enhances the accuracy of flood predictions and informs effective management strategies. These models simulate how rainfall translates into runoff, crucial for understanding flood dynamics (Krishna Pasupuleti, 2024). They simulate water flow and inundation patterns, providing insights into flood extent and depth (Renu et al., 2025). Machine learning methods, particularly deep learning, have shown improved accuracy in flood modeling compared to traditional approaches, although they lack the incorporation of expert knowledge (Karim et al., 2023). Combining hydrologic models with machine learning, such as integrating HEC-HMS outputs with artificial neural networks, has demonstrated enhanced performance in flood simulations (Renu et al., 2025).

Flood modeling, particularly hydraulic approaches, plays a crucial role in understanding and managing flood risks. These models simulate water flow and inundation patterns, providing essential data for infrastructure design and flood defense strategies. The integration of advanced technologies and methodologies enhances the accuracy and effectiveness of these models, which can significantly mitigate the impacts of flooding. Different hydrodynamic models are employed based on the complexity of the riverine topography. For instance, HEC-RAS (1D) and MIKE 21 (2D) are commonly used to simulate flow behavior and inundation areas (Vilca et al., 2025; Papaioannou et al., 2016). The use of geospatial data, satellite imagery, and high-resolution digital elevation models (DEMs) improves prediction accuracy and supports better decision-making (Vilca et al., 2025; Papaioannou et al., 2016).

Flood inundation modeling is a critical aspect of urban flood risk assessment, particularly in areas like Beletweyne, which face significant flood threats. Various software tools, including HEC-RAS, are employed to simulate flood scenarios and assess vulnerabilities. This overview synthesizes existing knowledge on flood modeling, HEC-RAS, Google Earth Engine, and urban flood risk assessment. Flood modeling encompasses various approaches, including hydrologic, hydraulic, and numerical methods. Recent advances highlight the integration of remote sensing and GIS technologies, which enhance the accuracy of flood predictions and risk assessments (Kumar et al., 2023). Models like HEC-RAS and IBER 2D have shown good agreement in flood depth and velocity estimations, crucial for urban planning (Djafri et al., 2024). HEC-RAS is widely used for simulating two-dimensional flood scenarios. It allows for detailed analysis of flood dynamics, including the impact of land cover and urban infrastructure on flood behavior (Jeong et al., 2024). Studies indicate that HEC-RAS can effectively produce flood inundation maps, which are essential for urban flood management (Ansarifard et al., 2024). Google Earth Engine (GEE) facilitates the integration of satellite imagery and geospatial data for flood monitoring and assessment. Its capabilities in processing large datasets enable real-time flood risk evaluations, which are vital for timely disaster response in urban settings (Prashar et al., 2023). Urban flood risk assessment involves evaluating vulnerabilities and resilience strategies. Comprehensive frameworks that integrate multiple assessment methods, including multi-criteria decision-making and hydrological modeling, are essential for effective urban flood management (Prashar et al., 2023). The complexity of urban systems necessitates a collaborative approach to enhance resilience against flooding. In contrast, while advanced modeling techniques and tools are beneficial, challenges remain in data accuracy and model selection, which can significantly impact flood risk assessments. Continuous research and development are necessary to address these limitations and improve urban flood resilience strategies (Kumar et al., 2023).

2.5 HEC-RAS model

2.5.1 Introduction

The HEC-RAS (Hydrologic Engineering Center - River Analysis System) model is a sophisticated tool developed by the U.S. Army Corps of Engineers for hydraulic and hydrologic modeling. It is widely utilized for simulating river flow, floodplain dynamics, and water quality assessments. The model supports both one-dimensional and two-dimensional flow simulations, making it versatile for various applications, including flood risk management and agricultural water quality analysis. One of the key features of HEC-RAS is its ability to simulate flow under both steady and unsteady conditions, allowing for accurate predictions of water surface profiles and flood extents (Zainal & Abu Talib, 2024). Additionally, it integrates hydrological data with GIS tools to enhance flood hazard mapping and management strategies (Crenganiș et al., 2024; Saini & Barik, 2024). The model also utilizes discrete cross-sections to define floodplain geometry, which is crucial for accurate floodplain mapping (Saini & Barik, 2024). HEC-RAS is employed in various applications, including flood risk assessment, where it evaluates flood heights and inundation areas to aid in urban planning and disaster preparedness (Hardiyanto et al., 2024; Siakara et al., 2024). It also plays a role in water quality management, particularly in agricultural scenarios, by computing the impacts on water quality, demonstrating its multifaceted utility (Zainal & Abu Talib, 2024). However, while HEC-RAS is a powerful tool for flood modeling, its effectiveness can be limited by the availability of high-resolution topographical data, which is often lacking in developing regions (Saini & Barik, 2024). The model requires extensive calibration and validation against observed data to ensure reliability, which can be resource-intensive(R, 2023). HEC-RAS 2D with rain-on-grid capabilities allows for accurate modeling of extreme rainfall events and their impacts on runoff (Ansori et al., 2023).

2.5.2 Key features and modules

HEC-RAS (Hydrologic Engineering Center's River Analysis System) is a versatile tool for hydraulic modeling, particularly relevant for flood analysis in Beletweyne City, Somalia. Its key features include 1D and 2D flow modeling, unsteady flow simulation, and the analysis of hydraulic structures, which are crucial for understanding flood dynamics and mitigation strategies. The software enables unsteady flow simulations, essential for predicting flood behavior during varying conditions. This feature is particularly useful in regions like Beletweyne, where flash floods are common (Ibrahim et al, 2024). HEC-RAS includes modules for analyzing hydraulic structures, such as bridges and levees, which are critical for flood management. The model can compute bridge scour and assess the stability of channels (Husain, 2017).

2.6 Google Earth Engine (GEE)

2.6.1 Introduction

The introduction of Google Earth Engine (GEE) in flood mapping has revolutionized the way researchers and practitioners approach flood risk assessment and management. GEE's cloud-based platform allows for the integration of various remote sensing data, machine learning algorithms, and user-friendly applications, making it accessible for both technical and non-technical users. This transition has led to more efficient and accurate flood mapping methodologies. This application utilizes multimodal remote sensing and advanced algorithms to enhance water body extraction, particularly in challenging environments with dense vegetation and cloud cover (Li & Demir, 2024). In Tetouan, Morocco, GEE was employed to assess flash flood susceptibility using machine learning techniques, achieving a high accuracy of 96% in identifying at-risk areas (Sellami & Rhinane, 2024). GEE facilitated the mapping of glacial lake outburst floods, providing temporal flood extent analysis and insights into land use impacts (Halder & Bose, 2024). By leveraging publicly available datasets and deep learning models, GEE has enabled the creation of detailed flood susceptibility maps, crucial for disaster risk management (Mangkhaseum et al., 2024). The combination of SAR and optical data within GEE has proven effective for continuous flood monitoring, even under adverse weather conditions (Giannone et al., 2024).

The capabilities for processing and analyzing large volumes of geospatial flood data, such as satellite imagery and Digital Elevation Models (DEMs), have significantly advanced through the integration of various technologies and methodologies. These advancements enable more accurate flood monitoring, assessment, and management, particularly in real-time scenarios. One of the key elements in this progress is the utilization of satellite data. The Copernicus Sentinel satellites, for instance, provide high-resolution data suitable for flood detection. Sentinel-1's C-band Synthetic Aperture Radar (SAR) offers all-weather monitoring with a resolution of 10 meters, while Sentinel-2's optical data is effective under clear conditions, providing a resolution of 20 meters (Lacava et al., 2024). Furthermore, the integration of data from multiple satellite sources enhances flood extent mapping and depth estimation, utilizing algorithms like RAPID and SWD for improved accuracy (Yang et al., 2024). In terms of geospatial data processing, Google Earth Engine (GEE) has emerged as a pivotal platform that facilitates the integration of historical satellite data and DEMs. This enables efficient identification of flood-prone areas and depth assessment, proving essential in analyzing flood events across various regions (Hiep et al., 2023; Lacava et al., 2024). Additionally, by employing DEMs alongside satellite imagery, researchers can classify flood-vulnerable areas, thereby enhancing disaster risk management strategies (Assaidi et al., 2024). Advanced modeling techniques have also contributed to this field. For example, post-processing workflows such as the Quantile-based Filling and Refining (QFR) technique improve the accuracy of flood inundation maps generated from remote sensing data, particularly in urban settings (Li et al., 2024)

2.6.2 Applications of Flood Modeling

Google Earth Engine (GEE) has emerged as a powerful tool in flood-related research, particularly in regions like Somalia, where the extraction of hydrological data, flood inundation mapping, and impact assessment are critical. The integration of remote sensing technologies within GEE facilitates comprehensive flood monitoring and management strategies that are essential for disaster preparedness. One of the key capabilities of GEE is its ability to extract hydrological data through the analysis of satellite imagery, including Synthetic Aperture Radar (SAR) and optical data from Sentinel-1 and Sentinel-2 satellites. This functionality is crucial for continuous monitoring, even in adverse weather conditions (Giannone et al., 2024). Additionally, the MultiRS Flood Mapper application enhances water body extraction by utilizing multimodal remote sensing and advanced algorithms, making it accessible for both technical and non-technical users (Li & Demir, 2024). In terms of flood inundation mapping, GEE has been effectively applied to create flood distribution maps. For instance, studies conducted in Trinidad demonstrated the delineation of flood areas using SAR data (Ramsewak et al., 2024). Similarly, in Quang Tri Province, GEE facilitated the identification of flooded areas and the assessment of flood depths, providing timely insights crucial for disaster management (Giang Hoang Hiep et al, 2023). Furthermore, the integration of flood maps with infrastructure data allows for visual assessments of flood impacts, which aids in disaster response planning (Ramsewak et al., 2024). GEE's ability to amalgamate various data types enhances decision-making processes in vulnerable regions, contributing to more effective disaster mitigation strategies (Hiep et al., 2023). Overall, GEE represents a significant advancement in flood research, providing essential tools for monitoring and managing flood risks in areas prone to hydrological challenges.

2.4 Model calibration and validation

Model calibration and validation are essential procedures that enhance the accuracy and reliability of computational models across various fields. These processes ensure that models accurately represent real-world systems, which is critical for informed decision-making and effective application in practice.

Calibration involves iteratively adjusting model parameters to align simulated results with experimental or analytical data, ensuring accuracy within established standards (Cataño-Lopera, 2023). One prominent method utilized in this process is the Kennedy and O'Hagan (KOH) framework, which addresses model inadequacies and identifiability issues, thereby enhancing model performance in complex scenarios (Sung & Tuo, 2024). Furthermore, employing a statistically sound approach to calibration can significantly improve predictive performance, as evidenced in traffic flow models (Würth et al., 2023). Calibration often involves modifying parameters such as Manning's roughness coefficients. For instance, a study on the Tigris River reported a calibration range of 0.018–0.020, achieving a high Nash-Sutcliffe coefficient (NSE) close to 1, indicating strong model performance (Sabeeh & Alabdraba, 2022). Calibration relies heavily on field data. The study on the Guddu Barrage used in-situ gauge data to calibrate water levels, achieving differences between simulated and observed levels ranging from -0.1718 m to +0.1521 m (Saeed & Zaidi, 2022).

Model validation processes, which include verification and convergence tests, are crucial for assessing the reliability of computational simulations (Cataño-Lopera, 2023). A robust validation framework increasingly relies on model-driven methods based on causal relationships rather than purely data-driven approaches, allowing for more meaningful insights (Mandelli et al., 2023). Additionally, establishing a unified framework for validation can address inconsistencies in the literature, ultimately improving overall modeling practices (Ting et al., 2023). Validation involves testing the model against separate datasets. The validated model for the Guddu Barrage showed discrepancies from -0.232 m to 0.138 m, confirming its predictive accuracy (Saeed & Zaidi, 2022). Metrics such as the coefficient of determination (R^2) and NSE are commonly used to evaluate model performance. The Tigris River study demonstrated a close relationship between observed and simulated flow discharges, reinforcing the model's validity (Sabeeh & Alabdraba, 2022).

Flood mapping using Google Earth Engine (GEE) and the HEC-RAS model involves a combination of advanced modeling techniques and remote sensing data, which are crucial for effective calibration and validation. This integration enhances the accuracy of flood predictions and provides critical insights for flood risk management. In terms of calibration techniques, HEC-RAS utilizes both 1D and 2D modeling to simulate flood scenarios. Calibration involves adjusting parameters, such as Manning's roughness coefficient, based on observed data to ensure that simulated water levels align closely with actual measurements (Jaafar et al, 2023; Saeed & Zaidi, 2022). Additionally, regression analysis serves as a statistical method to validate water surface elevations against observed data, allowing for fine-tuning of model parameters (Trambadia et al., 2023). For validation techniques, remote sensing data plays a pivotal role. Satellite imagery and Flood Inundation Maps (FIM) derived from remote sensing provide a benchmark for validating model predictions. These maps capture real flooding events and offer spatial continuity that enhances model evaluation (Cohen et al., 2024; Trambadia et al., 2023). Furthermore, multi-scenario testing is employed, where different flood scenarios based on varying return period are simulated to assess model performance under diverse conditions, as observed in studies focusing on urban flood hazard mapping (Jaafar et al., 2023; Romanian Waters National Administration, Someș-Tisa Water Basin Administration, Maramureş Water Management System, Hortensiei, Baia Mare, Romania, et al, 2023). In South Jakarta, GEE was utilized to map flood-prone areas, achieving an overall accuracy of 91% and a Kappa accuracy of 83% (Akbar Mursaliin et al., 2025). In the Kelantan River Basin, GEE processed Sentinel-1 SAR data to create flood maps, validated through site inspections, achieving 57-60% accuracy (GeoInformatic Unit, Geography Section, School of Humanities, Universiti Sains Malaysia et al., 2024). Various studies employed metrics such as Kappa and AUC to validate flood models, ensuring reliable results for decision-making (Mursaliin et al., 2025; Lamichhane et al., 2024).

Ground truthing through site inspections and comparisons with historical data enhances the credibility of GEE-derived flood maps (GeoInformatic Unit, Geography Section, School of Humanities, Universiti Sains Malaysia et al, 2024).

2.7 Flood risk assessment in urban areas

2.7.1 Vulnerability and Exposure

Urban flooding poses significant risks to cities like Beletweyne, Somalia, where understanding vulnerability and exposure is crucial for assessing flood impacts. Vulnerability refers to the susceptibility of individuals and infrastructure to flood hazards, while exposure denotes the degree to which these elements are at risk of being affected by flooding. The interplay between these factors shapes the overall flood risk in urban environments.

Several factors contribute to vulnerability. Physical vulnerability is influenced by the design and quality of the built environment. Poorly constructed buildings and inadequate drainage systems can exacerbate the impacts of flooding (Bernardini et al., 2024). Additionally, social vulnerability plays a role, as demographic factors such as age, income, and education levels affect how communities perceive and respond to flood risks. Higher education and income levels are often correlated with better-coping strategies and resilience in the face of flooding (Salhi et al., 2024). Furthermore, institutional vulnerability is critical, as the effectiveness of local governance and emergency response systems significantly impacts flood risk management (Vaca et al., 2024).

Figure 2.1: A school in Beletweyne inundated by floodwaters, demonstrating the high vulnerability of critical social infrastructure and the disruption to educational services

Source: https://blogs.icrc.org/somalia/2019/11/05/pictures-flood-response-by-boats-in-beledweyne-somalia/

In assessing exposure, geospatial analysis is essential for mapping flood exposure and identifying high-risk areas. Research has shown that urbanization tends to increase exposure, particularly in densely populated regions (Rahayu, 2023). Additionally, the temporal dynamics of user exposure can vary throughout the day, influenced by population density and activity patterns. These variations can be effectively assessed using spatiotemporal methodologies (Bernardini et al., 2024). Overall, a comprehensive understanding of vulnerability and exposure is vital for developing effective strategies to mitigate the risks associated with urban flooding in Beletweyne.

The interplay among socio-economic factors, infrastructure, and land-use patterns significantly influences vulnerability in urban settings, making it crucial to understand these dynamics to develop effective disaster mitigation strategies, particularly against floods. Socio-economic factors are closely linked to vulnerability, with lower income and education levels, as well as higher proportions of marginalized groups, correlating with increased flood risk (Islam & Meng, 2024). In urban areas, these socioeconomic inequalities manifest spatially, affecting access to resources and services, which further exacerbates vulnerability (Iglesias-Pascual et al, 2023). Additionally, factors such as age, gender, and disability play critical roles in determining social vulnerability, as highlighted in various studies (Bigandata et al., 2023).

Infrastructure quality is vital for community resilience; areas with better access to social services like healthcare and education tend to exhibit lower vulnerability (Iglesias-Pascual et al, 2023). Furthermore, the resilience of infrastructure is influenced by land use patterns, with densely populated areas facing higher risks during disruptions. Land-use patterns significantly impact vulnerability as well, with residential and public service areas being more susceptible to disruptions (Zhao et al., 2022). Urban planning that addresses socioeconomic disparities can help mitigate vulnerability by ensuring an equitable distribution of resources and services (Iglesias-Pascual et al, 2023). Understanding these interconnected factors is essential for enhancing urban resilience against flooding.

2.7.2 Flood impacts

Urban flooding poses significant threats to urban environments, leading to loss of life, extensive property damage, and disruption of infrastructure, which collectively result in social and economic turmoil. The interconnected nature of urban systems exacerbates these impacts, as flooding can trigger cascading failures across various sectors, including transportation, utilities, and emergency services. Urban flooding can lead to fatalities, particularly in densely populated areas where evacuation is challenging (Zang et al., 2024). Property damage is substantial, with economic losses often exceeding millions; for instance, indirect losses can be 2.43 times greater than direct losses (K. Liu et al., 2024). Vulnerable populations, such as those in low-income neighborhoods, face heightened risks due to inadequate infrastructure (Roldán-Valcarce et al, 2023). Flooding disrupts critical infrastructure, including roads and emergency services, which can hinder recovery efforts (Zang et al., 2024). The Urban Flooding Open Knowledge Network highlights the interconnectedness of urban systems, where failures in one sector can lead to widespread disruptions (Yeghiazarian & Lilit Yeghiazarian, 2024). Economic impacts extend beyond immediate damage, affecting local businesses and employment (Liu et al., 2024). Socially, floods can exacerbate inequalities, as marginalized communities often lack resources for recovery (Roldán-Valcarce et al., 2023).

2.7.3 Flood Risk Management

Flood risk management strategies encompass both structural and non-structural measures, each playing a crucial role in mitigating the impacts of flooding. Structural measures, such as levees and floodwalls, are designed to provide immediate protection against floodwaters inundating urban areas. However, these barriers can create a false sense of security among residents, potentially leading to increased vulnerability in flood-prone regions (Dyca et al., 2024). Additionally, micro-scale solutions, which involve localized measures like flood proofing buildings and employing nature-based solutions, can significantly enhance community resilience (Vanelli et al., 2024).

On the other hand, non-structural measures focus on long-term resilience and adaptability. Early warning systems, enhanced by advanced modeling techniques such as machine learning, improve flood prediction and public awareness, allowing for timely evacuations (Ruidas et al., 2024). Furthermore, effective land use planning that integrates blue-green infrastructure into urban development promotes sustainable water management. This approach helps to reduce flood risk by facilitating natural water absorption and mitigating the impact of heavy rainfall (Dyca et al., 2024; Alshaikh et al., 2023). Together, these strategies underscore the importance of a comprehensive approach to flood risk management that balances immediate protection with long-term sustainability.

Community-based approaches to flood risk reduction are essential for enhancing resilience and preparedness among affected populations. These strategies emphasize the importance of active participation from local communities, fostering a sense of ownership and responsibility toward disaster management. Active community involvement is crucial for effective flood management, as demonstrated by initiatives in Balonggabus Village, where residents engaged in cleaning drainage systems and participated in the planning and evaluation of disaster management programs (Makhfud & Mursyidah, 2024). Increased community awareness contributes to better preparedness and response; communities informed about risks are more likely to take proactive measures to protect themselves (Makhfud & Mursyidah, 2024).

Moreover, successful flood risk reduction necessitates collaboration between government entities and communities. Governments can provide critical resources such as early warning systems and evacuation infrastructure, while communities can contribute by engaging in activities like cleaning waterways and organizing local environments. This partnership enhances the effectiveness of flood mitigation strategies, as both parties bring unique resources and knowledge to the table (Bosowa University et al., 2024).

In addition, innovative community-based disaster risk reduction (CBDRR) strategies are vital to address existing gaps, such as ineffective early warning systems and inadequate training (Ziwanai, 2024). Implementing nature-based solutions, such as biopori practices, can empower communities to manage flood risks sustainably, creating a more resilient environment (Candra Partarini & Wirastri, 2024). Overall, these community-based approaches underscore the importance of involvement, collaboration, and innovation in flood risk management.

2.3 Data requirement

High-quality data is essential for effective flood modeling, as it significantly enhances the accuracy and reliability of predictions. Key data types include Digital Elevation Models

(DEMs), hydrological data, land use-land cover data, and meteorological data, each contributing uniquely to the modeling process. High-resolution DEMs, particularly those derived from LIDAR, improve flood inundation mapping by accurately representing terrain features. Studies show that using DEMs from the 3D Elevation Program enhances flood extent predictions by approximately 80% compared to lower-quality datasets (Aristizabal et al., 2024). Accurate DEMs are essential for hydrodynamic modeling, as they provide critical topographic data. Filtering techniques that remove non-ground elevations can enhance DEM accuracy, leading to improved flood depth estimations (Sahid, 2024). The integration of Digital Surface Models (DSMs) can further refine flood predictions by incorporating land surface macrostructures, leading to significant improvements in predicted flood areas and travel times (Pizzileo et al., 2024). Hydrological data, including river flow rates, soil moisture levels, and groundwater conditions, are equally important for understanding how precipitation and surface runoff contribute to flooding. Real-time streamflow data, for instance, can enhance the timing and magnitude predictions of floods, thereby improving early warning systems (Wang et al., 2020). Accurate rainfall data, such as the CHRain dataset, is crucial for capturing the spatiotemporal characteristics of floods. This dataset demonstrates a high correlation with actual measurements, indicating its effectiveness in hydrological modeling (Nguyen et al., 2024). The combination of meteorological data with historical flood impact data allows for a more comprehensive understanding of flood dynamics, particularly in urban settings where rapid response is critical (Lombardo et al., 2024). Understanding land use and cover is vital for assessing flood risk and impacts. High-resolution data can inform models about how urbanization affects runoff and flood behavior, enabling better emergency management strategies (Lombardo et al., 2024). Accurate spatio-temporal precipitation data is essential for reliable flood risk assessment, particularly in regions with limited gauge observations, such as Malaysia (Muraleedharan et al., 2024).

The challenges associated with hydrological data acquisition in flood data-scarce regions like Somalia are multifaceted, primarily stemming from inadequate monitoring networks, logistical difficulties, and the need for innovative modeling approaches. These challenges hinder effective flood management and response strategies, particularly in regions prone to extreme weather events. Flood challenges in data-scarce regions like Somalia are exacerbated by limited hydrological data, which hinders effective flood management and forecasting. Recent studies highlight the integration of remote sensing and hydrological modeling as crucial strategies to address these challenges. The use of models such as HEC-HMS and HEC-RAS has shown promise in simulating flood events and predicting flood depths, with significant findings indicating peak flood discharges and depths that can inform mitigation strategies (Ibrahim et al., 2024). Many developing regions, including Somalia, lack robust ground monitoring networks due to deteriorating infrastructure and financial constraints (Ekeu-Wei, 2018). The absence of reliable hydrological data leads to flawed flood management decisions, exacerbating vulnerability during flood events (Ekeu-Wei, 2018). Recent advancements in physics-informed deep learning models have shown promise in simulating hydrological processes with limited data, outperforming traditional models (Zhong et al., 2024, 2024). These models utilize upstream-downstream relationships to optimize simulations using minimal downstream data, making them suitable for data-scarce regions (Zhong et al., 2024). Integrating remote sensing data, such as CHIRP satellite rainfall products, has improved flood modeling accuracy in Somalia (Ibrahim et al., 2024). IoT-driven monitoring systems can provide real-time data, enhancing early warning capabilities and enabling proactive flood management (Jimale et al., 2023). The Bakaano-Hydro framework combines hydrology with machine learning to enhance flood forecasting reliability, outperforming existing global platforms in data-scarce regions (Duku, 2025). Event-based flood scaling frameworks allow for better predictions by simulating various rainfall events and analyzing peak discharges (Li et al., 2020). Global datasets are often inadequate for local conditions, complicating model calibration (Abu-Saymeh et al., 2023).

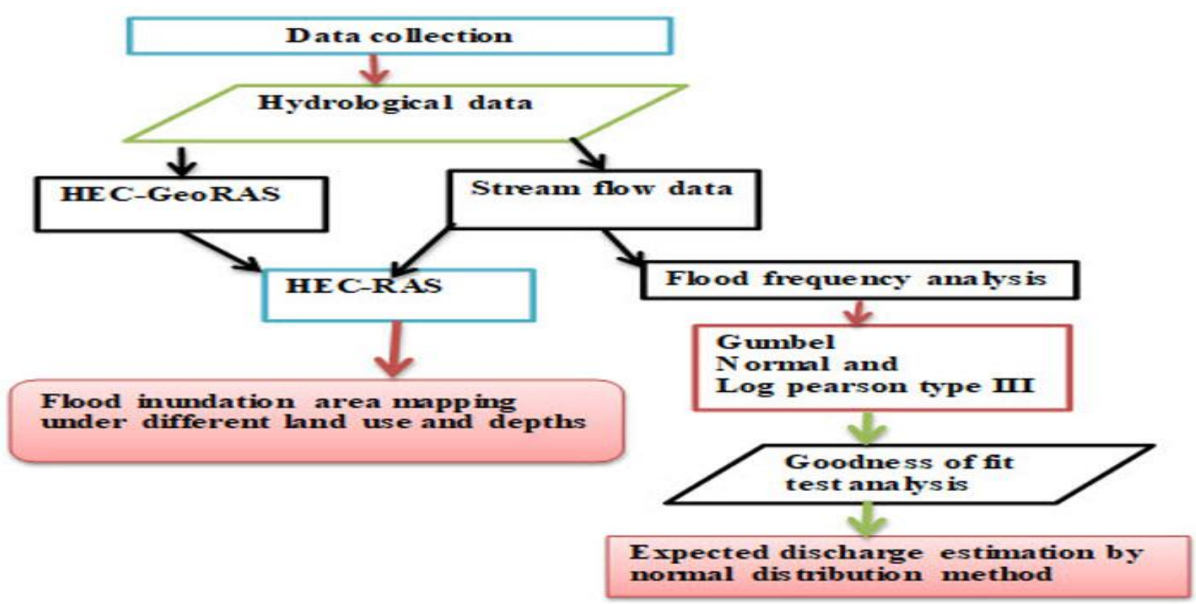

Figure 2.2: HEC-RAS hydrological data and simulation

Source: (Gambella University et al., 2024)

2.4 Comparison of Manning's n Values

To ensure the hydraulic resistance parameters used in this study were physically realistic, the calibrated Manning's n values were cross-referenced with standard literature (Chow, 1959) and recent regional studies on the Shebelle River (Ibrahim et al., 2023; SWALIM, 2009). As summarized in Table 2.1, the values adopted for the main channel (0.035) and floodplains align closely with established benchmarks for the Horn of Africa's hydrological conditions.

Table 2.1: Comparison of Adopted Manning's Roughness Coefficients with Regional Studies

Land Use / Cover Type	Current Study (n)	Ibrahim et al. (2023) (n)	Chow (1959) Range (n)	Justification for Variation
Main Channel (River)	0.035	0.033 – 0.040	0.025 – 0.040	Matches typical values for winding natural channels with weeds/stones (Shebelle context).
Built-Up Area (Urban)	0.08	0.080 – 0.100	0.060 – 0.120	Accounts for obstruction by buildings and fences in Beletweyne city blocks.
Agriculture (Cropland)	0.045	0.040 – 0.050	0.030 – 0.050	Represents seasonal crops (maize/sorghum) prevalent in the floodplain.
Shrubland / Scrub	0.06	0.06	0.050 – 0.080	Typical of the scattered bushland surrounding the urban fringe.
Bare Land	0.025	0.025 – 0.030	0.020 – 0.030	Smooth, packed earth surfaces common in non-vegetated zones.

MATERIALS AND METHODS

3.1 Study area description

3.1.1 Geographical Location and Administrative Context

In Figure 3.1, Beletweyne City serves as the strategic capital of the Hiran region in central Somalia. Geographically, the city is situated at approximately 4°44' N latitude and 45°12' E longitude, located within the wider Shebelle River Valley. The city is positioned approximately 332 km north of the national capital, Mogadishu, and lies close to the Ethiopian border (approximately 30 km). This proximity to the Ethiopian highlands, where the Shebelle River originates, makes Beletweyne the first major urban center in Somalia to receive river flows from the upstream catchment, rendering it uniquely vulnerable to rapid changes in discharge. The city is physically divided into eastern and western sections by the Shebelle River, which meanders directly through the urban core. This division creates two distinct administrative and residential zones, connected by limited bridge infrastructure, which becomes critical during flood events. The study area for this research encompasses not only the municipal boundaries of Beletweyne but also the surrounding floodplain areas that are integral to the region's agricultural economy and are frequently inundated during high-flow events.

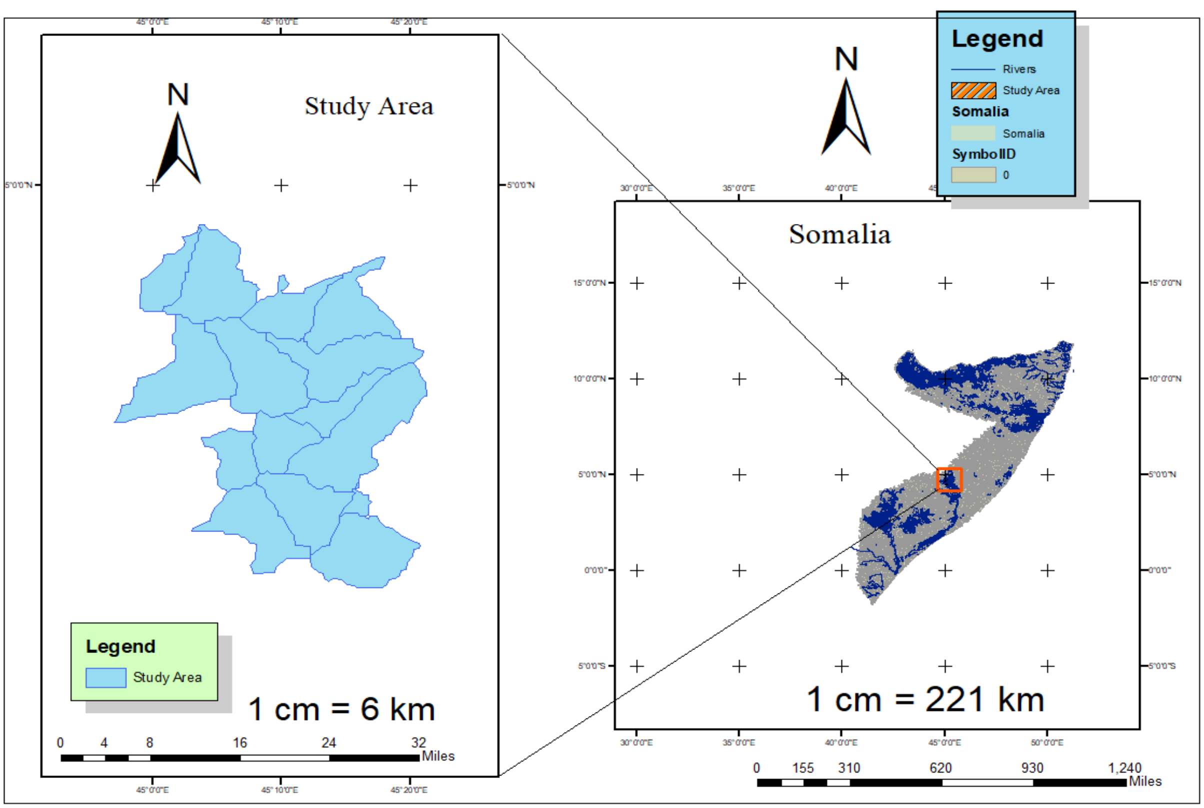

Figure 3.1: Study Area

3.2 Data

Flood inundation mapping in Beletweyne City, Somalia, requires a combination of hydrological, hydraulic, and geospatial data. Essential data includes historical streamflow and rainfall records, a high-resolution Digital Elevation Model (DEM), river geometry data, land use/land cover information, and soil data. To accomplish this goal, a high-resolution digital elevation model with a resolution of 30 m × 30 m was obtained from the Alaska Satellite Facility https://vertex.dac.asf.alaska.edu Google Earth Engine (GEE) can be a valuable tool for accessing and processing remotely sensed data, such as high-resolution imagery and DEMs, to support the modeling process. The HEC-RAS model can then be used to simulate flood inundation based on these data inputs, providing valuable information for flood risk assessment and planning for mitigation. The integration of ArcGIS with HEC-Geo RAS allows for efficient digitization of river features, facilitating the creation of accurate cross-sections for modeling (Kumar & Jha, 2022; Pandya & Vadodaria, 2018). The Manning's roughness coefficient is critical for simulating flow characteristics. Studies have shown that adjusting this coefficient can yield similar stage-discharge relationships in both DEM-extracted and field-measured cross-sections (Pramanik et al, 2010). To plot the region of the floodplain that has been inundated by flooding, the River Analysis System (RAS) needs flow data (profile). The table 3.1, shows the data needed and their sources, Hydro-meteorological data were gathered from the Somalia Meteorological Agency, the Somalia Ministry of Water (MoW), and the Somalia Water and Land Information Management in FAO (SWALIM) to achieve these goals.

Table 3.1: Data needed and their sources

Data needed	Purpose	Source
Streamflow data	1D/2D simulations	SWALIM
Stream geometry	An input for HEC-RAS	Extracted from DEM
DEM 30m	Terrain file creation	Alaska Satellite Facility
LULC Map	To assign Manning's n	Online available RS sources
Historical flood level data	Calibration	SWALIM
Sentinel 2 10m	Land use and Land cover classification	Copernicus RS products

Sentinel-1	2D model validation	RS product
Landsat-8 (OLI)	Pre-flood images and during-flood images	Earth Explorer

3.2.1 Topography and Geomorphology

The topography of the study area in Figure3.2 is characterized by a generally flat, low-lying floodplain, which significantly contributes to its flood susceptibility. Analysis of the Digital Elevation Model (DEM) acquired for this study reveals that elevations range from a high of 277 meters above sea level (masl) in the peripheral highlands to a low of 175 masl at the river outlet. The geomorphology is dominated by the Shebelle River's alluvial plain. The river channel itself exhibits a high degree of sinuosity (meandering), which naturally slows flow velocities but increases the likelihood of bank overtopping at bends and meander loops. The surrounding terrain slopes gently toward the river, creating a natural trough that traps floodwaters. In the immediate vicinity of the city, the riverbanks are often lower than the flood stages recorded during peak rainy seasons, leading to direct overflow into the "Built-Up" and "Cropland" areas.

For this study, a 30-meter resolution Digital Elevation Model (DEM) derived from the Alos World 3D (AW3D) was selected as the primary topographic input for the hydraulic simulation. This resolution was chosen based on a critical balance between data availability, computational efficiency, and the specific scale of the flood analysis.

While higher-resolution datasets (such as 1m LiDAR) are ideal for urban flood modeling, they are currently unavailable for the Beletweyne region due to the high costs of acquisition and data scarcity characteristic of the study area. Conversely, coarser datasets (such as 90m DEMs) were rejected as they fail to capture essential floodplain geometry and river channel definition required for accurate inundation mapping. The 30m DEM offers a practical compromise, providing sufficient topographical detail to delineate the main river channel and broad floodplain features while maintaining a manageable file size that ensures computational efficiency during complex 2D unsteady flow simulations. This resolution is widely accepted in hydrological literature for reach-scale and floodplain-scale analyses where the primary objective is to identify general inundation extents rather than property-level micro-drainage features.

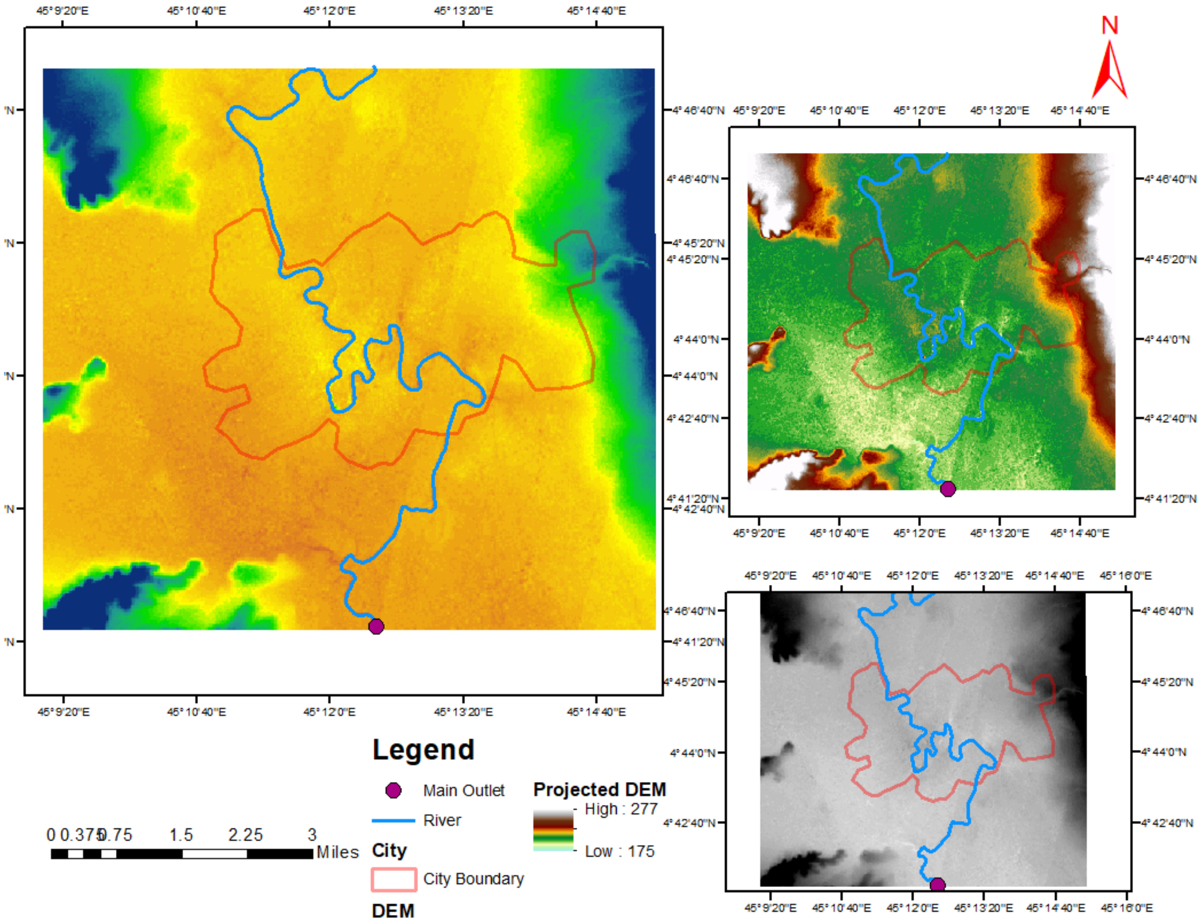

Figure 3.2: Digital Elevation Model of the study area

3.2.2 Soil Characteristics and Infiltration Capacity

The soil composition of the Beletweyne study area is predominantly characterized by alluvial deposits derived from the Ethiopian highlands. As shown in Table 3.2, the dominant soil texture is Clay to Silty Clay, which exhibits specific hydrological behaviors critical to flood modeling. Under dry conditions, these soils often form deep cracks (characteristic of Vertisols), allowing initial rapid infiltration. However, once saturated, the heavy clay content causes the soil to swell and seal, significantly reducing the infiltration rate to less than 2 mm/hr. (Hydrologic Soil

Group D). This low permeability results in high surface runoff volumes during peak rainfall events, exacerbating the flood risk in the flat terrain of Beletweyne.

Table 3.2: Estimated Soil Infiltration Properties for Beletweyne Floodplain

Soil Texture Class	Hydrologic Soil Group (SCS-CN)	Dry Infiltration Rate (mm/hr.)	Saturated Infiltration Rate (mm/hr.)	Runoff Potential
Clay / Silty Clay	D	> 20 mm/hr. (Initial)	< 1.5 mm/hr.	Very High
Sandy Loam	B	30 - 40 mm/hr.	10 - 20 mm/hr.	Moderate
Silt Loam	C	10 - 20 mm/hr.	2 - 5 mm/hr.	High

Source: SWALIM (FAO)

3.2.3 Hydrological Data

Observed annual river flow in Figure 3.3, spanning the 46 years from 1980 to 2025. The dataset is fundamental for characterizing the long-term hydrological regime of the basin and reveals a pronounced inter-annual variability in flow, which underscores the system's sensitivity to climatic drivers. This variability is starkly illustrated by the contrast between the year of highest flow, 2024, which recorded an average of 195.85 m3/s, and the year of lowest flow, 2025, with an average of just 30.09 m3/s within one and a half months. Analyzing this historical data is essential for understanding long-term trends in water resource availability. It provides the necessary baseline for assessing the frequency and magnitude of extreme wet and dry period within the study area.

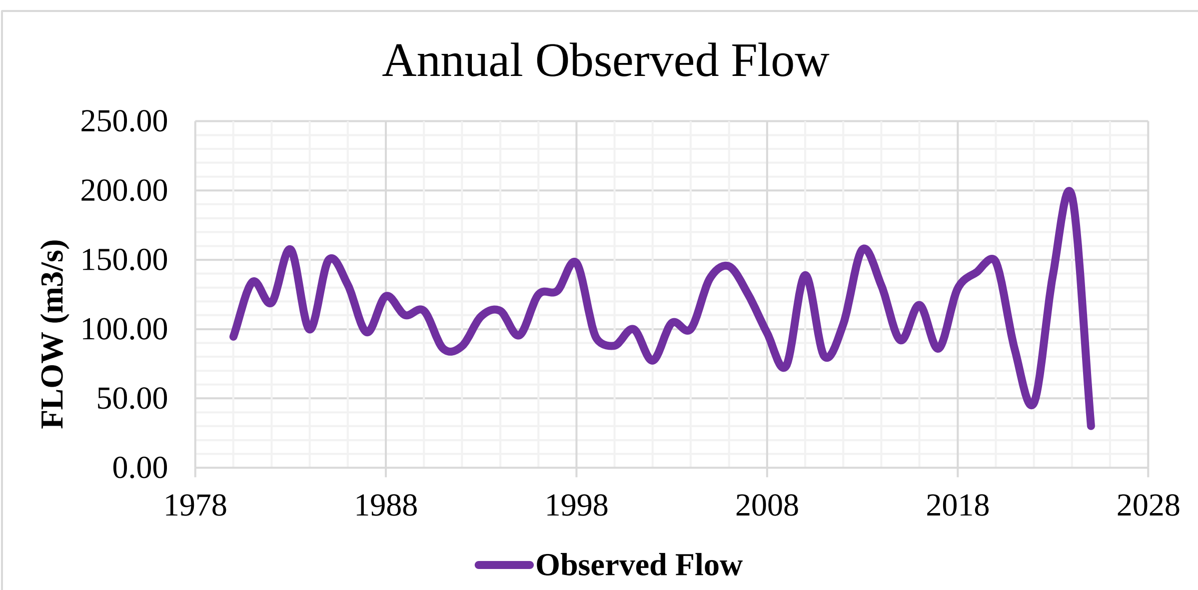

Figure 3.3: Average Annual Observed River Flow (m3/s)

3.2.4 River level data 1980-2025

This hydrological investigation is based on a derived time-series dataset in Figure 3.4, representing the annual mean river levels for the period 1980-2025. This 46-year record, which condenses daily observations into a single mean value for each year, provides a robust statistical foundation for a quantitative trend analysis. An initial examination of the data immediately highlights the period's hydrological extremes: the highest annual mean level (185.3157) was recorded in the year 2024, while the lowest annual mean level (184.5617) was registered in 2025. This pronounced variability, particularly the recent peak and subsequent (likely partial-year) low, underscores the necessity of a formal statistical analysis to distinguish long-term secular trends from short-term fluctuations and to understand the changing dynamics of the river's regime.

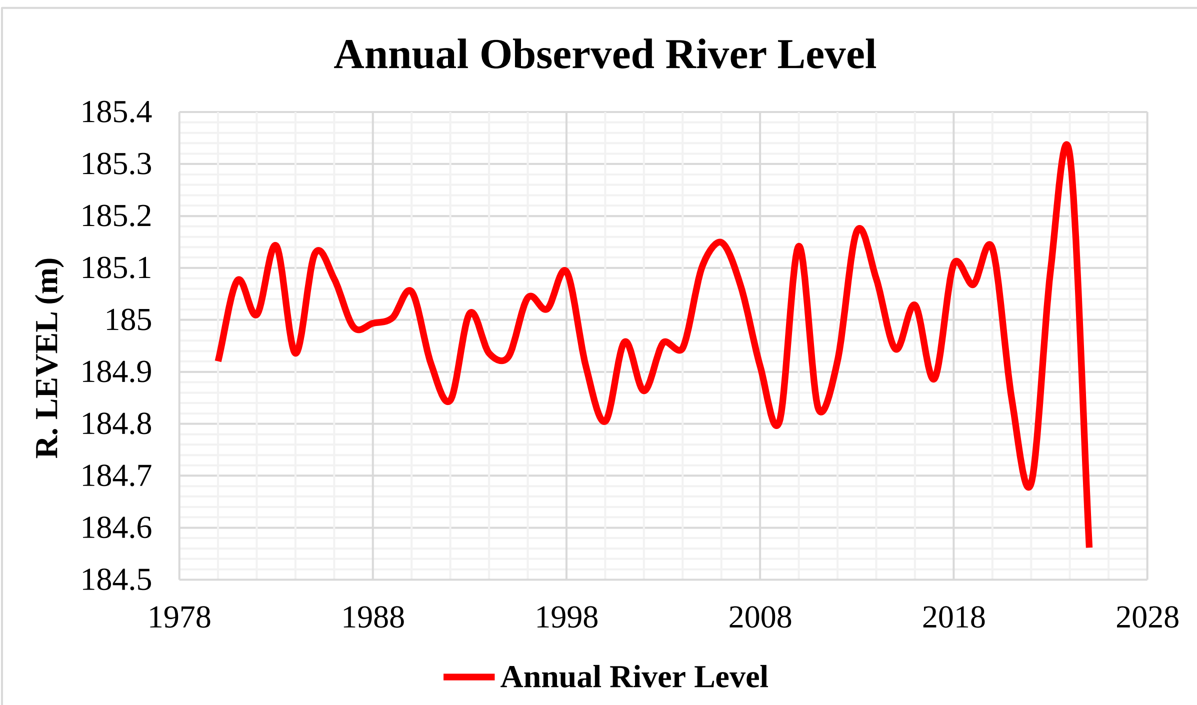

Figure 3.4: Average annual river level (m)

3.2.5 Observed Flow

The observed hydrograph for October-November 2019 in Figure 3.5, is characterized by two distinct flood peaks. The first is a moderate, slow-onset peak of 385 m3/s in mid-October. This is overshadowed by a second, much more severe "flash" event in early November, which saw the flow rise rapidly to the period's maximum of 470.076 m3/s on November 2nd. The sharp nature of the second event is a critical finding, suggesting the catchment is highly responsive to intense rainfall. This detailed, bimodal behavior provides excellent data for calibrating and validating a sophisticated hydraulic model.

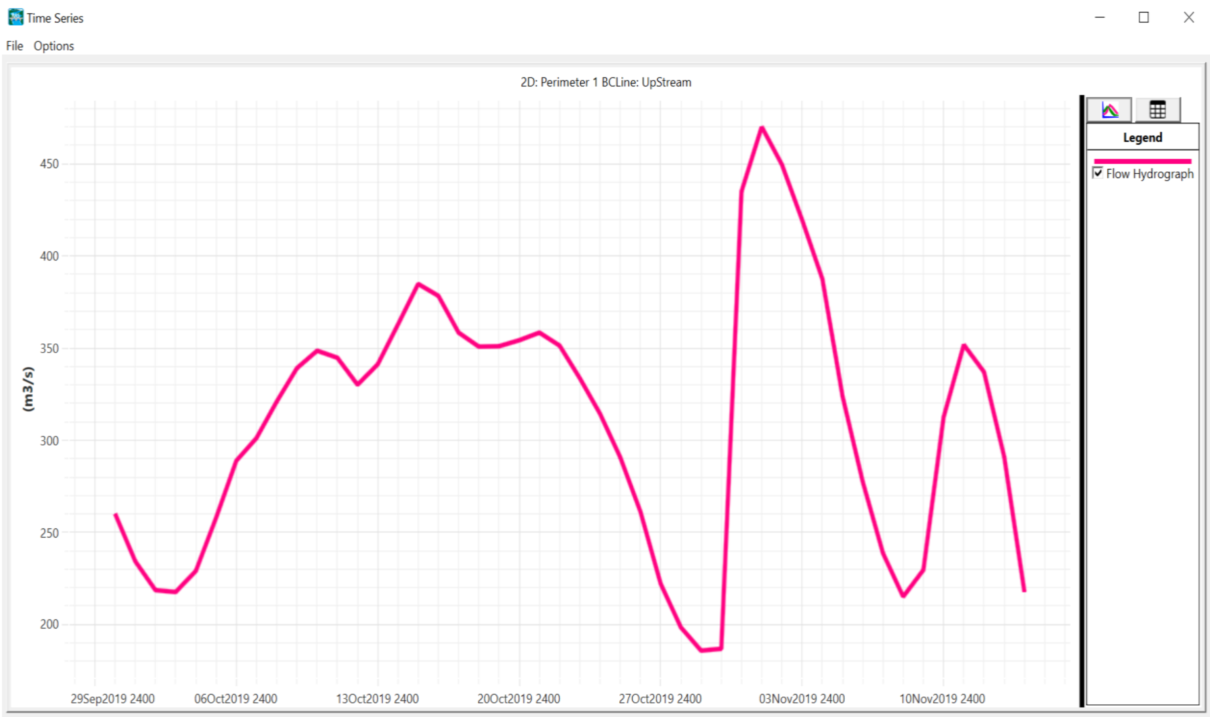

Figure 3.5: Observed flow hydrograph

3.2.6 Observed Level

Figure 3.6 the foundational field data for this hydraulic study consists of a time series of observed daily water surface elevations, recorded from October 1st to November 15th, 2019. This dataset serves as the definitive ground truth, documenting the river's actual response to flood events during this period and capturing a peak water level of 186.22 meters on November 2nd, 2019. These real-world measurements are the most critical component for the research, as they provide the essential benchmark against which the hydraulic model's performance is measured. Ultimately, this observed data is used for the crucial processes of model calibration and validation, with the primary objective of ensuring that the models' simulated outputs reliably replicate the actual hydraulic conditions of the river system.

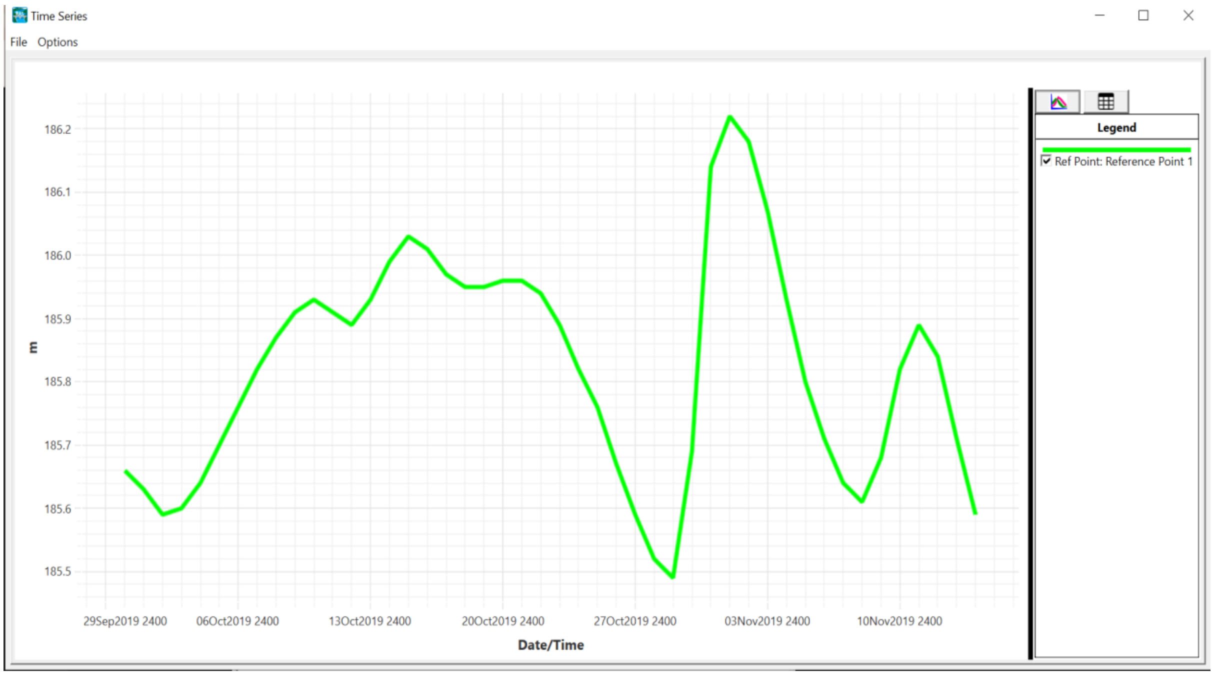

Figure 3.6: Observed River Level

3.2.7 Land Use and Land Cover of the Study Area

The Land Use/Land Cover (LULC) map for the study area in Figure 3.7 reveals a distinct pattern of land utilization organized around a central river system. The landscape is categorized into several classes: Built-up Area, Cropland, Forest, Shrubland, Vegetation, Bare land, and Water body. A detailed spatial analysis shows a concentrated Built-up Area, representing the urban core, situated directly along the river's path. This urban center is almost surrounded by extensive tracts of Cropland, indicating that agriculture is the predominant land use in the city's immediate vicinity. Beyond this agricultural belt, the periphery of the study area transitions into large expanses of Bare land. This concentric arrangement highlights a classic river-dependent settlement, where urban and agricultural activities are clustered in proximity to the water source, which flows towards a designated outlet. The map, scaled at 1 inch to 1.01 miles, illustrates that land use is fundamentally structured by its proximity to this central hydrographic feature.

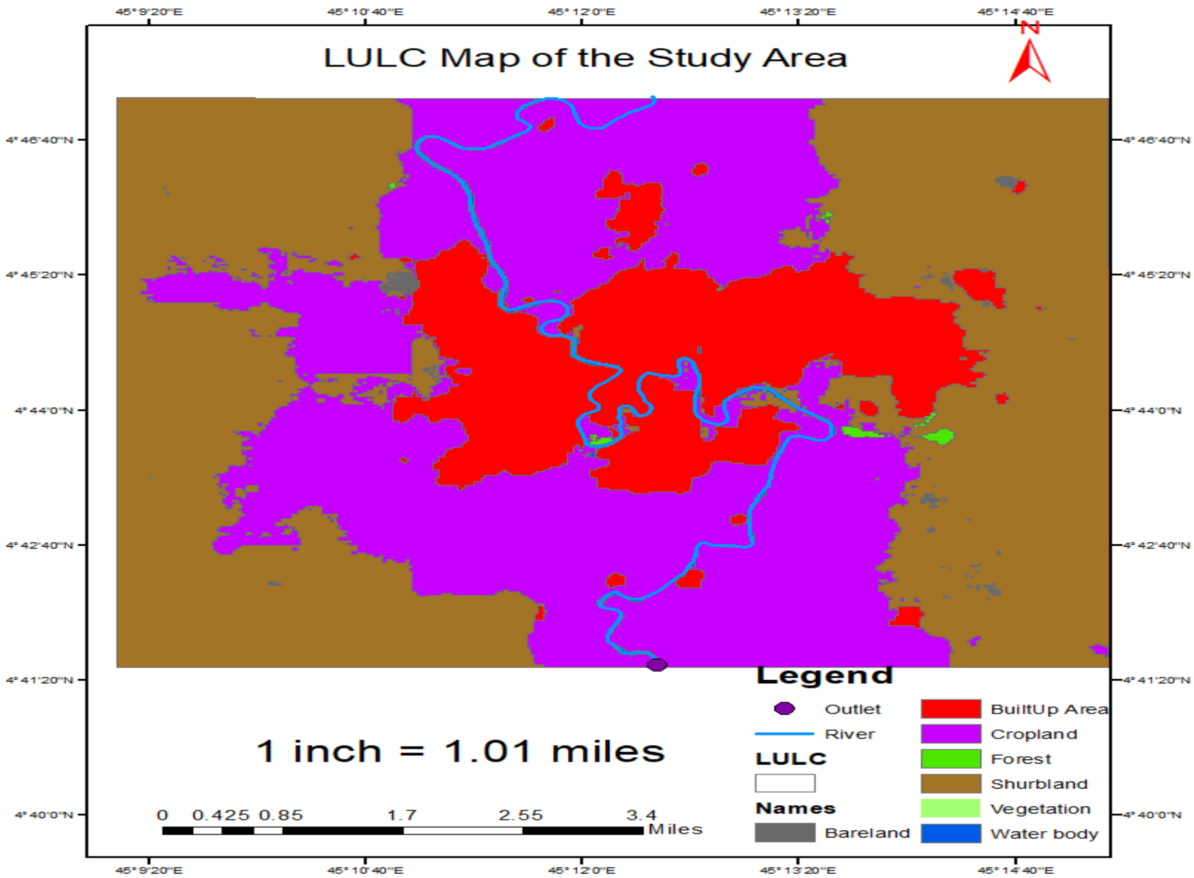

Figure 3.7: Land Use and Land Cover map of the Study Area

Land Use/Land Cover (LULC) classification was performed for the study area to establish a baseline for analysis. The results in table 3.3 indicate a landscape heavily influenced by both natural vegetation and human activity across its 117.28 km² extent. The most prevalent LULC type is Shrubland, accounting for nearly half of the area (45.90%), followed closely by Cropland (37.25%). This suggests that agricultural practices and natural vegetation are the primary determinants of surface runoff characteristics. Furthermore, Built-Up Area constitutes a significant 15.86%, highlighting the influence of urbanization on the watershed's imperviousness. To facilitate hydraulic modeling, each of the seven identified LULC categories was assigned an appropriate Manning's roughness coefficient (n), which quantifies the resistance to overland flow and is fundamental to the simulations presented in the subsequent chapters.

Table 3.3: Assigned Manning's n coefficient in each LULC Type

Code	LULC Type	Area (km2)	Percentage
1	Water body	0.638	0.544%
2	Forest	0.221	0.188%
4	Vegetation	0.001	0.001%
5	Cropland	43.682	37.247%
7	Built-Up Area	18.602	15.861%
8	Bareland	0.308	0.262%
11	Shrubland	53.827	45.897%

3.2.8 Materials and Tools

The materials and software packages that have been used for this thesis work include the following, but are not limited to:

HEC-RAS and HEC-GEORAS (pre- and post-processing)

ArcGIS

Digital camera

Global Mapper

Global Positioning System (GPS)

Field car

Motor cycle

Google earth

Note book

Minitab

Sigma Plot

Spell stat

3.3 Data Analysis

Adequacy: - the method through which the length of the record of data is measured. The observed record is merely a sample of the total population of floods that have occurred and may occur again. If the sample is too small, the probabilities derived cannot be expected to be reliable.

Nevertheless, available streamflow records are enough to provide an analysis of the problem.

Consistency: - If the conditions relevant to recording at a rain gauge station have significantly changed during the recording period, inconsistencies would appear in the station's rainfall data.

- Some of the common causes for the inconsistency of the records are:
- Shifting of the rain gauge station to a new location
- The neighborhood of the station is undergoing a marked change
- Change in the ecosystem due to calamities, such as forest fires, landslides, and
- Occurrence of observational error from a certain date

The inconsistency of the records can be checked using a double mass curve (DMC) technique, which is mainly useful when there are multiple nearby data stations. However, only one gauging station exists, making it impossible to verify the data's consistency.

Accuracy: - used to check the homogeneity of data. Most flow records are satisfactory in terms of intrinsic accuracy, and if they are not, there is little that can be done with them. If the reported flows are unreliable, they are not a satisfactory basis for frequency analysis. Even though reported flows are accurate, they may be unsuitable for probability analysis of change in the catchments that have caused a change in the hydrologic characteristic, if the record is not internally homogeneous.

3.4 Regional Flood Frequency Analysis

Regional flood frequency analysis using the HEC-RAS model and Google Earth Engine (GEE) integrates advanced hydrological modeling with geospatial data processing to enhance flood risk assessment. This approach allows for effective mapping of flood inundation areas and estimation of peak flows across various return period, leveraging both historical data and real-time satellite imagery. HEC-RAS is utilized for simulating river hydraulics and flood inundation mapping. Studies have shown its effectiveness in estimating flood extents for different return period, such as 25, 50, and 100 years, with specific peak flow values derived from statistical methods like the Normal distribution (Gambella University et al., 2024). The model's outputs can be validated against historical flood data, ensuring reliability in flood risk assessments (Namara et al., 2022).

The HEC-RAS model (version 6.5) is a powerful tool for hydraulic flood modeling, capable of performing 2D unsteady flow simulations based on full shallow water (SW) and diffusion wave (DW) equations. The choice of 2D diffusion wave equations in this study is particularly advantageous due to their stability and speed in modeling unsteady flow, which is critical for accurate flood predictions (Blandford & Ormsbee, 1993; Stelling & Verwey, 2005). These equations facilitate detailed 2D channel and floodplain mapping, allowing for effective flood risk assessment and management (Murillo & García-Navarro, 2012; Salajegheh et al., 2009). The integration of these equations within the HEC-RAS framework enhances the model's flexibility, making it suitable for various flood scenarios and improving the overall efficiency of floodplain delineation (Salajegheh et al., 2009; Wang, 2014). The equation is expressed as:

$$\frac{\partial h}{\partial t} + \frac{\partial (hu)}{\partial x} + \frac{\partial (hv)}{\partial y} = 0 \qquad (1)$$

Where h represents the depth of the water, u represents the velocity of the water along the X-axis, v represents the velocity of the water along the y-axis, t represents time, and x and Y represents location information. In Equation (1), the first term represents($\frac{\partial h}{\partial t}$), the rate of Change in water depth over time, whereas the second ($\frac{\partial (hu)}{\partial x}$) and third($\frac{\partial (hv)}{\partial y}$) terms represent the fluxes of water (the rates of flow of water) in the x and y directions, respectively.

The momentum equations are derived from the shallow water equations (SWE), which assume a thin layer of water where vertical momentum is negligible (Liang, 2011). By ignoring acceleration terms, the equations reduce to a form emphasizing gravitational and frictional forces, facilitating easier computational modeling. The zero-inertia model, which omits local and convective acceleration, is noted for its computational efficiency, particularly in low subcritical flow scenarios. This model allows for adaptive time-stepping and improved mass balance accuracy, addressing limitations found in previous models (Dey, 2025, p. 2). In urban settings, such as the Fukuoka flood disaster, the momentum equations incorporate resistance from buildings and bottom shear stresses, enhancing the model's accuracy in predicting flood behavior. The model's effectiveness is demonstrated through simulations that adjust for varying roughness coefficients, reflecting real-world conditions (Hashimoto & Park, 2008).

$$S0x - Sfx - \frac{\partial h}{\partial x} = 0 \tag{2}$$

Also, the y-axis

$$S0y - Sfy - \frac{\partial h}{\partial y} = 0 \tag{3}$$

S0x and S0y are bed slopes in the x and y directions, respectively. $\frac{\partial h}{\partial x}$ And $\frac{\partial h}{\partial y}$ represent the slopes of the water surface in the x and y directions, respectively. Sfx and Sfy are the friction slopes in the x and y directions, respectively.

The bed slope term expressed in the momentum equations can be computed from the underlying elevation data (DEM). In contrast, the friction slope terms are determined via Manning's equation, which relates friction (flow resistance) to depth and velocity.

$$\text{Sfx} = n^2 u \sqrt{\frac{n^2+v^2}{h^{4/3}}} \tag{3}$$

$$\text{Sfx} = n^2 v \sqrt{\frac{n^2+v^2}{h^{4/3}}} \tag{4}$$

Where n is Manning's roughness coefficient; u and v are the velocity components in the x and y directions, respectively; h is the water depth; and u2 + v2 represents the total velocity magnitude.

GEE can enhance flood frequency analysis by providing high-resolution satellite imagery and geospatial data, facilitating real-time monitoring of flood events and land use changes. The combination of HEC-RAS and GEE allows for dynamic updates to flood models, improving the accuracy of inundation mapping and enabling timely disaster response strategies (Kalita, 2024). Various statistical methods, including the Log Pearson Type III and Gumbel distributions, are employed to estimate design floods, which are crucial for calibrating models like HEC-RAS (Alexandre et al., 2024; Namara et al., 2022). Bayesian hierarchical models have also been explored to account for spatial variability and improve the precision of flood predictions across large regions (Sampaio & Costa, 2021).

Frequency analysis is a method that involves examining historical records of hydrologic events to estimate the likelihood of future occurrences. Water resource projects need to be planned for events that cannot be precisely predicted in terms of timing. Therefore, accurately estimating the probability that streamflow will meet or exceed a specific value is essential.

The basic assumptions in statistical flood frequency analysis are the independence and stationarity of the flow data series and that the data come from the same distribution. Before FFA was done, filling of missed flow data, homogeneity, independence, and consistency of collected flow data were checked. The flood frequency analysis (FFA) involves the calculation of the statistical probability that a flood of a certain magnitude will occur in a certain period of time. Each flood is recorded and ranked in order of magnitude, with the highest rank being assigned to the largest flood. The return period is the likely time interval between floods of a given magnitude and is a product of the length of the streamflow record and the rank of the event. Ultimately, the FFA assigns a recurrence interval to the annual peaks of the recorded time series and uses this information to develop a relationship linking recurrence interval with flood magnitude.

At present, there is no universally accepted frequency distribution model for frequency analysis of extreme floods. If a prediction is to be based on a set of hydrologic data, then the distribution that best fits the set of data may be expected to give the best estimates, usually an extrapolation of the probability of an event occurring. The probability distributions for this study were:-

After having the annual flood maximum series, probability distributions have been analyzed. The most common distributions used in the case of the Lower Shebelle gauging site data are as follows.

- Normal
- Log normal

- Gumbel (EV-I)
- Pearson type III and
- Log Pearson Type III distributions.

To find the annual flood maximum series of the catchment located in the sub-basin area, the above-mentioned method of frequency analysis can be used.

3.5 Model sensitivity

The sensitivity of the HEC-RAS model can be evaluated using different methods that examine how input parameter changes impact model outputs. These methods are essential for assessing flood prediction accuracy and enhancing model performance.

Morris Method: This approach evaluates the influence of individual parameters on model outputs by analyzing the elementary effects of varying parameters. It is particularly useful for identifying which parameters have the most significant impact on results (Bellos et al., 2020).

Global Sensitivity Analysis (GSA): GSA examines the effects of input parameters collectively, allowing for a comprehensive understanding of their interactions. For instance, varying the floodplain Manning coefficient demonstrated significant changes in peak discharge and flood arrival times (Silva et al., 2024).

Monte Carlo Simulation: This method propagates uncertainty through the model by running numerous simulations with varied parameters, providing a statistical distribution of potential outcomes (Bellos et al., 2020).

3.5.1 Parameters Influencing Sensitivity

Cross Section Spacing

The distance between cross sections can significantly affect flow predictions, with closer spacing often yielding more accurate results (Hu & Walton, 2008).

Manning Coefficient

Variations in this coefficient can lead to substantial differences in flood outputs, as shown in studies where changes resulted in up to 54% variation in peak discharge (Silva et al., 2024).

Expansion Ratio and Weir Discharge Coefficient

These parameters also play critical roles in determining flow characteristics and should be carefully calibrated (Hu & Walton, 2008).

3.6 HEC-RAS Tools

The Hydraulic Engineering Center's River Analysis System (HEC-RAS) is a powerful software developed by the U.S. Army Corps of Engineers. It allows for detailed hydraulic analysis, including one-dimensional steady and unsteady flow modeling, sediment transport simulation, and water temperature analysis. The system combines a user-friendly graphical interface with robust analysis tools, data management, and reporting features.

3.6.1 Standard Workflow for Inundation Mapping

Creating a flood inundation map with HEC-RAS typically involves five key stages:

- A digital representation of the ground surface, either as a Digital Elevation Model (DEM) or a Triangulated Irregular Network (TIN), is prepared using GIS software like ArcGIS.
- The HEC-GeoRAS extension for ArcGIS is used to extract the necessary river geometry from the terrain model. This includes defining the stream centerline, cross-sections, bank lines, and flow paths.
- The geometric data is imported into HEC-RAS, which then runs hydraulic calculations to determine the water surface elevation for given flow conditions.
- The calculated water levels from HEC-RAS are exported back into the GIS environment.
- In GIS, the water surface data is overlaid onto the terrain model to create the final flood inundation map.

3.6.2 Data Preparation and Model Setup

To build the hydraulic model, the terrain data (DEM/TIN) is first processed in HEC-GeoRAS. This tool helps delineate the river's physical characteristics. Simultaneously, a land use map is analyzed to assign Manning's 'n' values, a coefficient representing surface roughness, to each cross-section. This combined geometric and roughness data is then exported as a single file for HEC-RAS.

Within HEC-RAS, this geometry is reviewed and refined. Flow data, such as the peak flows for various return period (e.g., 100-year flood), is then entered. The primary goal is to use this flow data to simulate the corresponding water surface elevations along the entire river.

Performing Hydraulic Analysis in HEC-RAS

The process within the software follows a structured procedure:

- A new project is created to store all geometric, flow, and simulation data.
- The prepared geometric data is imported, and flow conditions are entered. This can be done for steady flow (a constant peak flow) or unsteady flow (a flow that changes over time, like a flood hydrograph).
- HEC-RAS performs the hydraulic computations based on the entered data.
- The software provides various ways to view the output, including water surface profiles, cross-section plots, tables, and rating curves.

For a reliable unsteady flow model, calibration is essential. This involves adjusting model parameters until the simulated results closely match observed historical flood data. Furthermore, analyzing the model's accuracy, stability, and sensitivity is crucial to ensure the final results are dependable.

3.7 Computational methodology

HEC-RAS is an integrated software system, designed for interactive use in a multi-tasking environment. The system comprises a graphical user interface (GUI), separate analysis components, data storage and management capabilities, graphics, mapping, and reporting facilities. The HEC-RAS system contains the following river analysis components in figure 3.8 for (1) one-dimensional steady flow water surface profile computations; (2) one-dimensional and/or two-dimensional unsteady flow simulation; (3) quasi-unsteady or fully unsteady flow movable boundary sediment transport computations (1D and 2D); and (4) one-dimensional water quality analysis. A key element in Figure 3.8 is that all four components use a common geometric data representation and common geometric and hydraulic computation routines. In addition to the four river analysis components, the system contains several hydraulic design features that can be invoked once the water surface profiles are computed. HEC-RAS also has an extensive spatial data integration and mapping system (HEC-RAS Mapper). HEC-RAS is designed to perform one-dimensional and two-dimensional hydraulic calculations for a full network of natural and constructed channels, overbank/floodplain areas, levee-protected areas; etc. The following is a description of the major capabilities of HEC-RAS (HEC-RAS user manual 6.5.1). HEC-RAS effectively models flood scenarios, as demonstrated in studies where it accurately predicted flood extents and inundation volumes in urban areas (Riswanto & Nanda, 2023; Yusuf et al., 2023).

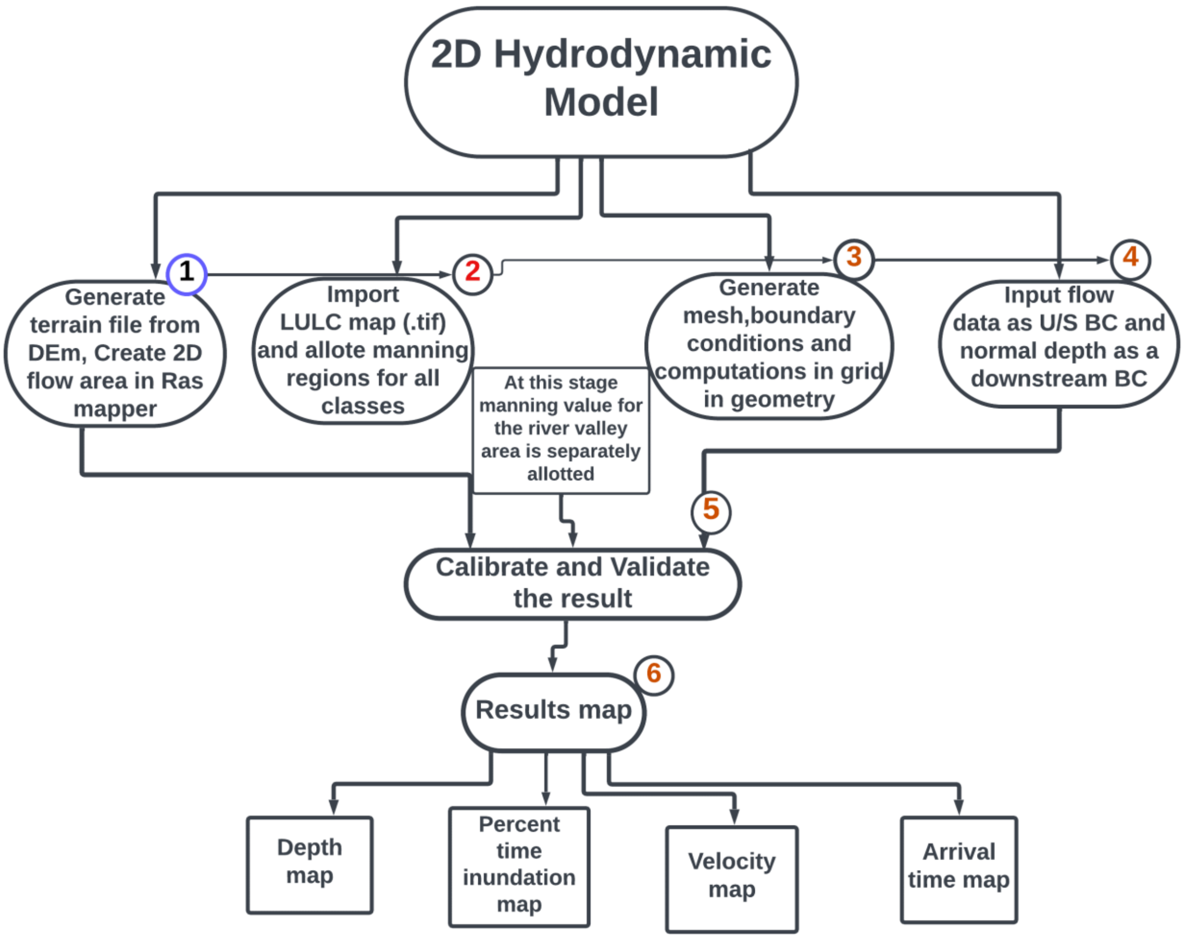

Figure 3.8: Conceptual framework of the 2D simulating HEC-RAS model

3.7.2 2D Flow Area

Figure 3.9 illustrates a foundational component of the HEC-RAS model configuration: the 2D Flow Area defined for the Beletweyne study reach. This user-defined computational mesh, superimposed over the terrain and satellite imagery, delineates the precise spatial domain where the two-dimensional hydraulic calculations will be performed. By encompassing the main river channel and the expansive adjacent floodplains, this grid serves as the digital environment where the model will solve the shallow water equations. The extent and resolution of this 2D Flow Area are critical setup parameters, as they directly govern the model's ability to simulate the complex, two-dimensional hydrodynamics of floodwater spreading across the topography, ultimately determining the spatial accuracy of the final inundation maps.

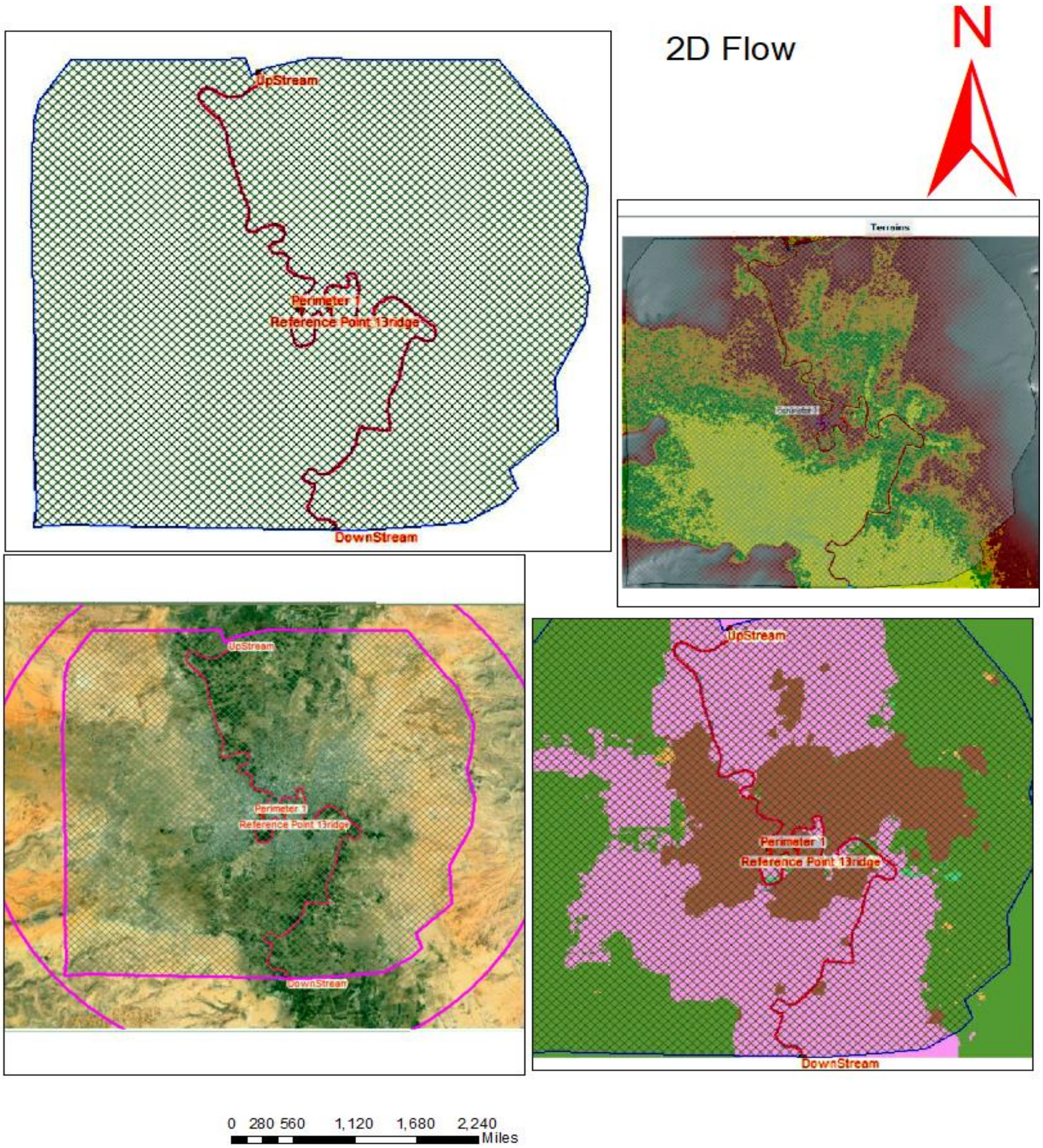

Figure 3.9: 2D Flow Area

3.7.3 Justification for 2D Model Selection

While 1D hydraulic models are computationally efficient, they were deemed insufficient for the complex floodplain dynamics of Beletweyne. A comprehensive comparison was conducted (Table 3.6) to justify the selection of the 2D Unsteady Flow engine for this study.

The Beletweyne floodplain is characterized by flat topography where floodwaters spread laterally in multiple directions, creating complex overland flow paths that a 1D cross-section cannot capture. The 2D model accurately solves for these multi-directional flows, identifying independent flow paths through the urban core and agricultural fields.

Table 3.4: Comparative Analysis and Justification for Model Selection

Criteria	1D Model (HEC-RAS)	2D Model (HEC-RAS)	Justification for Selection in this Study
Flow Direction	Longitudinal only (Downstream)	Multi-directional (X and Y)	Floodwaters in Beletweyne spread laterally into streets, which 1D cannot map.
Topography	Discrete Cross-Sections	Continuous Digital Terrain (Mesh)	2D captures the continuous terrain, including depressions and elevated roads.
Velocity	Average velocity at Cross-Section	Detailed Velocity Vectors	Required to identify high-risk zones where velocity > 2 m/s.
Mapping	Interpolated (Linear)	Direct Spatial Calculation	1D interpolation misses details between lines; 2D provides pixel-perfect accuracy.
Complexity	Low (Fast)	High (Computationally intensive)	The higher computational the cost is justified by the need for accuracy in urban risk mapping.

3.8 Statistical performance

Statistical performance metrics are essential tools for quantitatively evaluating the accuracy and reliability of a 2D HEC-RAS model. These metrics provide a framework for comparing simulated results with observed data, allowing modelers to assess the model's performance rigorously and systematically. Common metrics include Root Mean Square Error (RMSE), Nash-Sutcliffe Efficiency (NSE), and Percent Bias (PBIAS), each offering unique insights into different aspects of model accuracy.

RMSE is a critical metric for assessing the model's accuracy in simulating hydraulic conditions. In the study of the Karoon River, the RMSE for the water stage during validation was reported as 0.1 m, indicating a high level of accuracy in the model's predictions. RMSE was computed for intermediate gauging stations for the Lower Tapi River, demonstrating the model's effectiveness in capturing flood peaks (Timbadiya et al., 2011). For instance, a study on the Purna River achieved an R^2 value of 0.9679, indicating a strong correlation between observed and simulated data (Pathan et al., 2024).

$$\text{RMSE} = \frac{1}{n}\sum_{i=1}^{n}(y_i - y^{\wedge}{}_i)^2$$

Where;

N is the number of data points

Yi represents observed values

$Yi^{\wedge}$ represents predicted values

Effective validation of a model involves calibration, comparison with observed data, and statistical analysis. This process ensures that the model accurately simulates real-world conditions, which is crucial for reliable flood management and water quality assessments. Statistical metrics, such as Nash-Sutcliffe Efficiency (NSE) and R^2 values, are commonly used to quantify the model's performance, with NSE values of 0.86 indicating a strong predictive capability (Tamiru & Wagari, 2022).

$$\text{NSE} = 1 - \frac{\Sigma(\text{simulated} - \text{observed})^2}{\Sigma\,(\text{observed} - \text{mean (observed)})^2}$$

Measures the relative magnitude of the residual variance to the observed data variance.

NSE values range from -∞ to 1.1

NSE = 1 indicates perfect model performance.

NSE = 0 indicates that the model's predictions are no better than the mean of the observed data.

NSE < 0 indicates that the mean of the observed data is a better predictor than the model.

The Coefficient of Determination (R^2) is a statistical measure that indicates the proportion of the variance in the dependent variable that can be explained by the independent variable(s) in a regression model. It ranges from 0 to 1, where:

R^2 values range from 0 to 1.

Higher R^2 values indicate better model performance.

The PBIAS (Percent Bias) is a crucial statistical index used to validate HEC-RAS models to assess the accuracy of simulated flow against observed data. It provided insight into the systematic error of the model predictions, indicating whether the model tends to overestimate or underestimate flow values. A PBIAS value close to zero signifies a good model performance, while values beyond ±10% may indicate significant bias. Studies have shown that models with PBIAS values within ±10% are generally considered acceptable, as seen in various watershed analyses (Zhang et al, 2022; Zulaeha et al, 2020).

$$\text{PBIAS} = \frac{\sum \text{Oi} - \text{Si}}{\sum \text{Oi}} \text{x} 100\%$$

Where:

Oi= Observed value

Si = Simulated value

The summation is conducted over all observations.

3.9 Google Earth Engine platform

Machine learning techniques save time and do not require properly configured equipment; researchers have recently directed their attention toward simulations based on these algorithms. The Google Earth Engine platform in Figure 3.10 shows the findings in a terminal and offers an interface for working with JavaScript object notation (JSON). GEE has more than 40 years of data preserved and available via the platform's scripts. Among other things, GEE is well-known for its environmental mapping, NDVI (normalized difference vegetation index), air pollution, hazard management, and atmospheric analysis. A few sections of the study demonstrate the application of GEE for flood mapping due to a recent methodology (Trambadia et al., 2023).

Sentinel-1A and Sentinel-1B play a crucial role in flood inundation mapping through their advanced Synthetic Aperture Radar (SAR) capabilities. These satellites provide all-weather, day-and-night imaging, which is essential for timely flood detection and monitoring. Their integration with other data sources enhances the accuracy and reliability of flood mapping methodologies. The satellites offer a spatial resolution of 10 meters and a temporal resolution of sub-weekly when both are operational, facilitating frequent updates on flood extents (Lacava et al, 2024). Combining SAR intensity and interferometric coherence from Sentinel-1 data allows for a more nuanced understanding of flood dynamics, as seen in the mapping of the Derna, Libya flood event (Hotaki et al, 2024). The integration of Sentinel-1 with optical data from Sentinel-2 can further improve flood mapping accuracy, leveraging the strengths of both satellite types (Lacava et al, 2024).

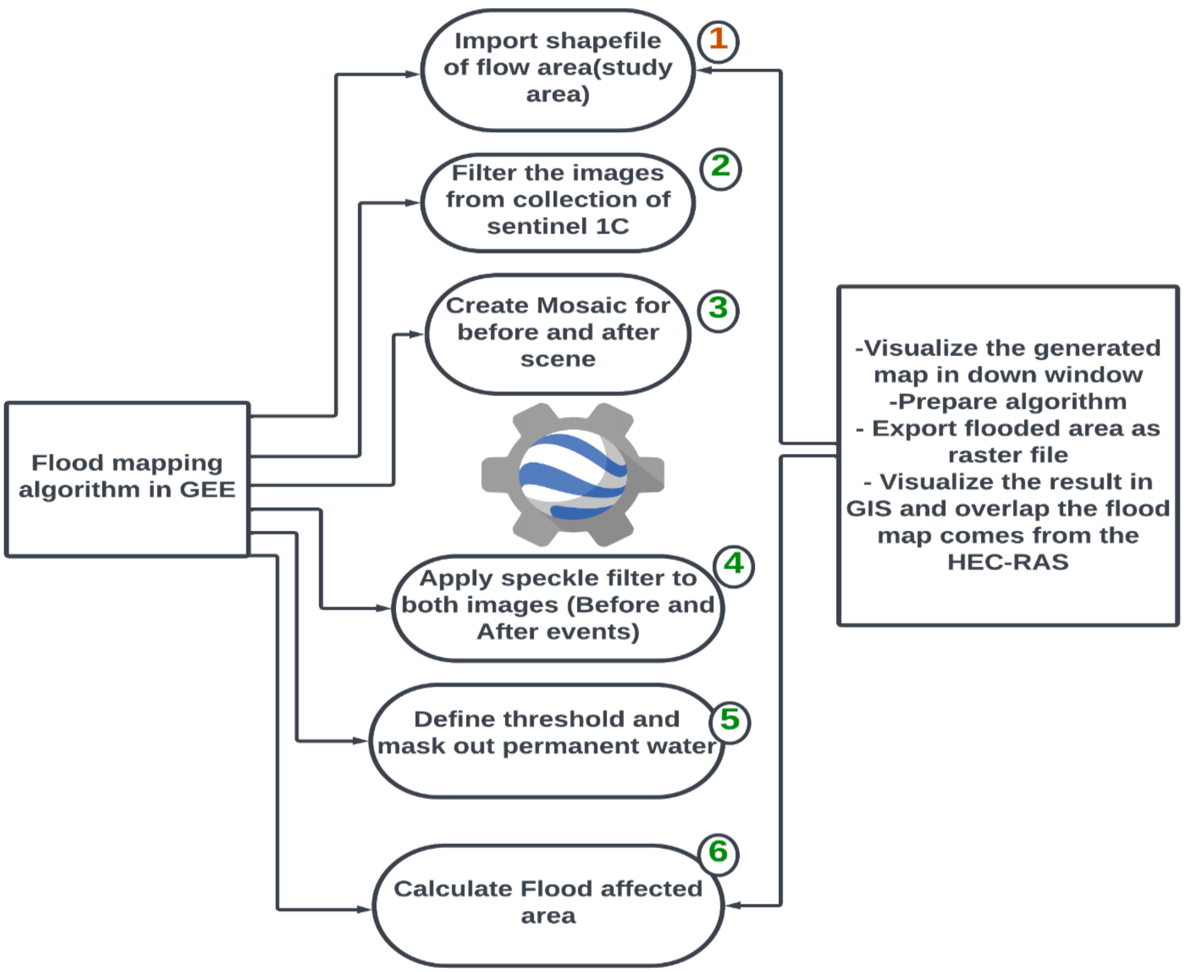

Figure 3.10: Process algorithm showing the flood inundation mapping via the GEE platform

The integration of machine learning with HEC-RAS has been shown to enhance validation accuracy, as seen in the Baro River Basin, where flood extents were validated against NDWI data with 96% agreement (Tamiru & Wagari, 2022). In this study, the inundation map generated in HEC-RAS was checked with the water body delineated using the Normalized Difference Water Index (NDWI). NDWI uses Green (Band-2) and near-infrared (Band-4) bands of remote sensing images to extract a water body, in which near-infrared (NIR) and short-wave infrared (SWI) are used as the main input. Based on overlapping areas, the HEC-RAS inundation map and the LANDSAT 8 remotely sensed imagery derived from https://earthexplorer.usgs.gov/ in NDWI were evaluated for performance.

$$\text{NDWI} = \frac{(\text{NIR}-\text{SWI})}{(\text{NIR}+\text{SWI})}$$

Using the intersect tool in the Analysis toolbox of ArcGIS (ver.10.4), the percentage of overlapped area between the water body designated in NDWI and HEC-RAS software was calculated. The raster formats of the two results (NDWI and HEC-RAS) were first converted into vectors (Polygons) using a conversion tool, and ArcGIS's geometry calculation methods were then used to determine the relevant shape areas. Both polygons were remapped to the same geographic coordinate system (Afgoye UTM Zone 38 N), and the percentage of overlapped regions was computed (Tamiru & Wagari, 2022).

Overlapping percentage (%) = $\frac{(\text{Layer 1 (Km2)})}{(\text{Layer 2 (Km2)})}$ Layer 1 is the area of the water body delineated in NDWI from flood events, and Layer 2 is the area of the inundation map generated in HEC-RAS.

RESULTS AND DISCUSSION

4.1 Flood frequency analysis Results

To select the best-fitting probability distribution for the Shebelle River flood frequency analysis, five distributions were evaluated. Normal, Log-Normal, and Gumbel (EV-I), Pearson Type III, and Log-Pearson Type III. The selection was based on the Akaike Information Criterion (AIC), Bayesian Information Criterion (BIC), and Nash-Sutcliffe Efficiency (NSE) (Table 3.4). As shown in Table 3.4, the Log-Pearson Type III distribution demonstrated a superior fit compared to the Normal and Gumbel methods, achieving a high Coefficient of Determination (R^2 = 0.83) and NSE (0.83). While the Pearson Type III distribution also performed well, the Log-Pearson Type III is widely recommended for hydrological extremes involving skewed data. Consequently, Log-Pearson Type III was selected to project the 25, 50, and 100-year return period floods, ensuring the most accurate boundary conditions for the hydraulic model.

Table 3.1: Goodness-of-Fit Statistical Metrics for Distribution Selection

Probability Distribution	AIC	BIC	D	R^2	NSE	Rank
Log Pearson type III	518.23	523.72	0.224	0.829	0.875	1
Pearson type III	511.41	516.9	0.24	0.851	0.837	2
Normal	531	534.66	0.246	0.718	0.712	3
Log Normal	533	538.49	0.246	0.718	0.712	4
Gumbel	566.11	569.77	0.318	0.571	-0.46	5

4.2 Sensitivity Analysis Results

To identify the parameters with the most significant influence on the model's predictive accuracy, a sensitivity analysis was conducted by varying key input parameters within a range of ±10% to ±25% from their calibrated baseline values. The analysis focused on three primary variables: Main Channel Roughness (n_{ch}), Floodplain Roughness (n_{fp}), and Slope Boundary Conditions (S). The results, summarized in Table 3.5, indicate that the model is most sensitive to changes in the Main Channel Roughness (n_{ch}). An increase of 25% in n_{ch} resulted in a corresponding increase in peak water surface elevation (WSE) of 0.85 meters, significantly altering the flood extent. In contrast, the model showed lower sensitivity to variations in the floodplain roughness and slope, which resulted in minor WSE deviations of less than 0.3 meters. This finding underscores the critical importance of accurately characterizing the river channel geometry and vegetation during the calibration process.

Table 3.2: Sensitivity Analysis of Key Model Parameters on Peak Water Surface Elevation (WSE)

Parameter	Baseline Value	Adjustment (%)	Adjusted Value	Resulting WSE (m)	Change in WSE (m)	Sensitivity Ranking
Main Channel	0.035	0.25 -0.25	0.044 0.026	186.05 184.65	0.85 -0.55	High
Floodplain	0.045	0.25 -0.25	0.056 0.034	185.35 185.08	0.15 -0.12	Medium
Slope	0.0003	0.1 -0.1	0.00033 0.00027	185.22 185.18	0.02 -0.02	Low

4.3 1D Steady Model Results

4.3.1 1D Cross-Sectional View

Figure 4.1 presents a representative 1D cross-sectional view, a primary output from the HEC-RAS hydraulic simulation, illustrating the river's computed response to the 100-year design flood. This plot contrasts the ground's topographical profile, showing the main channel and the adjoining left and right bank (overbank) areas, with the simulated Water Surface Elevation (WSE) for this specific flood event. The visualization clearly indicates that the flood discharge significantly exceeds the main channel's conveyance capacity, resulting in extensive overbank flooding across the adjacent floodplains. This cross-sectional data, which provides the precise flood depth and lateral inundation extent at this station, is a fundamental unit of analysis that, when interpolated along the river reach, forms the geospatial basis for the final flood inundation map.

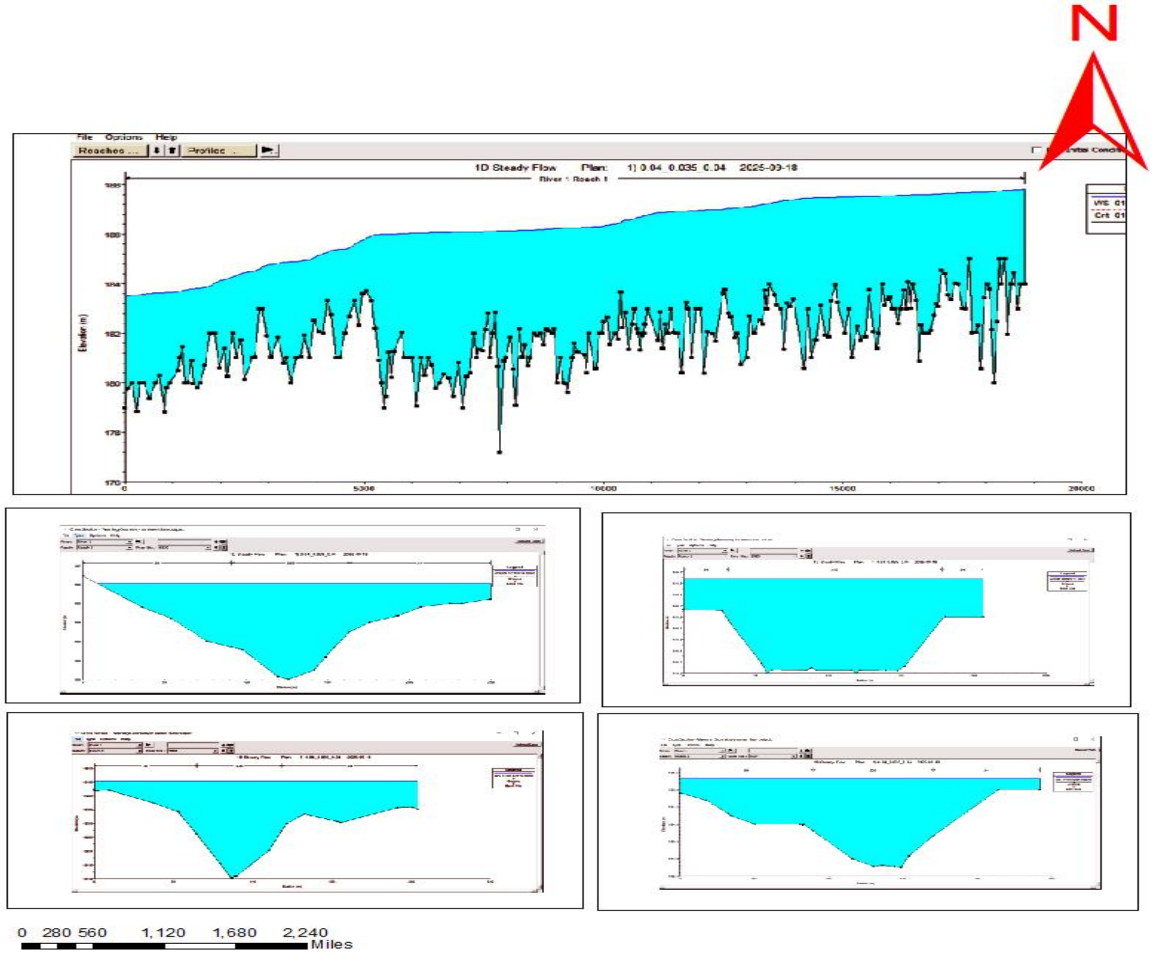

Figure 4.1: 1D Cross-sectional View

4.3.2 25-year return period and a 50-year return period

The provided flood inundation maps in Figure 4.2 illustrate two different storm scenarios for the Shebelle River in Beletweyne City, Somalia: a 25-year return period and a 50-year return period. The map for the 25-year event shows projected flood depths ranging from 0.00 meters up to a maximum of 3.7951 meters. As expected, the 50-year return period map indicates a more severe flooding event, with corresponding flood depths increasing significantly to a maximum of 5.9691 meters. Both maps clearly delineate the river, the city boundary, and a main outlet, providing a clear visual comparison of the increased inundation area and depth associated with the larger, less frequent storm event.

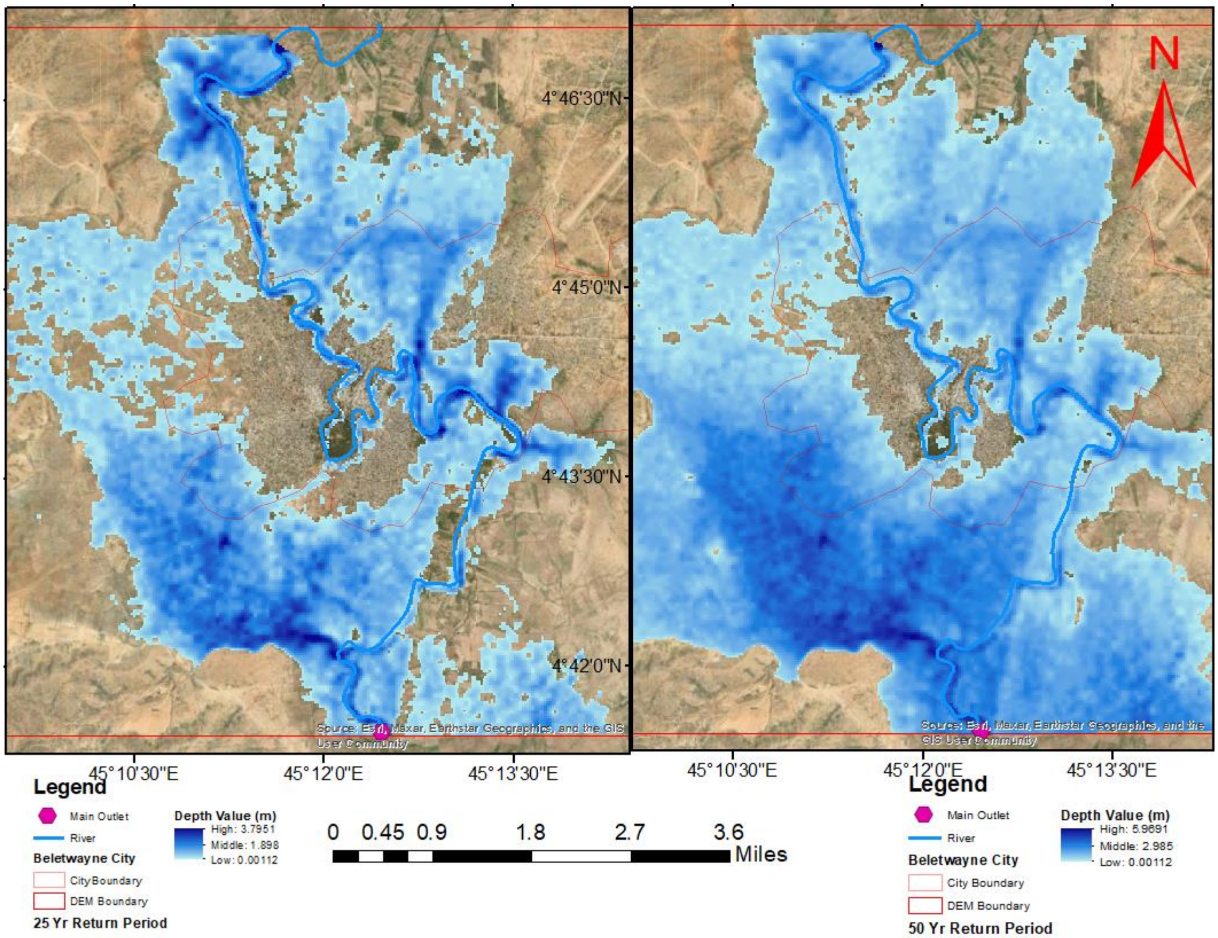

Figure 4.2: Comparison of simulated flood inundation depths (m) for 25-year and 50-year return period in Beletweyne City, Somalia

4.3.3 Analysis of 100-Year Flood Scenario for the Shebelle River

The map in Figure 4.3 illustrates the simulated 100-year return period flood event, presenting two key visualizations. The first map details the Depth Values, showing a maximum flood depth of 8.575 meters and a minimum of 0.00 meters. The second map shows the corresponding Water Surface Elevation (WSE) for the same 100-year event, with values ranging from a low of 185.029 meters to a high of 198.126 meters. Both maps clearly identify the river, city boundary, and main outlet. The table 4.1 escalating impact of flood events on local populations and infrastructure by comparing predictive return period (25 to 100 years) against the catastrophic observed totals from 2019. It highlights a critical trend where recent flooding levels are significantly outpacing historical models, placing vital assets like the Regional Hospital and Ugas Khalif Airport at extreme risk.

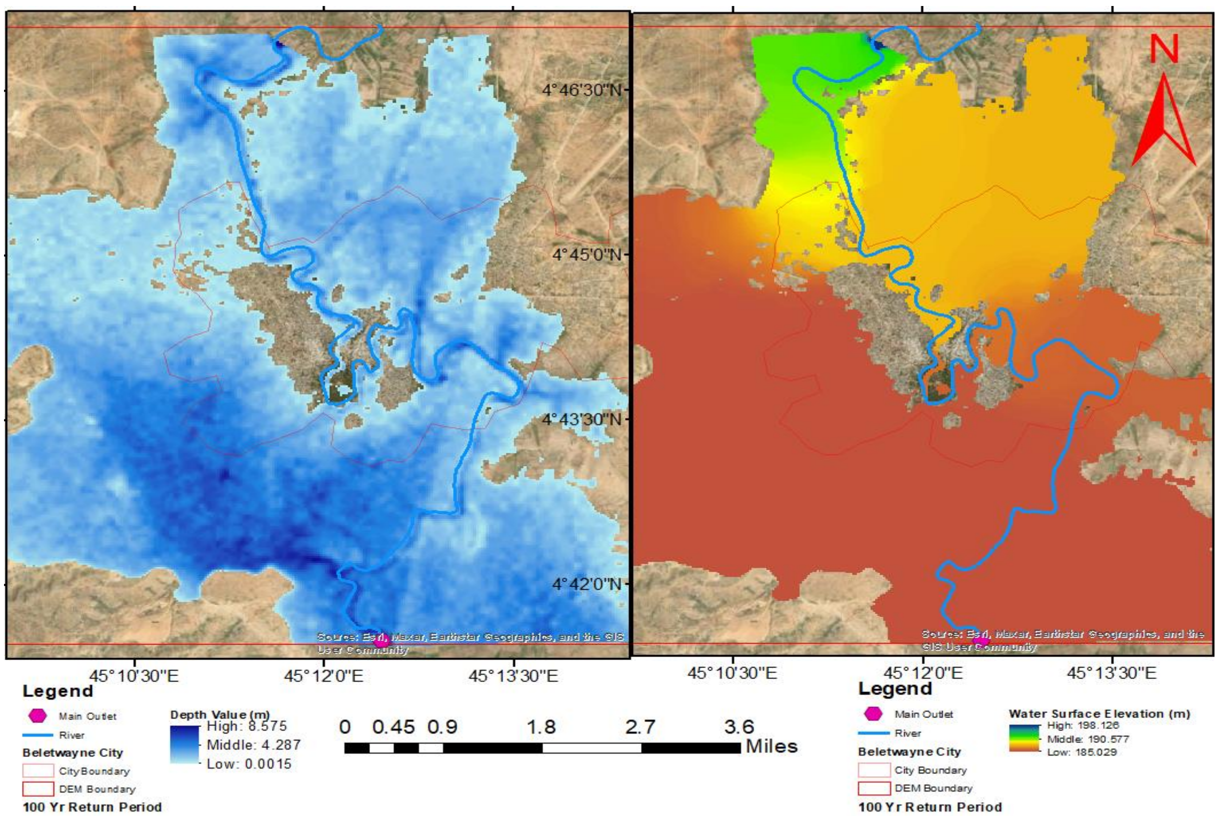

Figure 4.3: Simulated flood maps for the 100-year return period in Beletweyne City

Table 4.3: Summary of Simulated Flood Scenarios for Beletweyne City

Return Period	Max Flood Depth (m)	Inundation Area (km²)	Population Affected	Critical Infrastructure Impacted
25-Year	3.7951 m	4.87	65,000 – 80,000	Central Market (Suuqacaol) Bundo-weyn Bridge approaches, Residential Sectors (Hawa-tako)
50-Year	5.969 m	8.56	110,000 – 130,000	Regional Hospital, Primary Schools, Mosques in central districts, Main paved roads
100-Year	8.575 m	11.65	>180,000	Government Administrative Buildings, Ugas Khalif Airport road, Power/Water Supply Stations
Observed (2019)	186.22 m (WSE)	20.0 km²	230,000 (Displaced)	Widespread destruction of housing, agricultural land and suspension of transport

Population estimates were derived by overlaying the flood extent map with estimated population density layers (approx. 4,000–6,000 persons/km² in core urban zones) derived from World Pop data for Somalia.

4.4 2D Unsteady Model Results

4.4.1 Depth Map

The Figure 4.4 clearly illustrates the primary geospatial output of the 2D HEC-RAS simulation: a detailed flood inundation and depth map for the Beletweyne study area. This map provides a comprehensive, spatially-distributed visualization of the flood event's full extent and severity across the entire floodplain. The color-coded legend quantitatively represents the water depth in meters, clearly delineating the deepest sections of the main channel (shown in red, ~2.6m) from the shallower, inundated overbank areas (shown in green and blue, ~0.4m to 1.6m). This final map is the critical deliverable of the hydraulic modeling process, as it directly translates complex hydraulic calculations into an intuitive and actionable tool for identifying high-risk zones, validating the model against observed data, and informing all subsequent flood risk management and urban planning decisions.

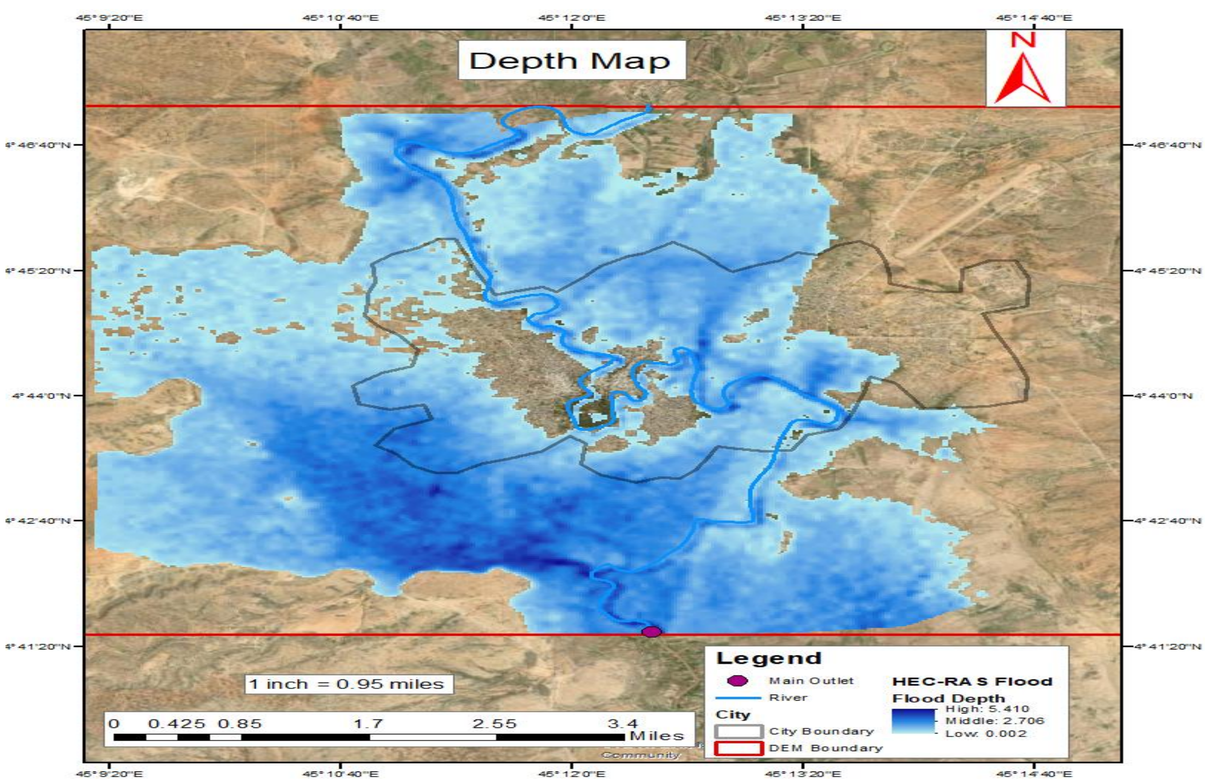

Figure 4.4: Depth of Flood

4.4.2 Percentage Time of Inundation

This Figure4.5 presents a Percent Inundation map, a key temporal output derived from the 2D HEC-RAS unsteady flow simulation. Unlike a static depth map that illustrates the maximum flood extent at a single moment, this map visualizes the duration of inundation over the entire simulated flood event. The color ramp, ranging from 0% (blue) to 100% (red), quantifies the percentage of the total simulation time that each specific grid cell was submerged. Areas shown in red, such as the main river channel, represent locations that were inundated for nearly 100% of the event, while the cooler-colored areas on the floodplain fringes represent transient flooding that occurred only during the peak of the hydrograph. This temporal analysis is critically important for assessing the persistence of flooding, a key variable in determining agricultural crop damage, infrastructure service disruption, and the viability of evacuation routes.

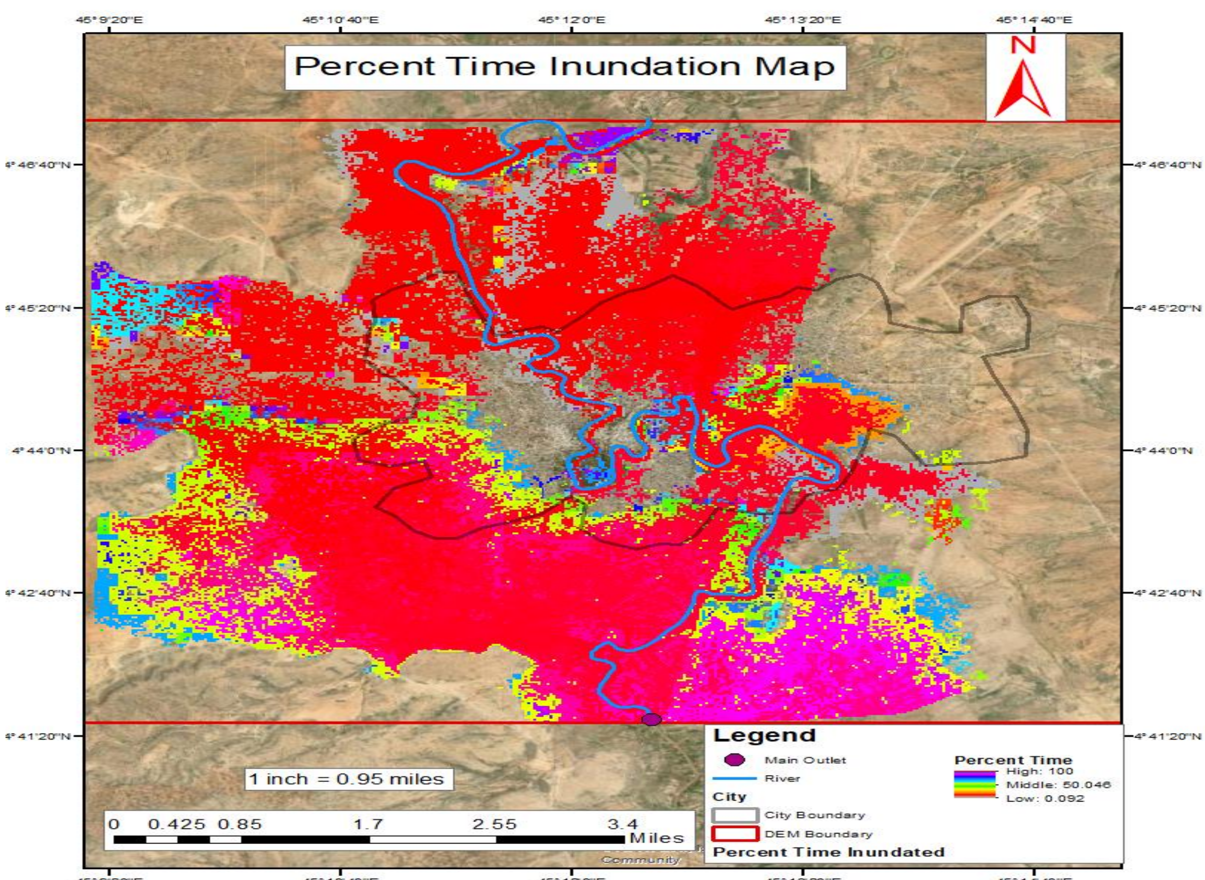

Figure 4.5: Visualization of the percent time inundation map

4.4.3 Velocity Map

Figure 4.6 displays the simulated water velocity map, a key hydrodynamic output from the 2D HEC-RAS model that measures floodwaters' speed in meters per second (m/s). This map clearly shows a distinct difference in flow behavior between the main channel and the overbank areas. Velocities peak at around 2.0 m/s (indicated in red) within the main river channel, where conveyance is greatest. In contrast, the nearby floodplains have much lower velocities (close to 0 m/s, shown in blue), indicating calmer, ponded water. This distribution of velocity is vital for a thorough risk assessment, as it directly affects the flood's erosive potential, the forces damaging buildings and infrastructure, and the identification of high-risk zones.

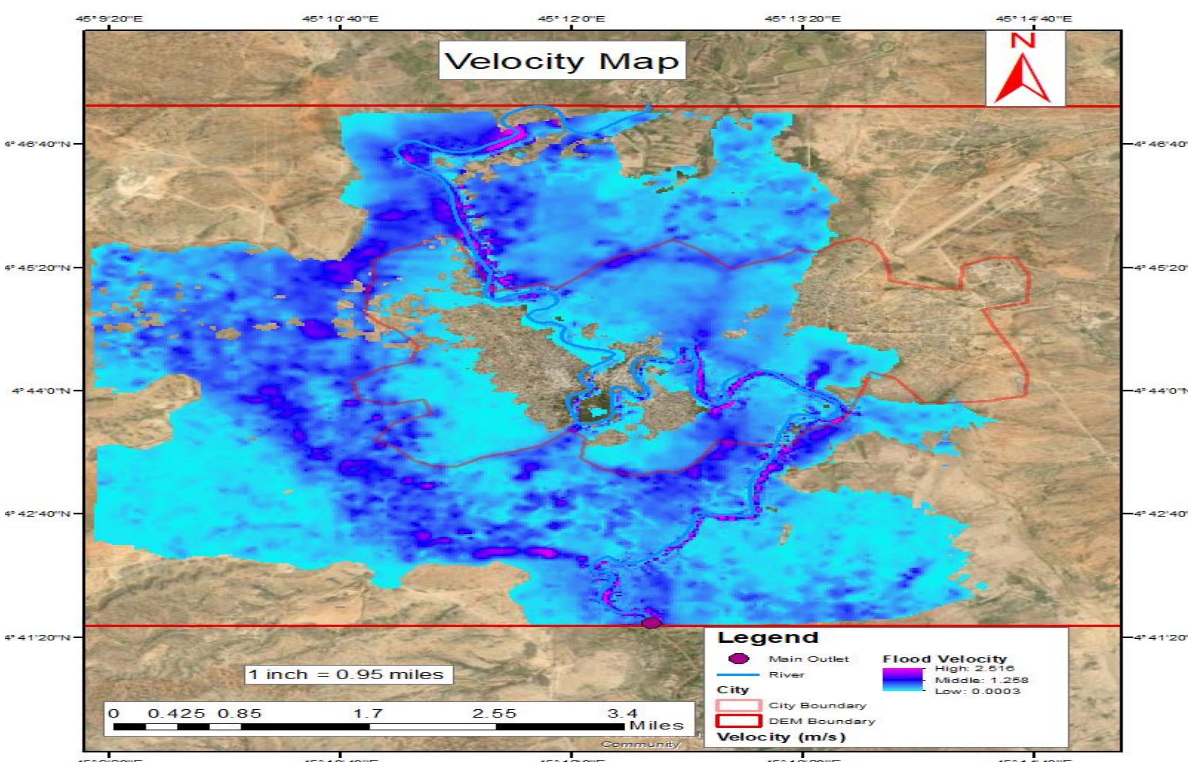

Figure 4.6: Velocity Map

4.4.4 Arrival Time map

The Figure 4.7 presents a critical temporal output from the hydraulic simulation: the Flood Arrival Time Map. This map illustrates the progressive propagation of the flood wave across the study area, quantifying the elapsed time in hours from the start of the event to the initial arrival of water at each location. The spatial pattern indicates that inundation begins within the main river channel (shown in blue, representing a Low of 0 hours) and subsequently spreads laterally across the floodplain. The arrival time's increase with distance and elevation from the river, moving through the middle ranges (yellow/orange, 508.5 hours) and reaching a maximum of 1017 hours (red/pink) at the most distal inundated areas. This temporal analysis is paramount for disaster preparedness, as it directly informs the available warning lead time for specific neighborhoods, guiding the prioritization of evacuation orders and the deployment of emergency response resources.

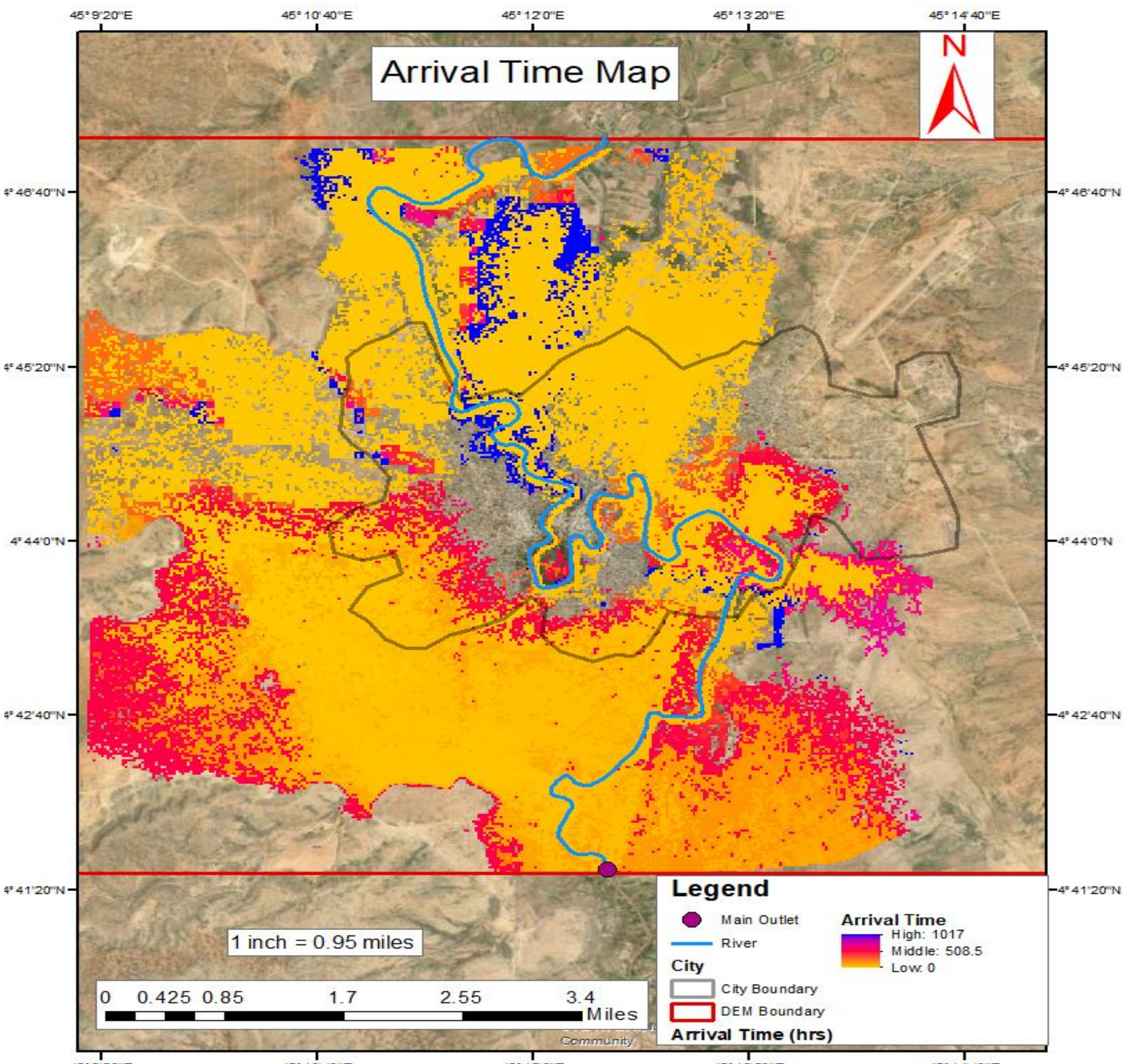

Figure 4.7: Visualization of water arrival time (hrs) at various locations

4.4.5 Visualization of Map results from HEC-RAS Model and GEE

This Figure 4.8 shows a critical comparative analysis by overlaying two distinct flood inundation datasets for the Beletweyne study area. The first dataset is the simulated flood extent generated by the HEC-RAS hydraulic model, representing the predicted inundation resulting from a specific design flood (e.g., a 100-year return period). This is contrasted with the second dataset, the observed flood extent, which has been delineated from satellite imagery (such as Sentinel-1 SAR) processed within the Google Earth Engine (GEE) platform, capturing the empirical footprint of an actual historical flood event. The primary objective of this composite map is to facilitate a direct spatial validation of the hydraulic model, allowing for a quantitative and qualitative assessment of its performance by comparing the predicted flood boundaries against the satellite-observed reality.

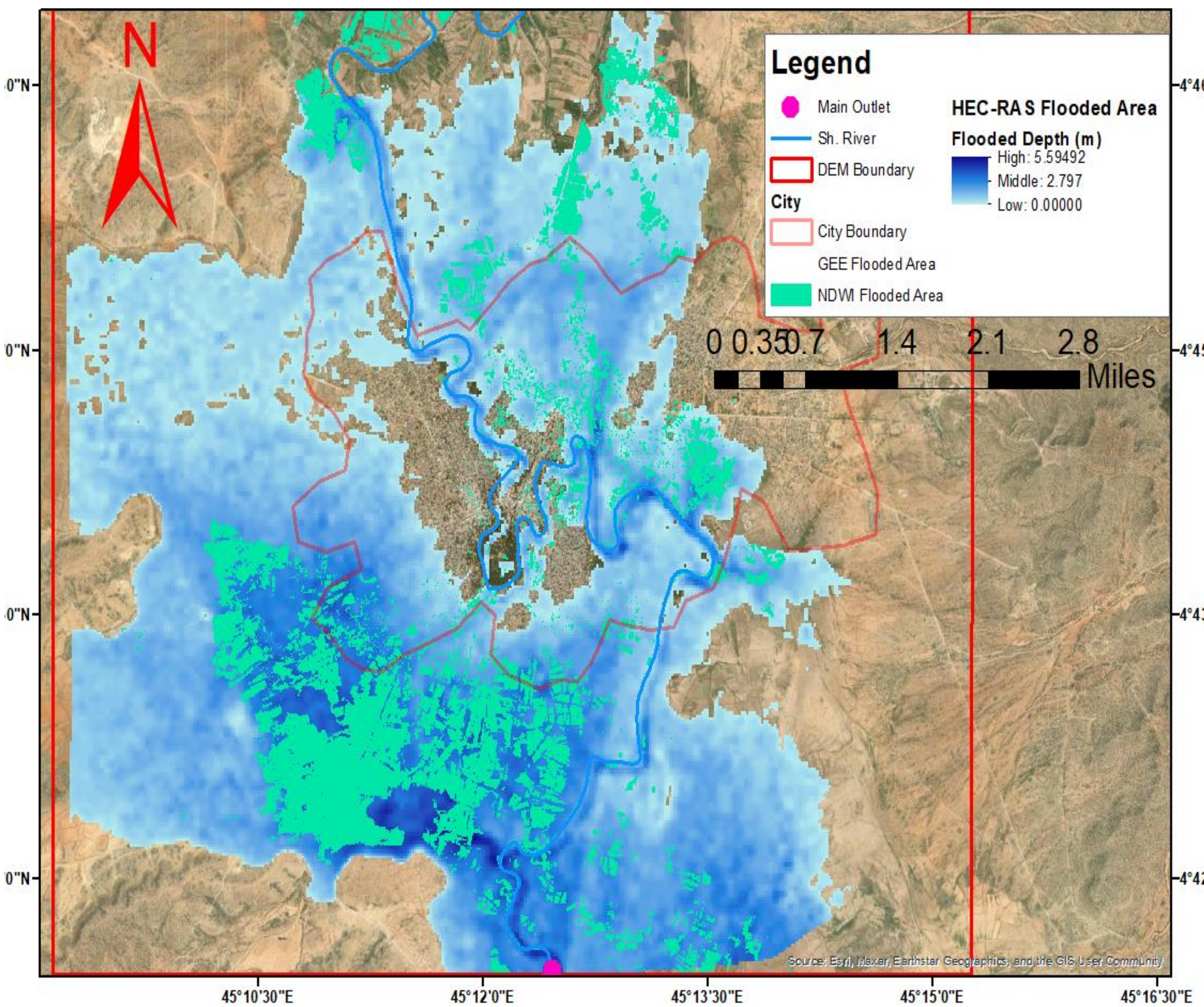

Figure 4.8: Overlapping Visualization of HEC-RAS inundation boundary map and sentinel-1band image

To validate the spatial accuracy of the hydraulic model, a quantitative overlay analysis was conducted comparing the HEC-RAS simulated flood extent against the observed flood extent derived using the Normalized Difference Water Index (NDWI) in Google Earth Engine. As detailed in Table 4.2, the analysis yielded a 54.106% spatial overlap between the two datasets.

The HEC-RAS model simulated a total inundation area of 9.88 km², which is comparable in magnitude to the 9.03 km² detected by the NDWI satellite analysis. The intersection (overlapping area) was calculated at 4.45 km². While the total areas are similar, the moderate overlap percentage suggests that while the model captures the core flood zones, there are differences in the exact spatial distribution. These discrepancies may be attributed to the limitations of optical remote sensing (NDWI) in detecting water under dense vegetation or cloud cover, compared to the hydraulic model, which simulates the maximum theoretical extent based on terrain.

Table 4.4: Quantitative Comparison of Inundation Areas (NDWI vs. HEC-RAS)

Parameter	Area / Value	Description
GEE - NDWI	9.03 km²	Flooded area extracted using NDWI
Simulated Area (HEC-RAS)	9.88 km²	Total maximum inundation area from the 2D model.
Area of Intersection	4.45 km²	A common area where both Model and Satellite detected flooding.
Overlap Percentage	54.106%	Calculated as: (Intersection/Observed Area)*100

4.5 Calibration

4.5.1 Manning's n-value adjustment

Manning's n-value adjustment is a critical process in hydrological modeling, particularly in flood modeling using HEC-RAS. Manning's n is a coefficient used in Manning's equation to estimate flow velocity in open channels, accounting for the roughness of the channel surface. This coefficient is influenced by factors such as vegetation, channel shape, and materials. The importance of accurately selecting and adjusting Manning's n values cannot be overstated, as it directly affects the simulation of flow behavior, including water surface elevations, flow velocities, and inundation extents, which are vital for flood hazard assessments.

The calibration yielded n-values of 0.045 for the main channel and 0.047 for the floodplain, indicating strong agreement with observed profiles (Hadi & Almansori, 2023). An n-value of 0.042 was determined, demonstrating good predictive accuracy (Soomro et al, 2021). A value of 0.035 was accepted based on relative percentage differences within acceptable limits (Jaafar et al, 2023). A lower n-value of 0.025 was found to provide acceptable agreement in another study (Abbas et al, 2020).

Careful adjustment enhances model accuracy, leading to more reliable flood behavior simulations and improved hazard management strategies.

4.5.2 Flood stage comparison

Flood stage comparison is a crucial technique in calibrating a 2D HEC-RAS model, as it directly assesses the model's ability to predict water levels during flood events accurately. This process involves using historical flood stage data gathered from gauge stations located along the river or floodplain of interest. By comparing the simulated water surface elevations generated by the model with the observed flood stages recorded during specific flood events, modelers can identify discrepancies and make necessary adjustments to improve accuracy. Calibration may include tweaking parameters such as Manning's n values, which represent the roughness of the channel, or adjusting the model's geometric representation of the floodplain.

This iterative process is essential because it ensures that the model reflects real-world conditions and behaviors during flooding.

4.5.3 Inundation extent assessment

Inundation extent assessment is a vital technique used in the calibration and validation of 2D HEC-RAS models, focusing on the accuracy of simulated flood extents compared to actual observed inundation areas during flood events. The calibrated model is used to generate inundation maps, which help in assessing the potential impact of floods on communities and infrastructure (Afzal et al, 2022; Tamiru & Wagari, 2022).

This process involved comparing the model's predicted flood boundaries, derived from simulations, against historical data obtained from satellite imagery, aerial photographs, or on-the-ground surveys taken during significant flooding events. By overlaying the simulated inundation maps with these observed data sources, modelers can visually and quantitatively evaluate how well the model replicates the actual areas that were inundated.

Figure 4.9: Aerial observation of the extensive flood inundation in Beletweyne, this observed reality serves as a qualitative benchmark for validating the spatial accuracy of the HEC-RAS simulated flood boundaries

Source: https://apnews.com/article/somalia-flooding-beledweyne-el-nino-2f624d796152c1f56206de688318d34f

4.5.4 Validation

Independent flood stage comparison

Independent flood stage comparison is a critical validation technique used to assess the accuracy and reliability of a 2D HEC-RAS model. This method involves comparing the simulated flood stages produced by the model with independent observed data from gauge stations that were not utilized during the calibration process. By using data from these independent sources, modelers can evaluate how well the model predicts water surface elevations during flood events, providing an unbiased assessment of its performance. Validation performed by comparing model outputs with observed flood extents. In the Mahanadi River study, the HEC-RAS model's flood extent was validated against satellite-derived data, achieving F1 and F2 values of 0.85 and 0.74, respectively (Surwase et al, 2019).

4.5.5 Observed hydrograph analysis

Observed hydrograph analysis is a fundamental validation technique used in the assessment of a 2D HEC-RAS model's performance. This method focuses on comparing the simulated hydrographs that depict the change in flow rate over time generated by the model against observed hydrographs collected from gauge stations during flood events. For instance, in the Wiroko Sub-Watershed, discrepancies in peak discharge (Qp) were only 0.8%, while the time to peak (Tp) differed by 1.93 hours (Ansori et al, 2024). By analyzing these hydrographs, I evaluated the model's ability to accurately reproduce the temporal dynamics of river flow, which is crucial for understanding flood behavior. Studies have shown that HEC-RAS 2D models can closely replicate observed hydrographs.

4.6 Analysis of 1D Model Calibration

Figure 4.10 provides a crucial graphical representation of the 1D model calibration process, visually plotting the time-series data from the October 2019 event. It directly contrasts the observed water levels, magenta line, which represent the empirical ground truth, against the simulated water surface elevations from the five HEC-RAS model Iterations shown in various other colors. The graph makes the model's performance immediately apparent: a significant and persistent discrepancy exists, with all five simulation iterations substantially underestimating the actual observed water levels throughout the entire period. This clear visual divergence highlights the model's initial struggle to replicate the event's magnitude, underscoring the necessity of the iterative calibration process to refine parameters and improve predictive accuracy.

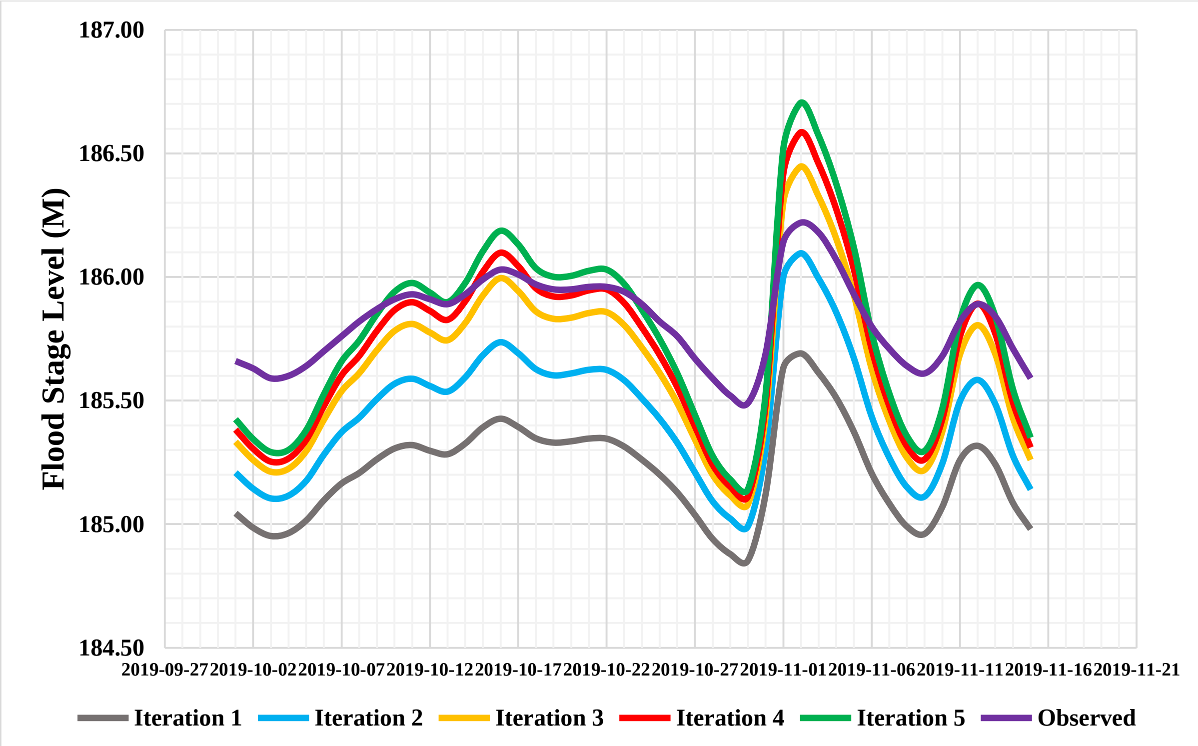

Figure 4.10: 1D Unsteady Flow Model Calibration Comparing Observed Water Levels to Simulated Iterations (October 2019 Event)

4.7 Analysis of 2D Model Calibration

Figure 4.11 details the 2D hydraulic model calibration, a crucial step in validating the model's performance against real-world conditions. The analysis is founded on the time-series data from the October 2019 event, which compares observed water surface elevations against the results of four distinct Iterations of the 2D HEC-RAS model. The accompanying graph provides a clear visual representation of this comparison, plotting the final calibrated model output against the observed data Magenta line. Unlike the initial 1D trials, this visualization demonstrates a strong congruence between the simulated and observed hydrographs, showing that the calibrated 2D model successfully replicates both the timing and the magnitude of the flood peak, thereby establishing a high confidence in its predictive capabilities.

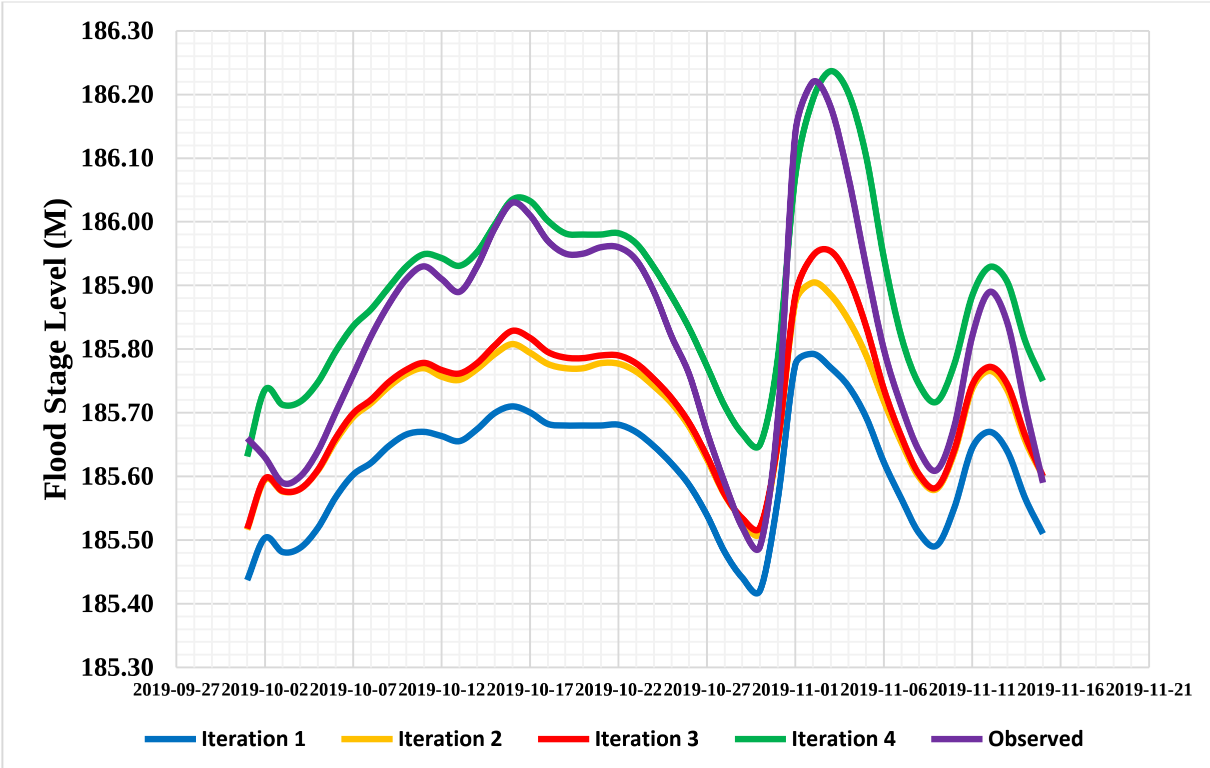

Figure 4.11: 2D Model Calibration Comparing Observed Water Levels to Simulated Iterations (October 2019 Event)

The graphs in figure 4.12 depict critical performance metrics for a study on 2D flood inundation modeling in Beletweyne, Somalia. The first graph compares the Root Mean Square Error (RMSE) and the Nash-Sutcliffe Efficiency (NSE) across multiple model calibration iterations. The notable decrease in RMSE and the corresponding increase in NSE indicate progressive model improvement and better predictive accuracy of water levels. The second graph presents a scatter plot of observed versus simulated water levels, showcasing a high correlation (R^2 = 0.9262) and a close fit to the perfect 1:1 line, demonstrating that the model reliably simulates measured water levels in the area. Together, these visualizations underscore the model's efficacy in depicting flood inundation dynamics in the region.

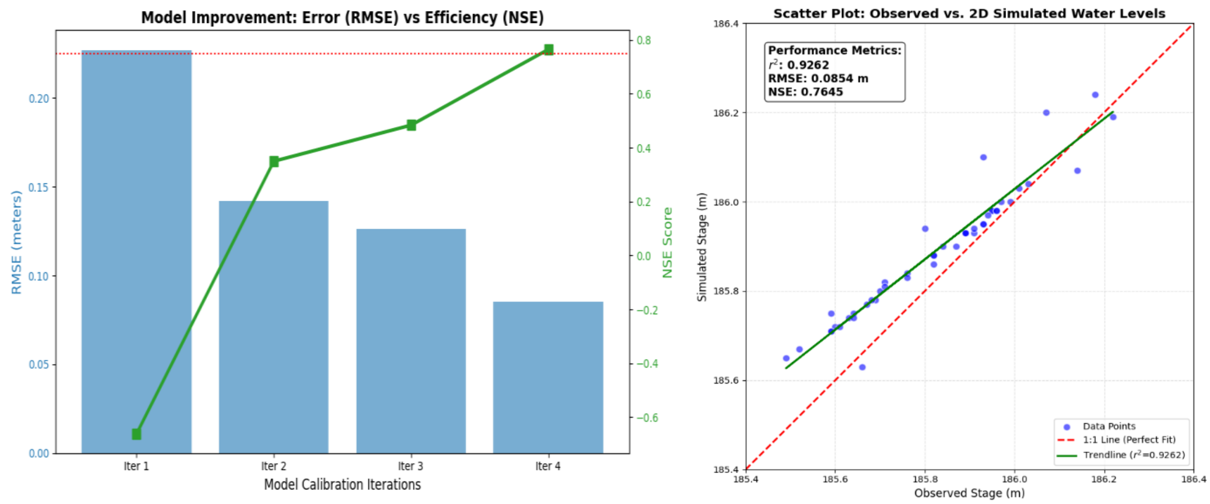

Figure 4.12: Graphs illustrating RMSE and NSE over calibration iterations, and the correlation between observed and simulated water levels in Beletweyne

4.8 1D Model Calibration and Parameter Optimization

Table 4.3 summarizes the calibration process for the 1D unsteady flow model, detailing the five iterations undertaken to find a suitable Manning's 'n' roughness coefficient. The 'n' value was systematically adjusted, starting from 0.015 in Iteration 1 and progressively increasing to 0.023 in Iteration 5. The corresponding Coefficient of Determination R^2 is listed for each attempt, quantifying the model's goodness-of-fit. The results clearly demonstrate a highly successful calibration progression: the R^2 value shows a consistent improvement from an initial 0.375 (Iteration 1) to a final, very strong fit of 0.923 (Iteration 5). This indicates that the final model configuration (Iteration 5, n is 0.023) is capable of accurately replicating the observed event.

Table 4.5: 1D Model Calibration Iterations, Manning's 'n' Adjustments, and Resulting R^2 Improvement

LULC	I1	R^2 Of I1	I2	R^2 Of I2	I3	R^2 Of I3	I4	R^2 Of I4	I5	R^2 Of I5
Water	0.05		0.06		0.065		0.07		0.075	
Forest	0.12		0.13		0.14		0.15		0.155	
Vegetation	0.075		0.08		0.085		0.09		0.095	
Cropland	0.04	**0.375**	0.055	**0.67**	0.06	**0.765**	0.065	**0.845**	0.07	**0.923**
Built Up	0.12		0.13		0.14		0.15		0.155	

Bare land	0.03		0.04		0.05		0.06		0.07	
Shrub land	0.05		0.06		0.065		0.07		0.075	

4.9 Calibration Iterations and 2D Model Performance

This table4.4 presents a comprehensive summary of the 2D model calibration methodology, documenting the systematic adjustment of the key hydraulic parameter, Manning's 'n' roughness coefficient, based on Land Use/Land Cover (LULC) classification. It details the specific 'n' values assigned to each LULC type (Water Body, Settlement, Bare Land, and Cropland) across four distinct iterations. The direct impact of this iterative refinement is quantified by the Coefficient of Determination R^2, which is listed at the bottom of each column. The table clearly illustrates a successful progression in model performance, starting from an initial, poor-fitting model (Iteration 1, R^2 is 0.345) and culminating in the final calibrated model, Iteration 4, which achieved a strong statistical agreement with the observed data (R^2 is 0.8903).

Table 4.6: Summary of 2D Model Calibration Iterations, Manning's 'n' Values by LULC, and Resulting R^2 Scores

LULC Type	Iteration 1	R^2 Of Iteration 1	Iteration 2	R^2 Of Iteration 2	Iteration 3	R^2 Of Iteration 3	Iteration 4	R^2 Of Iteration 4
Water	0.05		0.065		0.075		0.0875	
Forest	0.12		0.15		0.18		0.21	
Vegetation	0.075		0.093		0.112		0.131	
Cropland	0.04	**0.34**	0.05	**0.65**	0.06	**0.75**	0.07	**0.89**
Built-Up	0.12		0.15		0.18		0.21	
Bareland	0.03		0.0375		0.045		0.05	
Shurbland	0.05		0.0625		0.075		0.085	

Table 4.5 deeply interprets the calibration results, demonstrating a significant performance difference between the 1D and 2D hydraulic models. The 2D HEC-RAS model (Iteration 4) achieved a 'Very Good' performance rating with an NSE of 0.76 and an RMSE of 0.09 m, indicating it can replicate observed water levels with high precision (Table 4.6).In contrast, while the 1D model showed a strong correlation with the observed data trends (R^2 = 0.99), it

yielded a negative NSE value (-0.38). This discrepancy suggests that while the 1D model accurately captures the timing of the flood wave, it suffers from a systematic vertical offset, likely due to the inability of 1D cross-sections to represent the complex floodplain storage in the Beletweyne area fully. Consequently, the 2D model was selected for the final flood inundation mapping.

Table 4.7: Statistical performance metrics for 1D and 2D HEC-RAS models

Model Type	Best Iteration	R^2	NSE	RMSE (m)	PBIAS (%)	Performance Rating
1D Model	Iteration 5	0.9875	-0.375	0.206	0.024	Poor (Bias)
2D Model	Iteration 4	0.9258	0.763	0.086	-0.036	Very Good

4.10 Interpretation of Flood Scenarios (25, 50, 100-Year)

The simulation of the three return periods quantifies the escalating nature of flood risk in Beletweyne. The 25-year event is already sufficient to inundate low-lying residential sectors, but the jump to a maximum depth of 8.58 m in a 100-year event indicates a fundamentally destructive scenario that would breach all existing natural embankments. These results imply that the 100-year flood is a catastrophic threshold where current city infrastructure particularly in the Hawa-tako and Bundo-weyn sectors becomes entirely untenable.

4.11 Comparison of Simulated Results with Regional Studies

To assess the reliability of the hydraulic model developed in this research, the simulated maximum flood depth for the 100-year return period was rigorously compared against findings from established regional literature and historical field observations. This benchmarking process is essential to evaluate whether the 2D unsteady flow approach provides a more realistic representation of Beletweyne's complex floodplain compared to traditional methods. The table below summarizes the results of this study alongside the 1D HEC-RAS simulations reported by Ibrahim et al. (2024) and SWALIM (2009), as well as the observed water levels from the extreme 2020 flood event.

Table 5.8: Comparison of Simulated Flood Results with Regional Studies and Observations

Study / Source	Methodology	100-Year Max Depth	Key Difference / Observation
Current Study (2025)	HEC-RAS 1D (Steady)	8.58 m	Captures lateral flow and urban "pile-up" effects.
Ibrahim et al. (2024)	HEC-RAS 1D (Steady)	7.53 m	Underestimates depth by 1m due to 1D averaging.
SWALIM (2009)	HEC-RAS 1D (Steady)	7.82 m	Based on the theoretical rating curve (Q_{100}=701m^3/s).
FAO/SWALIM (2020)	Field Observation	8.25 m	Observed Bankfull Level during the extreme 2020 floods.

4.12 Justification of Methodological Assumptions

To ensure the reliability of the hydraulic simulation, several key assumptions were made and validated against the local context

4.12.1 Manning's Roughness Coefficients n

The assigned values were justified by cross-referencing standard literature with the specific landscape of Beletweyne. A value of 0.035 was assumed for the main channel to account for its winding nature and vegetation. In urban zones, a high n-value of 0.08 was assumed to simulate the high resistance and obstruction caused by dense housing and fences.

4.12.2 2D Diffusion Wave Equations

The choice of the 2D diffusion wave engine (zero-inertia model) is justified by its computational efficiency and stability in subcritical flow scenarios. This model omits local and convective acceleration to allow for faster, more stable simulations of complex urban inundation without sacrificing mass balance accuracy.

4.12.3 Boundary Conditions

The upstream flow hydrograph from the October 2019 event was assumed as the primary boundary condition because its bimodal behavior (two distinct peaks) provides a rigorous test for the model's temporal responsiveness.

4.13 Implications of Climate Change on Future Flood Frequency

The hydrological analysis presented in this study assumes a stationary climate regime based on historical discharge records (1980–2025). However, climate projections for the Greater Horn of Africa consistently indicate a shift towards intensified hydrological cycles. According to the IPCC Sixth Assessment Report (AR6), East Africa is projected to experience a significant increase in the frequency and intensity of extreme precipitation events, primarily driven by the strengthening of the Indian Ocean Dipole (IOD).

This warming trend has profound implications for the "100-year" flood scenario modeled in this thesis. The flood depth of 8.58 meters, currently defined as a 1% annual probability event, is likely to become more frequent. Research by Hirpa et al. (2019) suggests that under high-emission scenarios, today’s "100-year" floods in the Shebelle basin could shift to a 10-to-20-year recurrence interval by 2050.

Practically, this means the infrastructure designed today based on historical averages will be insufficient within two decades. The "safe" zones identified in the 25-year flood map (Figure 4.1) may effectively become high-risk zones. Consequently, future flood mitigation planning for Beletweyne must move beyond historical stationarity. Levees and floodwalls should be designed with an additional "climate freeboard" of at least 1.0 meter above the simulated 8.58m level to account for this non-linear increase in extreme flows. Furthermore, the definition of "flood-prone" areas for urban planning should be expanded to encompass the entire 100-year inundation boundary, rather than just the historically flooded zones.

4.14 Uncertainty Analysis and Model Limitations

While the calibrated HEC-RAS 2D model demonstrates a strong statistical fit ($R^2 = 0.89$), it is essential to acknowledge the inherent uncertainties associated with the input data and modeling assumptions. The primary source of uncertainty stems from the 30-meter resolution Digital Elevation Model (DEM). In dense urban environments like Beletweyne’s core, small-scale features such as boundary walls, narrow drainage channels, and raised road embankments are smaller than the 30m grid size. Consequently, the model may overestimate flood propagation speed in these specific zones as it treats the urban surface as a continuous roughness field rather than a series of physical obstructions. Additionally, the vertical accuracy of the open-source DEM (ALOS World 3D) typically ranges between ±5 meters. This implies that the simulated flood depths, particularly in shallow peripheral areas (0.5m – 1.0m depth), carry a margin of error. However, in the main floodplain where depths exceed 4 meters, this relative error decreases significantly. A secondary source of uncertainty is Manning's 'n' roughness coefficient. Although these values were calibrated iteratively, they remain static throughout the simulation. In reality, roughness changes dynamically as vegetation bends or is submerged. Sensitivity analysis (Section 3.5) indicated that a ±10% change in the main channel's Manning's n could alter water surface elevations by approximately ±0.45 meters. Therefore, the flood boundaries presented in this study should be interpreted as probabilistic risk zones rather than absolute deterministic lines.

4.15 Limitations of the Study

While this study successfully developed a flood inundation model for Beletweyne, several limitations should be acknowledged.

Topographic Resolution: The hydraulic modeling relied on a 30-meter resolution DEM. While sufficient for regional-scale mapping, this resolution may not capture fine-scale urban features (such as boundary walls or small drainage ditches) that influence local flow paths. Consequently, flood extents in densely urbanized zones should be viewed as the maximum potential inundation zones.

Data Scarcity: The study relied on a single gauging station at Beletweyne without upstream routing data, limiting the ability to validate the flood wave propagation speed over long distances.

Bathymetry Assumptions: The river channel geometry was approximated using width-depth relationships due to the unavailability of a comprehensive hydrographic survey. Future studies could improve accuracy by integrating high-resolution LiDAR data to resolve these micro-topographic features.

CONCLUSION AND RECOMMENDATIONS

5.1 CONCLUSION

This research demonstrates that the Shebelle River catchment is highly responsive to intense rainfall, meaning that flash flooding is a permanent and escalating threat to Beletweyne City. The study confirms that traditional 1D modeling is insufficient for this area; instead, the integration of 1D/2D HEC-RAS with Google Earth Engine provides the high-resolution spatial detail necessary to capture how floodwaters "pile up" against urban infrastructure like buildings and bridges. The validation of these models against satellite-observed extents confirms that they are a reliable foundation for real-world disaster management. The primary implication of this study is that local authorities now have a scientifically validated framework to move away from reactive emergency response toward proactive, risk-based urban planning. By utilizing the developed maps for flood velocity and arrival time, the city can prioritize the most vulnerable neighborhoods for early warning alerts and structural reinforcements. Ultimately, these tools are essential for safeguarding lives and ensuring that future infrastructure in the Shebelle River basin is resilient to increasingly frequent extreme flood events.

5.2 RECOMMENDATIONS

Based on the conclusions of this study, the following recommendations are proposed:

5.2.1 for Policymakers

Adopt Risk-Based Zoning: Immediately prohibit new permanent settlements within the 25-year floodplain (where depths reach 3.80 m).

Critical Infrastructure Protection: Relocate or heavily reinforce critical facilities (hospitals, power stations) located within the 100-year floodplain limit.

5.2.2 for Disaster Management Agencies

Evacuation Planning: Utilize the Flood Arrival Time Map to design evacuation protocols. Neighborhoods identified with "0-2 hour" arrival times must be prioritized for immediate early warning alerts.

Climate Adaptation: Acknowledge that the "100-year" event modeled here may become more frequent due to climate change. Flood defenses should be designed with a safety margin (freeboard) of at least 1.0 meter above the simulated 8.58 m level to account for future uncertainty.

5.2.3 for Engineers and Infrastructure Managers

Implement Targeted Structural Defenses: The Velocity Map should be used to identify high-risk zones (e.g., where high-velocity flow threatens the built-up area). These areas should be prioritized for structural interventions such as levees, floodwalls, or riverbank stabilization.

Retrofit Critical Infrastructure: All existing critical infrastructure (bridges, water treatment plants, power stations) located within the 100-year floodplain should be assessed and retrofitted to withstand the projected flood depths and velocities.

5.2.4 for Future Research

Acquire High-Resolution Topography: The 30m DEM used in this study was effective for a regional assessment. Future studies should be conducted using a high-resolution DEM (e.g., <5m resolution from drone-based LiDAR or photogrammetry) to improve model accuracy at the building and street level.

Incorporate Climate Change Scenarios: This study used historical flow data. It is recommended to re-run the hydraulic models using discharge data projected from future climate change scenarios to understand how flood risk may worsen in the coming decades.

Conduct a Full Socio-Economic Risk Assessment: This study focused on the physical hazard. The next logical step is to combine these hazard maps with socio-economic data (e.g., population density, building types, poverty levels) to conduct a full risk assessment, quantifying the potential economic damages and humanitarian impact for each scenario.

REFERENCE

. G. (2023). Conceptualization of Flooding Disaster: A Theoretical Perspective of Management. *Disaster Advances, 17*(2), 40–45. https://doi.org/10.25303/172da040045

Abbas, S. A., Al-Aboodi, A. H., & Ibrahim, H. T. (2020). Identification of Manning's Coefficient Using HEC-RAS Model: Upstream Al-Amarah Barrage. *Journal of Engineering*, *2020*, 1–7. https://doi.org/10.1155/2020/6450825

Abdullahi Mohamed Sheikh Ali & Mohamed Omar Mohamed. (2023). Climate change-induced floods and storms: Impacts of changing rainfall patterns in Somalia. *World Journal of Advanced Research and Reviews*, *20*(1), 1229–1233. https://doi.org/10.30574/wjarr.2023.20.1.1998

Abu-Saymeh, R. K., Godrej, A., & Alexander, K. A. (2023). Modeling Large River Basins and Flood Plains with Scarce Data: Development of the Large Basin Data Portal. *Hydrology*, *10*(4), 87. https://doi.org/10.3390/hydrology10040087

Afzal, M. A., Ali, S., Nazeer, A., Khan, M. I., Waqas, M. M., Aslam, R. A., Cheema, M. J. M., Nadeem, M., Saddique, N., Muzammil, M., & Shah, A. N. (2022). Flood Inundation Modeling by Integrating HEC–RAS and Satellite Imagery: A Case Study of the Indus River Basin. *Water*, *14*(19), 2984. https://doi.org/10.3390/w14192984

Akbar Mursaliin, M., Yanuarsyah, I., & Fatimah, F. (2025). Spatial Modeling of Flood Vulnerability Using Google Earth Engine (Case Study: Pasar Minggu, Pancoran and Tebet Districts). *E-Jurnal Penyelidikan Dan Inovasi*, *12*(2), 59–77. https://doi.org/10.53840/ejpi.v12i2.280

Alexandre, D. A., Chaudhuri, C., & Gill-Fortin, J. (2024). *Continental regional flood frequency analysis: Combining enhanced datasets and a Bayesian framework*. https://doi.org/10.20944/preprints202407.0789.v1

Alfieri, L., Libertino, A., Campo, L., Dottori, F., Gabellani, S., Ghizzoni, T., Masoero, A., Rossi, L., Rudari, R., Testa, N., Trasforini, E., Amdihun, A., Ouma, J., Rossi, L., Tramblay, Y., Wu, H., & Massabò, M. (2024). Impact-based flood forecasting in the Greater Horn of Africa.

Natural Hazards and Earth System Sciences, *24*(1), 199–224. https://doi.org/10.5194/nhess-24-199-2024

Ali, M. M. (2023). CAUSES AND IMPACTS OF FLASH FLOODS ON LIVES AND LIVELIHOODS IN HIRSHABELLE STATE OF SOMALIA. *Ecofeminism and Climate Change*, *4*(1), 51–55. https://doi.org/10.26480/efcc.01.2023.51.55

Lorenzo. (n.d.). *Comment on egusphere-2023-804* [Peer review]. https://doi.org/10.5194/egusphere-2023-804-RC2

Lorenzo, & Alfieri, L. (n.d.-a). *Reply on RC1* [Peer review]. https://doi.org/10.5194/egusphere-2023-804-AC1

Lorenzo, & Alfieri, L. (n.d.-b). *Reply on RC2* [Peer review]. https://doi.org/10.5194/egusphere-2023-804-AC2

Ansarifard, S., Eyvazi, M., Kalantari, M., Mohseni, B., Ghorbanifard, M., Moghaddam, H. J., & Nouri, M. (2024). *Simulation of floods under the influence of effective factors in hydraulic and hydrological models using HEC-RAS and MIKE 21*. https://doi.org/10.21203/rs.3.rs-4863234/v1

Ansori, M. B., Lasminto, U., & Gde Kartika, A. A. (2023). Reliability of Runoff Hydrograph Model for Extreme Rainfall Events using HEC-RAS 2D Flow Hydrodynamics Rain-On-Grid. *IOP Conference Series: Earth and Environmental Science*, *1276*(1), 012034. https://doi.org/10.1088/1755-1315/1276/1/012034

Ansori, M. B., Lasminto, U., & Kartika, A. A. G. (2024). Runoff Hydrograph Analysis of HEC-RAS 2D Flow Hydrodynamics Meteorological Rain-on-Grid on Observed Watershed: A Case Study of Wiroko Sub-Watershed. *International Journal on Advanced Science, Engineering and Information Technology*, *14*(2), 575–581. https://doi.org/10.18517/ijaseit.14.2.19813

Aristizabal, F., Chegini, T., Petrochenkov, G., Salas, F., & Judge, J. (2024). Effects of high-quality elevation data and explanatory variables on the accuracy of flood inundation mapping via Height Above Nearest Drainage. *Hydrology and Earth System Sciences*, *28*(6), 1287–1315. https://doi.org/10.5194/hess-28-1287-2024

Assaidi, H., Khomarudin, M. R., Badron, K., Ismail, A. F., & Ramza, H. (2024). Geospatial Data Integration for the Flood Vulnerable Area Classification in Jratunseluna Watershed. *Journal of Computer Networks, Architecture and High Performance Computing*, *6*(3), 1159–1169. https://doi.org/10.47709/cnahpc.v6i3.4233

Bellos, V., Tsakiris, V. K., Kopsiaftis, G., & Tsakiris, G. (2020). Propagating Dam Breach Parametric Uncertainty in a River Reach Using the HEC-RAS Software. *Hydrology*, *7*(4), 72. https://doi.org/10.3390/hydrology7040072

Bernardini, G., Ferreira, T. M., Baquedano Julià, P., Ramírez Eudave, R., & Quagliarini, E. (2024). Assessing the spatiotemporal impact of users' exposure and vulnerability to flood risk in urban built environments. *Sustainable Cities and Society*, *100*, 105043. https://doi.org/10.1016/j.scs.2023.105043

Bigandata, Y., Wahyuni, P., & Maharani, Y. N. (2023). KERENTANAN SOSIAL DAN EKONOMI PADA BENCANA BANJIR DI KELURAHAN SUTOJAYAN KABUPATEN BLITAR. *Indonesian Journal of Environment and Disaster*, *2*(1), 57–67. https://doi.org/10.20961/ijed.v2i1.688

Blandford, G. E., & Ormsbee, L. E. (1993). A diffusion wave finite element model for channel networks. *Journal of Hydrology*, *142*(1–4), 99–120. https://doi.org/10.1016/0022-1694(93)90007-V

Bosowa University, Harifuddin, H., Azuz, F., Bosowa University, Apriningsih, A., Pembangunan Nasional Veteran University, Hayati, A. N., State Islamic University ofSultan Aji Muhammad Idris, Yuldashev, A. A., Chirchik State Pedagogical University, Kuraesin, A. D., & Technology Muhammadiyah University. (2024). Flood Risk Reduction: A Government and Community Collaboration Perspective in Urban Communities. *Journal of Techno-Social*, *16*(1). https://doi.org/10.30880/jts.2024.16.01.005

Calvo-Solano, O., & Quesada-Román, A. (2024). Worldwide Research Trends and Networks on Flood Early Warning Systems. *GeoHazards*, *5*(3), 582–595. https://doi.org/10.3390/geohazards5030030

Candra Partarini, N. M., & Wirastri, M. V. (2024). Community-Based Flood Resilience: Upaya Mitigasi Banjir Kawasan Semi-Perkotaan Berbasis Nature Based Solution. *Jurnal Atma Inovasia*, *4*(2), 52–59. https://doi.org/10.24002/jai.v4i2.8692

Cataño-Lopera, Y. A. (Ed.). (2023). *Computational Fluid Dynamics Modeling in Water Infrastructure: Best Practices*. American Society of Civil Engineers. https://doi.org/10.1061/9780784485125

Cohen, S., Tian, D., Baruah, A., Liu, H., & Nikrou, P. (2024, November 27). *Use of Remote Sensing Flood Inundation Maps (FIM) for Evaluating Model-predicted FIM: Challenges and Strategies*. https://doi.org/10.5194/egusphere-egu24-2941

Composto, R., Tulbure, M. G., Tiwari, V., Gaines, M. D., & Caineta, J. (2024). *Quantifying Urban Flood Extent Using Satellite Imagery and Random Forest: A Case Study in Southeastern Pennsylvania*. https://doi.org/10.21203/rs.3.rs-3882712/v1

Conesa-Garcia, C., Caselles-Miralles, V., Sanchez Tomas, J. M., & Garcia-Lorenzo, R. (2010). Hydraulic Geometry, GIS and Remote Sensing, Techniques against Rainfall-Runoff Models for Estimating Flood Magnitude in Ephemeral Fluvial Systems. *Remote Sensing*, *2*(11), 2607–2628. https://doi.org/10.3390/rs2112607

Crenganiș, L. M., Pricop, C. I., & Diac, M. (2024). *Integrating ArcGIS and HEC-RAS for Flood Hazard Management: A Case Study of Ungheni, Iasi County, Romania*. https://doi.org/10.20944/preprints202404.1783.v1

Criss, R. E., & Nelson, D. L. (2021). *Stage-Based Flood Inundation Mapping*. https://doi.org/10.21203/rs.3.rs-841313/v1

Dey, S. (2025, March 15). *zeroInertiaFlowFOAM – a OpenFOAM®-based computationally efficient, mass-conservative, implicit zero-inertia flow model for flood inundation problems on collocated grid-systems. * https://doi.org/10.5194/egusphere-egu25-17402

Djafri, S. A., Cherhabil, S., Hafnaoui, M. A., & Madi, M. (2024). Flood modeling using HEC-RAS 2D and IBER 2D: A comparative study. *Water Supply*, *24*(9), 3061–3076. https://doi.org/10.2166/ws.2024.184

Duku, C. (2025). *Enhancing flood forecasting reliability in data-scarce regions with a distributed hydrology-guided neural network framework*. https://doi.org/10.5194/egusphere-2025-2294

Duvvuri, B., Gehring, J., & Beighley, E. (2024). Methodological evaluation of river discharges derived from remote sensing and land surface models. *Scientific Reports*, *14*(1), 25653. https://doi.org/10.1038/s41598-024-75361-w

Dyca, B., Hartmann, T., & Tempels, B. (2024). Land use planning and management for flood risk management. In J. Lamond, D. Proverbs, & N. Bhattacharya Mis (Eds.), *Research Handbook on Flood Risk Management* (pp. 71–85). Edward Elgar Publishing. https://doi.org/10.4337/9781839102981.00013

Ekeu-Wei, I. (2018). *Application of open-access and 3rd party geospatial technology for integrated flood risk management in data sparse regions of developing countries* [Application/pdf]. 10189885 B, 328 pages. https://doi.org/10.17635/LANCASTER/THESIS/217

Gambella University, Minywach, L. T., Lohani, T. K., Arba Minch University, Ayalew, A. T., & Arba Minch University. (2024). Inundation Mapping and Flood Frequency Analysis using HEC-RAS Hydraulic Model and EasyFit Software. *Journal of Water Management Modeling*. https://doi.org/10.14796/JWMM.C513

GeoInformatic Unit, Geography Section, School of Humanities, Universiti Sains Malaysia, Tew, Y. L., Tan, M. L., GeoInformatic Unit, Geography Section, School of Humanities, Universiti Sains Malaysia, Juneng, L., Department of Earth Sciences and Environment, Faculty of Science and Technology, Universiti Kebangsaan Malaysia, Osman, S., National Flood Forecasting and Warning Centre, Department of Irrigation and Drainage, Hassan, M. H., National Flood Forecasting and Warning Centre, Department of Irrigation and Drainage, Samat, N., GeoInformatic Unit, Geography Section, School of Humanities, Universiti Sains Malaysia, Chang, C. K., River Engineering and Urban Drainage Research Centre (REDAC), Universiti Sains Malaysia, Li, L., & School of Geography, Nanjing Normal University. (2024). Flood inundation mapping in the Kelantan River Basin, Malaysia, using Sentinel-1 SAR and

Google Earth Engine. *Malaysian Journal of Society and Space*, *20*(4). https://doi.org/10.17576/geo-2024-2004-02

Giang Hoang Hiep, Nguyen Thanh Bang, & Tran Dang Hung. (2023). APPLICATION OF GOOGLE EARTH ENGINE PLATFORM TO IDENTIFY FLOODED AREAS AND ASSESS FLOOD DEPTH IN QUANG TRI PROVINCE. *Tạp Chí Khoa Học Biến Đổi Khí Hậu*, *27*, 56–64. https://doi.org/10.55659/2525-2496/27.85964

Giannone, F., Guerrisi, E., Scaglione, M., & Di Francesco, S. (2024, March 11). *SAR and Optical Remote Sensing for Flood Mapping and Monitoring through GEE*. https://doi.org/10.5194/egusphere-egu24-19476

Hadi, Z. N., & Almansori, N. J. H. (2023). Estimation of Manning coefficient for the section between Al-Hindiya barrage and Al-Kufa barrage utilizing HEC-RAS. *Materials Today: Proceedings*, *80*, 2595–2601. https://doi.org/10.1016/j.matpr.2021.06.417

Halder, S., & Bose, S. (2024). Sustainable flood hazard mapping with GLOF: A Google Earth Engine approach. *Natural Hazards Research*, *4*(4), 573–578. https://doi.org/10.1016/j.nhres.2024.01.002

Hardiyanto, M. A., Amin, M., Triyono, S., & Ridwan, R. (2024). Kajian Hidrologi dan Analisis Kapasitas Pengaliran Penampang Sungai Way Kuripan terhadap Bencana Banjir Wilayah Bandar Lampung Berbasis Hec Ras. *Jurnal Agricultural Biosystem Engineering*, *3*(2), 256. https://doi.org/10.23960/jabe.v3i2.9539

Hashimoto, H., & Park, K. (2008). Two-dimensional urban flood simulation: Fukuoka flood disaster in 1999. *Flood Recovery, Innovation and Response I*, *I*, 59–67. https://doi.org/10.2495/FRIAR080061

Hotaki, M. S. F., Motagh, M., & Haghshenas Haghighi, M. (2024, November 27). *Flood inundation Mapping for the Sept. 2023 Derna, Libya flood event using Sentinel-1 SAR data: An Integration of SAR intensity and interferometric coherence*. https://doi.org/10.5194/egusphere-egu24-11215

Hu, H. H., & Walton, R. (2008). Advanced Guidance on Use of Steady HEC-RAS. *World Environmental and Water Resources Congress 2008*, 1–10. https://doi.org/10.1061/40976(316)201

Huaricallo Vilca, Y., Sanchez Benites, F., Del Carpio, F., Espinoza Eche, J., Bedia Guillen, C., & Ariza Flores, V. (2025). *Hydraulic Modeling for Flood Defense Design in River Basins: A Systematic Review Focused on Hydrological Extremes*. https://doi.org/10.20944/preprints202507.0395.v1

Husain, A. (2017). Flood Modelling by using HEC-RAS. *International Journal of Engineering Trends and Technology*, *50*(1), 1–7. https://doi.org/10.14445/22315381/IJETT-V50P201

Ibrahim, O. A., Goshime, D. W., Tekleab, S., & Absi, R. (2024). Flood Inundation mapping and mitigation options in data-scarce region of Beledwayne town in the Wabi Shebele River Basin of Somalia. *Natural Hazards Research*, *4*(2), 336–346. https://doi.org/10.1016/j.nhres.2023.11.001

Ibrahim, T., & Mishra, A. (2021). A Conceptual Design of Smart Management System for Flooding Disaster. *International Journal of Environmental Research and Public Health*, *18*(16), 8632. https://doi.org/10.3390/ijerph18168632

Iglesias-Pascual, R., Benassi, F., & Hurtado-Rodríguez, C. (2023). Social infrastructures and socio-economic vulnerability: A socio-territorial integration study in Spanish urban contexts. *Cities*, *132*, 104109. https://doi.org/10.1016/j.cities.2022.104109

Internal Displacement Monitoring Center (IDMC). (2021). *Impacts of Displacement: Flood displacement in Beledweyne, Somalia*. Internal Displacement Monitoring Center (IDMC). https://doi.org/10.55363/IDMC.VCAI4770

Islam, M. T., & Meng, Q. (2024). Spatial analysis of socio-economic and demographic factors influencing urban flood vulnerability. *Journal of Urban Management*, *13*(3), 437–455. https://doi.org/10.1016/j.jum.2024.06.001

Jaafar, J., Ali Musa, A. F., Othman, Z., Wan Yahaya, W. A., Koon, L. W., Baki, A., Wan Mohd Isa, W. A. R., & Abdullah, S. (2023). Application of HEC-RAS Model for Flood Inundation Mapping in Sungai Golok, Rantau Panjang. *International Journal of Academic Research in*

Progressive Education and Development, *12*(1), Pages 690-701. https://doi.org/10.6007/IJARPED/v12-i1/15297

Jansky, O. J. (2023). Improving Adaptive Capacity of Riverine Communities in Responding to Floods in Beledweyne District, Somalia. *Multidisciplinary Journal of Horseed International University (MJHIU)*, *1*(2), 35–54. https://doi.org/10.59336/9kdzm360

Jeong, C., Chegal, S. D., Kim, D. H., & Lee, S. O. (2024). Comparison of FLUMEN and HEC-RAS 2D Models for Flash-Flood Inundation Considering Land Cover and Building Presence. *Journal of the Korean Society of Hazard Mitigation*, *24*(4), 239–247. https://doi.org/10.9798/KOSHAM.2024.24.4.239

Jimale, A. D., Abdullahi, M. O., Ahmed, Y. A., Nageeye, A. Y., Abdullahi, B. S., & Jama, A. A. (2023). Mitigating the Impact of Floods: An IoT-Driven Monitoring and Alert System for Somalia's Rivers. *International Journal of Electrical and Electronics Engineering*, *10*(6), 120–125. https://doi.org/10.14445/23488379/IJEEE-V10I6P113

Kalita, N. (2024). Flood Inundation Mapping In Belsiri River Basin Linking HEC-RAS and HEC-GeoRAS Model and Flood Frequency Analysis. *International Journal of Lakes and Rivers*, *17*(1), 47–55. https://doi.org/10.37622/IJLR/17.1.2024.47-55

Karim, F., Armin, M. A., Ahmedt-Aristizabal, D., Tychsen-Smith, L., & Petersson, L. (2023). A Review of Hydrodynamic and Machine Learning Approaches for Flood Inundation Modeling. *Water*, *15*(3), 566. https://doi.org/10.3390/w15030566

Khan, I. R., Elmahdy, S. I., Rustum, R., Khan, Q., & Mohamed, M. M. (2024). Floods modeling and analysis for Dubai using HEC-HMS model and remote sensing using GIS. *Scientific Reports*, *14*(1), 25039. https://doi.org/10.1038/s41598-024-74736-3

Krishna Pasupuleti, M. (2024). Cutting-Edge Techniques in Hydrology: Modeling Water Systems and Mitigating Flood Risks. In *Advanced Hydrology Modeling: Tools for Simulating Water Systems and Flood Risks* (First Edition, pp. 24–41). National Education Services. https://doi.org/10.62311/nesx/932199

Kumar, R., & Jha, R. (2022). River Cross Section Extraction from Elevation Models for Lower Ganga Basin. In R. Jha, V. P. Singh, V. Singh, L. B. Roy, & R. Thendiyath (Eds.), *River and*

Coastal Engineering (Vol. 117, pp. 345–357). Springer International Publishing. https://doi.org/10.1007/978-3-031-05057-2_30

Kumar, V., Sharma, K., Caloiero, T., Mehta, D., & Singh, K. (2023). Comprehensive Overview of Flood Modeling Approaches: A Review of Recent Advances. *Hydrology*, *10*(7), 141. https://doi.org/10.3390/hydrology10070141

Lacava, T., Albano, R., Lahsaini, M., & Mazzariello, A. (2024, July 11). *On a multitemporal analysis of Copernicus Sentinel data for a robust and near-real time mapping of floods*. https://doi.org/10.5194/egusphere-plinius18-75

Lamichhane, S., Karki, N., Pandey, V. P., Joshi, P., & Dawadi, S. (2024). A synergic approach using the model and remote sensing data for flood monitoring in under-observed transboundary rivers. *Journal of Hydroinformatics*, *26*(10), 2489–2505. https://doi.org/10.2166/hydro.2024.056

Li, J., Lei, K., Zhang, T., Zhong, W., Kang, A., Ma, Q., & Feng, P. (2020). A framework for event-based flood scaling analysis by hydrological modeling in data-scarce regions. *Hydrology Research*, *51*(5), 1091–1103. https://doi.org/10.2166/nh.2020.042

Li, Z., & Demir, I. (2024). MultiRS flood mapper: A google earth engine application for water extent mapping with multimodal remote sensing and quantile-based postprocessing. *Environmental Modelling & Software*, *176*, 106022. https://doi.org/10.1016/j.envsoft.2024.106022

Li, Z., Demiray, B. Z., Muste, M., & Demir, I. (2024). *An Integrated Framework for Actionable Flood Warnings on Road Structures Using High Resolution Satellite Imagery*. https://doi.org/10.31223/X5TT4N

Liu, K., Wang, S., Chen, B., & Wang, H. (2024). Quantifying the direct and indirect impacts of urban waterlogging using input–output analysis. *Journal of Environmental Management*, *352*, 120068. https://doi.org/10.1016/j.jenvman.2024.120068

Liu, X., Sahli, H., Meng, Y., Huang, Q., & Lin, L. (2017). Flood Inundation Mapping from Optical Satellite Images Using Spatiotemporal Context Learning and Modest AdaBoost. *Remote Sensing*, *9*(6), 617. https://doi.org/10.3390/rs9060617

Lombardo, M., Totaro, V., Chiaravalloti, F., & Petrucci, O. (2024, August 16). *A systematic approach for flood-impact data retrieval in urban floods modelling*. https://doi.org/10.5194/ems2024-571

Makhfud, & Mursyidah, L. (2024). Community Participation in Flood Disaster Management. *Indonesian Journal of Law and Economics Review*, *19*(4). https://doi.org/10.21070/ijler.v19i4.1176

Mandelli, D., Gonzales, R., Wang, C., Abdo, M., Welker, Z., Balestra, P., Qin, S., & Petrov, V. (2023). A Causal Approach to Model Validation and Calibration. *Volume 7: Energy*, V007T08A082. https://doi.org/10.1115/IMECE2023-112430

Mangkhaseum, S., Bhattarai, Y., Duwal, S., & Hanazawa, A. (2024). Flood Susceptibility Mapping Using Publicly Available Big Data with Google Earth Engine and Deep Learning Algorithms. *2024 5th International Conference on Big Data Analytics and Practices (IBDAP)*, 38–43. https://doi.org/10.1109/IBDAP62940.2024.10689702

Mason, D. C., Bevington, J., Dance, S. L., Revilla-Romero, B., Smith, R., Vetra-Carvalho, S., & Cloke, H. L. (2021). Improving Urban Flood Mapping by Merging Synthetic Aperture Radar-Derived Flood Footprints with Flood Hazard Maps. *Water*, *13*(11), 1577. https://doi.org/10.3390/w13111577

Merga, B. B., Mamo, F. L., Moisa, M. B., Tiye, F. S., & Gemeda, D. O. (2023). Assessment of flood risk by using geospatial techniques in Wabi Shebele River Sub-basin, West Hararghe Zone, southeastern Ethiopia. *Applied Water Science*, *13*(11), 214. https://doi.org/10.1007/s13201-023-02019-9

Muraleedharan, S., Kezhkepurath Gangadhara, K., & Raja, B. (2024, November 27). *Comparison of precipitation datasets for representing flood characteristics in Malaysia * https://doi.org/10.5194/egusphere-egu24-9361

Murillo, J., & García-Navarro, P. (2012). Wave Riemann description of friction terms in unsteady shallow flows: Application to water and mud/debris floods. *Journal of Computational Physics*, *231*(4), 1963–2001. https://doi.org/10.1016/j.jcp.2011.11.014

Nabinejad, S., & Schüttrumpf, H. (2023). Flood Risk Management in Arid and Semi-Arid Areas: A Comprehensive Review of Challenges, Needs, and Opportunities. *Water*, *15*(17), 3113. https://doi.org/10.3390/w15173113

Namara, W. G., Damisse, T. A., & Tufa, F. G. (2022). Application of HEC-RAS and HEC-GeoRAS model for Flood Inundation Mapping, the case of Awash Bello Flood Plain, Upper Awash River Basin, Oromiya Regional State, Ethiopia. *Modeling Earth Systems and Environment*, *8*(2), 1449–1460. https://doi.org/10.1007/s40808-021-01166-9

Nguyen, C., Vaze, J., Mateo, C. M. R., Hutchinson, M. F., & Teng, J. (2024). *Very high spatial and temporal resolution rainfall data for accurate flood inundation modelling*. https://doi.org/10.5194/hess-2024-228

Osman, S. A., & Das, J. (2023). GIS-based flood risk assessment using multi-criteria decision analysis of Shebelle River Basin in southern Somalia. *SN Applied Sciences*, *5*(5), 134. https://doi.org/10.1007/s42452-023-05360-5

Pandya, K., & Vadodaria, D. G. P. (2018). *Use of ArcGIS to extract river geometry as an input to HEC-RAS for Flood Modelling*. *4*(12).

Papaioannou, G., Loukas, A., Vasiliades, L., & Aronica, G. T. (2016). Flood inundation mapping sensitivity to riverine spatial resolution and modelling approach. *Natural Hazards*, *83*(S1), 117–132. https://doi.org/10.1007/s11069-016-2382-1

Pathan, A. I., Agnihotri, P. G., Patel, D., Gandhi, P. J., Prieto, C., Mohseni, U., & Patidar, N. (2024). Use of Big Data for Flood Assessment Through HEC-RAS Model: A Study of Purna River of Navsari. In P. V. Timbadiya, P. L. Patel, V. P. Singh, & V. L. Manekar (Eds.), *Flood Forecasting and Hydraulic Structures* (Vol. 340, pp. 87–100). Springer Nature Singapore. https://doi.org/10.1007/978-981-99-1890-4_7

Petrochenko, O. V. (2023). The problem of flooding and analysis of the ways of its solution. *Environmental Safety and Natural Resources*, *46*(2), 5–22. https://doi.org/10.32347/2411-4049.2023.2.5-22

Pizzileo, S., Moretti, G., & Orlandini, S. (2024). Flood plain inundation modeling with explicit description of land surface macrostructures. *Advances in Water Resources*, *188*, 104713. https://doi.org/10.1016/j.advwatres.2024.104713

Pramanik, N., Panda, R. K., & Sen, D. (2010). One Dimensional Hydrodynamic Modeling of River Flow Using DEM Extracted River Cross-sections. *Water Resources Management*, *24*(5), 835–852. https://doi.org/10.1007/s11269-009-9474-6

Prashar, N., Lakra, H. S., Shaw, R., & Kaur, H. (2023). Urban Flood Resilience: A comprehensive review of assessment methods, tools, and techniques to manage disaster. *Progress in Disaster Science*, *20*, 100299. https://doi.org/10.1016/j.pdisas.2023.100299

Pulvirenti, L., Chini, M., & Pierdicca, N. (2020). InSAR Multitemporal Data over Persistent Scatterers to Detect Floodwater in Urban Areas: A Case Study in Beletweyne, Somalia. *Remote Sensing*, *13*(1), 37. https://doi.org/10.3390/rs13010037

Rahayu, P. (2023). Mapping Vulnerability to Flood in Urbanizing Watershed: The Case of Surakarta Urban Region. *IOP Conference Series: Earth and Environmental Science*, *1264*(1), 012013. https://doi.org/10.1088/1755-1315/1264/1/012013

Ramsewak, D., Jagassar, A., Woodward, K., Paz-Garcia, P., & Anderson, H. (2024). Detection of Two Major Flooding Events on the Island of Trinidad In 2018 and 2022 Using Google Earth Engine and Sentinel-1 SAR Imagery. *IGARSS 2024 - 2024 IEEE International Geoscience and Remote Sensing Symposium*, 3925–3929. https://doi.org/10.1109/IGARSS53475.2024.10642765

Renu, S., Reddy, B. S. N., Santhosh, S., Sreelekshmi, Lekshmi, V., Pramada, S. K., & Sridhar, V. (2025). Hydrologic and Hydraulic Modeling for Flood Risk Assessment: A Case Study of Periyar River Basin, Kerala, India. *Climate*, *13*(6), 129. https://doi.org/10.3390/cli13060129

Riswanto, S., & Nanda, M. P. (2023). Use of Hec-Ras Software to Analyze Floods in Joyoakan Urban Village, Surakarta City, Central Java. *Journal of Advanced Civil and Environmental Engineering*, *6*(1), 33. https://doi.org/10.30659/jacee.6.1.33-41

Rizeei, H. M. (n.d.). *Flood risk assessment using multi-sensor remote sensing, geographic information system, 2D hydraulic and machine learning based models*.

Roldán-Valcarce, A., Jato-Espino, D., Manchado, C., Bach, P. M., & Kuller, M. (2023). Vulnerability to urban flooding assessed based on spatial demographic, socio-economic and infrastructure inequalities. *International Journal of Disaster Risk Reduction*, *95*, 103894. https://doi.org/10.1016/j.ijdrr.2023.103894

Romanian Waters National Administration, Someș-Tisa Water Basin Administration, Maramureş Water Management System, St. Hortensiei 2A, 430294, Baia Mare, Romania, Ciurte, D. L., Mihu-Pintilie, A., Institute for Interdisciplinary Research, Science Research Department, "Alexandru Ioan Cuza" University of Iaşi (UAIC), St. Lascăr Catargi 54, 700107 Iaşi, România, Urzică, A., Research Center with Integrated Techniques for Atmospheric Aerosol Investigation in Romania, RECENT AIR, Laboratory of Interdisciplinary Research of Mountain Environment, Ion Gugiuman, Rarău Station for Research and Students Fellowships, 725100 Câmpulung-Moldovenesc, Suceava, România, Grozavu, A., & Faculty of Geography and Geology, Department of Geography, "Alexandru Ioan Cuza" University of Iaşi, Bd. Carol I 20A, 700505 Iaşi, Romania. (2023). INTEGRATING LIDAR DATA, 2D HEC-RAS MODELING AND REMOTE SENSING TO DEVELOP FLOOD HAZARD MAPS DOWNSTREAM OF A LARGE RESERVOIR IN THE INNER EASTERN CARPATHIANS. *Carpathian Journal of Earth and Environmental Sciences*, *18*(1), 149–169. https://doi.org/10.26471/cjees/2023/018/248

Ruidas, D., Pal, S. C., Saha, A., Roy, P., Pande, C. B., Islam, A. R. Md. T., & Islam, A. (2024). Flood hazard forecasting and management systems: A review of state-of-the-art modelling, management strategies and policy-practice gap. *International Journal of Disaster Risk Reduction*, *108*, 104539. https://doi.org/10.1016/j.ijdrr.2024.104539

Sabeeh, N. N., & Alabdraba, W. M. Sh. (2022). The Hydrodynamic Model using HEC-RAS: The case of Tigris River Downstream of Samarra Barrage (Iraq). *IOP Conference Series: Earth and Environmental Science*, *1120*(1), 012017. https://doi.org/10.1088/1755-1315/1120/1/012017

Saeed, F., & Zaidi, A. (2022). Application of Geohecras for 2D Flood Modeling of Downstream of Guddu Barrage. *IGARSS 2022 - 2022 IEEE International Geoscience and Remote Sensing Symposium*, 5543–5546. https://doi.org/10.1109/IGARSS46834.2022.9883618

Sahid. (2024). Enhancing Digital Elevation Model Accuracy for Flood Modelling – A Case Study of the Ciberes River in Cirebon Indonesia. *Forum Geografi*, *38*(1). https://doi.org/10.23917/forgeo.v38i1.1839

Saini, D. S., & Barik, D. K. (2024). Simulation of the Hydraulic Model HEC-RAS Coupled with GIS and Remote Sensing to Study the Effect of River Cross-section Width in Detecting Flood-prone Areas. *Journal of the Geological Society of India*, *100*(3), 367–376. https://doi.org/10.17491/jgsi/2024/173843

Salajegheh, A., Bakhshaei, M., Chavoshi, S., Keshtkar, A. R., & Najafi Hajivar, M. (2009). Floodplain mapping using HEC-RAS and GIS in semi-arid regions of Iran. *Desert*, *14*(1). https://doi.org/10.22059/jdesert.2010.21750

Salhi, A., Larifi, I., Salhi, H., & Heggy, E. (2024). Flooding in semi-unformal urban areas in North Africa: Environmental and psychosocial drivers. *Science of The Total Environment*, *929*, 172486. https://doi.org/10.1016/j.scitotenv.2024.172486

Sampaio, J., & Costa, V. (2021). Bayesian regional flood frequency analysis with GEV hierarchical models under spatial dependency structures. *Hydrological Sciences Journal*, *66*(3), 422–433. https://doi.org/10.1080/02626667.2021.1873997

Sellami, E. M., & Rhinane, H. (2024). Google Earth Engine and Machine Learning for Flash Flood Exposure Mapping—Case Study: Tetouan, Morocco. *Geosciences*, *14*(6), 152. https://doi.org/10.3390/geosciences14060152

Siakara, G., Gourgouletis, N., & Baltas, E. (2024). Assessing the Efficiency of Fully Two-Dimensional Hydraulic HEC-RAS Models in Rivers of Cyprus. *Geographies*, *4*(3), 513–536. https://doi.org/10.3390/geographies4030028

Silva, I. T. C. E., Santos, H. A., Pereira, L. C. O., & Nascimento, K. S. D. (2024). Global sensitivity analysis in flood mapping using HEC-RAS 2D: Effects of the floodplain manning coefficient for a dam-break case. *RBRH*, *29*, e38. https://doi.org/10.1590/2318-0331.292420240032

Soomro, S., Hu, C., Munir Babar, M., & Hyder Alias Aamir, M. (2021). Estimation of Manning's Roughness Coefficient Through Calibration Using HEC-RAS Model: A Case Study of Rohri Canal, Pakistan. *American Journal of Civil Engineering*, *9*(1), 1. https://doi.org/10.11648/j.ajce.20210901.11

Stelling, G. S., & Verwey, A. (2005). Numerical Flood Simulation. In M. G. Anderson & J. J. McDonnell (Eds.), *Encyclopedia of Hydrological Sciences* (1st ed.). Wiley. https://doi.org/10.1002/0470848944.hsa025a

Sung, C., & Tuo, R. (2024). A review on computer model calibration. *WIREs Computational Statistics*, *16*(1), e1645. https://doi.org/10.1002/wics.1645

Surwase, T., SrinivasaRao, G., Manjusree, P., Begum, A., Nagamani, P. V., & JaiSankar, G. (2019). Flood Inundation Simulation of Mahanadi River, Odisha During September 2008 by Using HEC-RAS 2D Model. In P. J. Rao, K. N. Rao, & S. Kubo (Eds.), *Proceedings of International Conference on Remote Sensing for Disaster Management* (pp. 851–863). Springer International Publishing. https://doi.org/10.1007/978-3-319-77276-9_77

Tabasi, N., Fereshtehpour, M., & Roghani, B. (2024). *A Review on Flood Risk Conceptual Frameworks and Development of Hierarchical Structures for Assessment Criteria* (Version 1). arXiv. https://doi.org/10.48550/ARXIV.2409.08803

Tamiru, H., & Wagari, M. (2022). Machine-learning and HEC-RAS integrated models for flood inundation mapping in Baro River Basin, Ethiopia. *Modeling Earth Systems and Environment*, *8*(2), 2291–2303. https://doi.org/10.1007/s40808-021-01175-8

Thakur, J. K., Singh, S. K., & Ekanthalu, V. S. (2017). Integrating remote sensing, geographic information systems and global positioning system techniques with hydrological modeling. *Applied Water Science, 7*(4), 1595–1608. https://doi.org/10.1007/s13201-016-0384-5

Timbadiya, P. V., Patel, P. L., & Porey, P. D. (2011). Calibration of HEC-RAS Model on Prediction of Flood for Lower Tapi River, India. *Journal of Water Resource and Protection*, *03*(11), 805–811. https://doi.org/10.4236/jwarp.2011.311090

Ting, S., Lymburn, T., Stemler, T., Sun, Y., & Small, M. (2023). *Model Calibration and Validation From A Statistical Inference Perspective* (Version 1). arXiv. https://doi.org/10.48550/ARXIV.2309.08562

Trambadia, N. K., Patel, D. P., Patel, V. M., & Gundalia, M. J. (2023). *Flood inundation assessment in the data-scarce region using hydrodynamic models and google earth engine -A case of Ghed region, Ozat River basin, Gujarat, India*. https://doi.org/10.21203/rs.3.rs-2321703/v1

Vaca, A. N. G., Rodríguez-Roda, I., Popartan, L. A., & Nuss-Girona, S. (2024). *Spatial Approach to Assess Multidimensional Vulnerability to Urban Flooding: A Proposal for Indicators*. https://doi.org/10.21203/rs.3.rs-4199231/v1

Vanelli, F., Lavagna, M., & Minifie, P. (2024). Flood management in the built environment: The micro-scale contribution to a distributed strategy. *IOP Conference Series: Earth and Environmental Science*, *1402*(1), 012012. https://doi.org/10.1088/1755-1315/1402/1/012012

Wang, C. H. (2014). Application of HEC-RAS Model in Simulation of Water Surface Profile of River. *Applied Mechanics and Materials*, *641–642*, 232–235. https://doi.org/10.4028/www.scientific.net/AMM.641-642.232

Wang, X., Zhang, H., Bertone, E., Stewart, R. A., & O'Halloran, K. (2020). Numerical Study of the Hydrodynamic and Sediment Transport Process in a Subtropical Water Reservoir: The Impacts of Storms and Winds. *Environmental Modeling & Assessment*, *25*(6), 843–860. https://doi.org/10.1007/s10666-020-09719-5

Werren, G., Reynard, E., Lane, S. N., & Balin, D. (2016). Flood hazard assessment and mapping in semi-arid piedmont areas: A case study in Beni Mellal, Morocco. *Natural Hazards*, *81*(1), 481–511. https://doi.org/10.1007/s11069-015-2092-0

Würth, A., Binois, M., & Goatin, P. (2023). Validation of Calibration Strategies for Macroscopic Traffic Flow Models on Synthetic Data. *2023 8th International Conference on Models and Technologies for Intelligent Transportation Systems (MT-ITS)*, 1–6. https://doi.org/10.1109/MT-ITS56129.2023.10241626

Xu, X., Li, J., & Tolson, B. A. (2014). Progress in integrating remote sensing data and hydrologic modeling. *Progress in Physical Geography: Earth and Environment*, *38*(4), 464–498. https://doi.org/10.1177/0309133314536583

Yang, Q., Shen, X., Zhang, Q., Helfrich, S., Kellndorfer, J. M., Straka, W., Hao, W., Steiner, N. C., Villa, M., Ruff, T., Torres, J. C. M., Lazzaro, R., & Jackson, C. (2024). Advanced Operational Flood Monitoring in the New Era: Harnessing High-Resolution, Event Based, and Multi-Source Remote Sensing Data for Flood Extent Detection and Depth Estimation. *IGARSS 2024 - 2024 IEEE International Geoscience and Remote Sensing Symposium*, 1366–1369. https://doi.org/10.1109/IGARSS53475.2024.10641791

Yang, Z., Huang, W., McKenzie, J. E., Xu, R., Yu, P., Ye, T., Wen, B., Gasparrini, A., Armstrong, B., Tong, S., Lavigne, E., Madureira, J., Kyselý, J., Guo, Y., & Li, S. (2023). Mortality risks associated with floods in 761 communities worldwide: Time series study. *BMJ*, e075081. https://doi.org/10.1136/bmj-2023-075081

Yeghiazarian, L. & Lilit Yeghiazarian. (2024, November 27). *The Urban Flooding Open Knowledge Network: From Real-Time Flood Forecasts to Cascading Failures Through Infrastructure, Ecosystems, Communities and Economy*. https://doi.org/10.5194/egusphere-egu24-13258

Yusuf, A., Ojo, R., Idrees, M. O., Balogun, A.-L., Salami, I. B., & Sani, O. S. (2023). Modelling flood hazards impacted by ungauged river in urbanised area using HEC-RAS and GIS. *Nigerian Journal of Technological Development*, *20*(2), 83–92. https://doi.org/10.4314/njtd.v20i2.1405

Zainal, N. N., & Abu Talib, S. H. (2024). Review paper on applications of the HEC-RAS model for flooding, agriculture, and water quality simulation. *Water Practice & Technology*, *19*(7), 2883–2900. https://doi.org/10.2166/wpt.2024.173

Zang, Y., Huang, J., & Wang, H. (2024). Dynamic impact assessment of urban floods on the compound spatial network of buildings-roads-emergency service facilities. *Science of The Total Environment*, *926*, 172007. https://doi.org/10.1016/j.scitotenv.2024.172007

Zhang, L., Dawadi, S., & Wilsnack, M. (2022). Prediction-Based Methodology for the Calibration and Uncertainty Analysis of Vegetation Flow Simulation with HEC-RAS Model. *World Environmental and Water Resources Congress 2022*, 410–421. https://doi.org/10.1061/9780784484258.038

Zhao, L., Wang, S., Wei, J., & Chen, R. (2022). Impacts of Land Use on Urban Road Network Vulnerability. *Journal of Urban Planning and Development*, *148*(3), 04022032. https://doi.org/10.1061/(ASCE)UP.1943-5444.0000862

Zhong, L., Lei, H., & Yang, J. (2024). Development of a Distributed Physics-Informed Deep Learning Hydrological Model for Data-Scarce Regions. *Water Resources Research*, *60*(6), e2023WR036333. https://doi.org/10.1029/2023WR036333

Zhu, J. (2010). GIS Based Urban Flood Inundation Modeling. *2010 Second WRI Global Congress on Intelligent Systems*, 140–143. https://doi.org/10.1109/GCIS.2010.264

Ziwanai, F. (2024). Re-Imagining Community-Based Disaster Risk Reduction Towards Building Resilient Rural Communities: In Z. Mbandlwa (Ed.), *Advances in Human Services and Public Health* (pp. 84–96). IGI Global. https://doi.org/10.4018/979-8-3693-2721-0.ch004

Zuhair Alshaikh, R., Adnan Abdulmunem, S., & Shakir Alkinani, A. (2023). A Review on Urban Planning and Its Role in Managing Flood Risks. *Urban Planning and Construction*, *1*(1), 1–8. https://doi.org/10.55121/upc.v1i1.104

Zulaeha, S., Nur Faridah, S., Achmad, M., & Mubarak, H. (2020). Prediksi Debit Aliran Sub-DAS Bantimurung Menggunakan Model HEC-HMS. *Jurnal Agritechno*, 71–76. https://doi.org/10.20956/at.v13i1.255

APPENDICES

Appendix A: Photographic Evidence of Flood Impacts

Appendix A-1: Impact on urban logistics and mobility, showing the depth of floodwaters on main city roads.

Source: https://www.somtribune.net/2019/11/02/somalia-dahabshiil-donates-150000-relief-assistance-to-floods-affected-people-in-beledweyne/

Appendix A-2: Aerial view of Beletweyne City showing the proximity of dense urban settlements to the Shebelle River banks, resulting the city's high exposure to riverine flooding

Source: (https://mustaqbalmedia.net/en/shabelle-river-floods-beledweyne-prompting-evacuations/)

Appendix A-2: Forced displacement and evacuation; families wading through inundated neighborhoods while transporting essential household assets to safer locations

Appendix A-3: Extensive inundation of semi-permanent housing units, demonstrating the magnitude of flood depth in residential zones lacking adequate flood defenses

Source: https://edition.cnn.com/2019/10/31/africa/somalia-floods-children-displaced-intl

Appendix A-4: Aerial overview of Beletweyne illustrating the extensive spatial footprint of the floodwaters affecting diverse residential neighborhoods

Appendix A-5: Aerial imagery highlighting the direct interface between the urban infrastructure of Beletweyne and the Shebelle River banks, demonstrating high exposure to flood risk

Source: https://himilonetwork.com/battling-climate-change-in-beledweyne-somalia-a-community-on-the-edge/

Appendix B: Study Area Geomorphology

Appendix B-1: The main channel of the Shebelle River flowing through Beletweyne, illustrating the riverbank geometry and channel morphology used for the hydraulic model setup

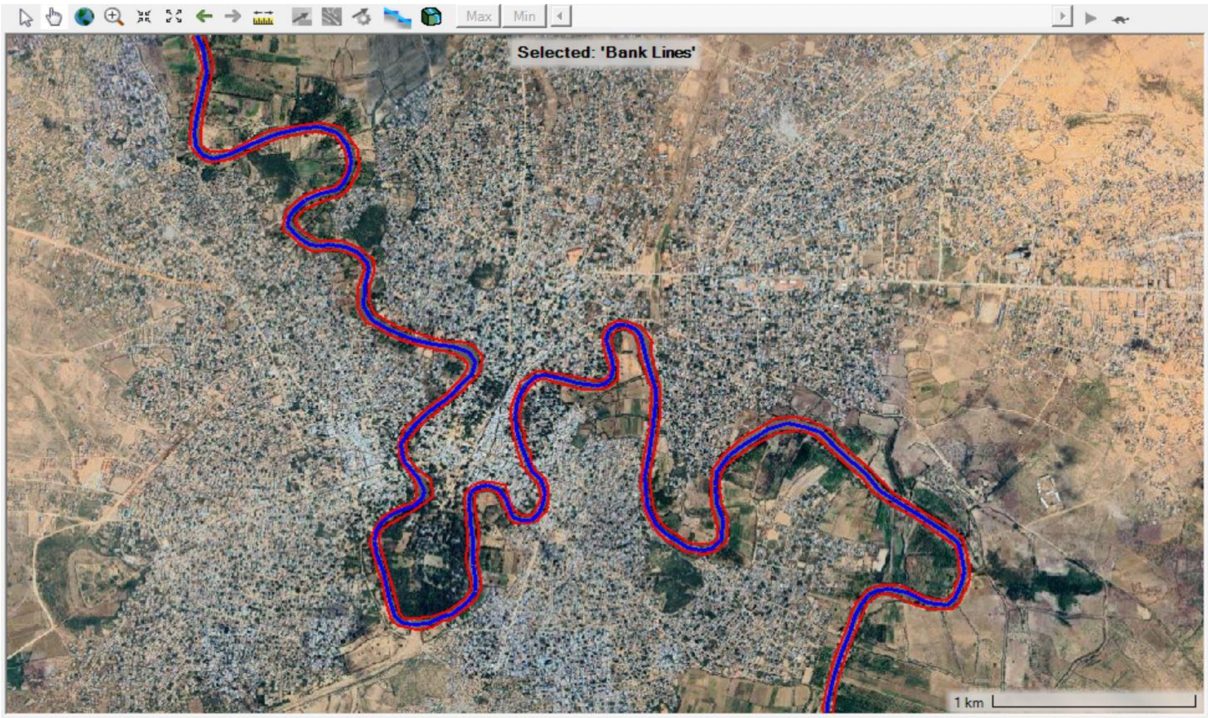

Appendix B-1: The interface between the Shebelle River and urban infrastructure, demonstrating the high exposure of settlements located along the riverbanks

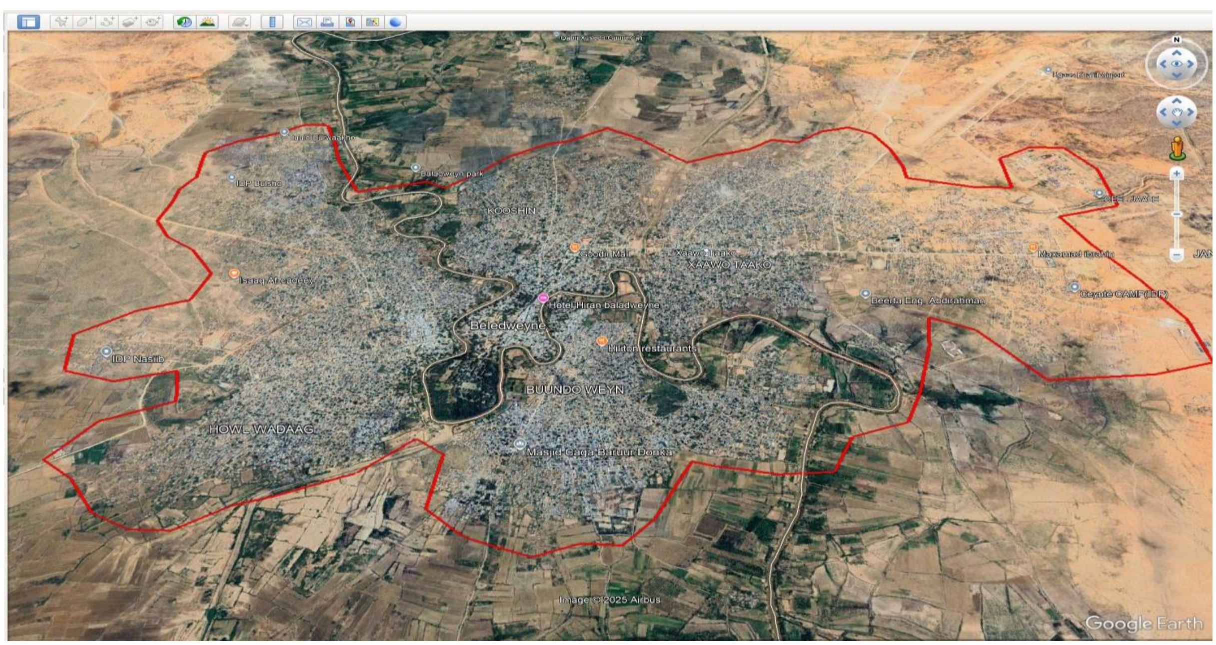

Appendix B-2: Satellite overview of the Shebelle River course through the Beletweyne district

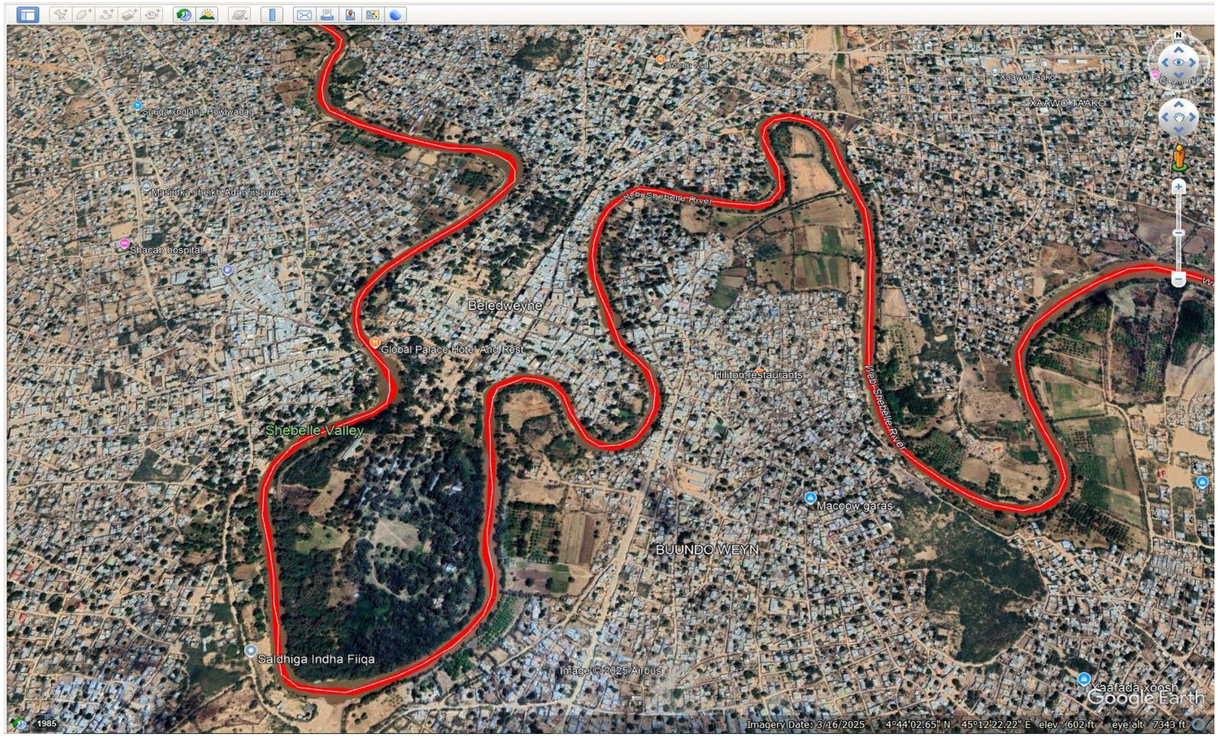

Appendix C: Hydrological Data and Model Simulation Outputs

Appendix C-1: Historical observed streamflow records (m³/s) for the Shebelle River at Beletweyne gauging station (1980–2025), utilized for flood frequency analysis

Time (Yrs.)	Observed Flow
1980	94.5268
1981	134.0520
1982	119.0021
1983	157.4595
1984	99.7525
1985	149.9986
1986	132.0075
1987	97.7208
1988	123.7960
1989	110.1278
1990	113.1637
1991	86.0480
1992	87.8071
1993	109.2375
1994	113.1847
1995	95.5140

1996	124.8363
1997	127.6791
1998	147.7457
1999	94.6935
2000	88.0532
2001	99.9813
2002	77.2831
2003	104.4623
2004	100.1161
2005	136.4827
2006	145.3406
2007	125.2674
2008	97.3186
2009	73.3644
2010	138.9277
2011	80.5009
2012	103.5902
2013	157.4570
2014	131.4326
2015	91.9901
2016	117.4137
2017	85.9413
2018	129.1603
2019	141.0687
2020	148.5722
2021	85.2391
2022	46.6370
2023	138.8985
2024	195.8491
2025	30.0865

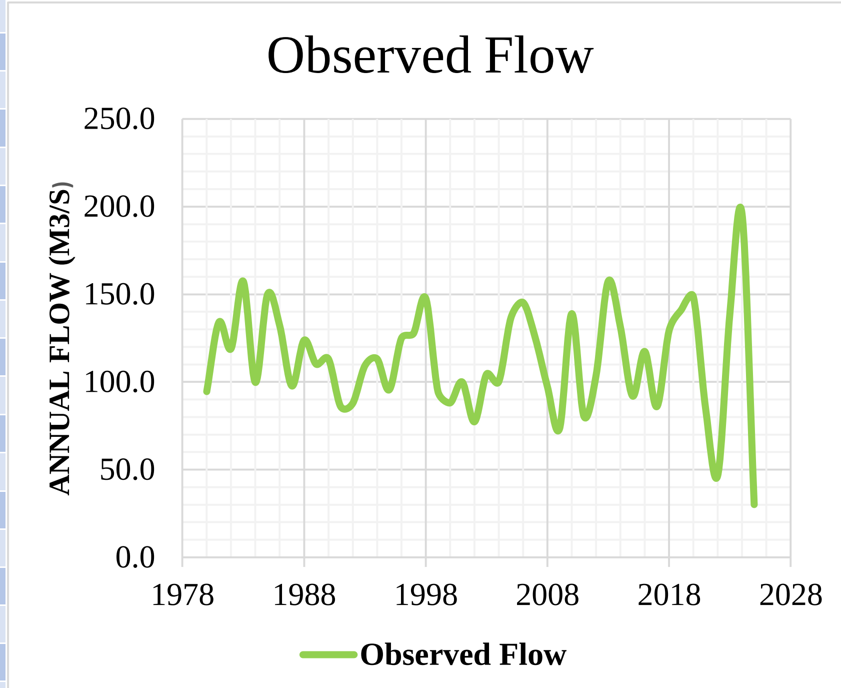

Appendix C-2: Annual mean water surface elevations (m) for the Shebelle River at Beletweyne (1980–2025), illustrating long-term hydrological trends

Year	Level (m)
1980	184.9203
1981	185.0761
1982	185.0101
1983	185.1428
1984	184.9357
1985	185.1275
1986	185.0787
1987	184.9861
1988	184.9935
1989	185.0038

1990	185.0543
1991	184.9153
1992	184.8455
1993	185.0126
1994	184.9358
1995	184.9292
1996	185.0427
1997	185.021
1998	185.0928
1999	184.9104
2000	184.8048
2001	184.9577
2002	184.8635
2003	184.9565
2004	184.9459
2005	185.1018
2006	185.1491
2007	185.0649
2008	184.9111
2009	184.8048
2010	185.1418
2011	184.8299
2012	184.9217
2013	185.1711
2014	185.079
2015	184.9436
2016	185.0284
2017	184.8866
2018	185.1075
2019	185.0676
2020	185.1372
2021	184.8468
2022	184.6857
2023	185.0948
2024	185.3157
2025	184.5617

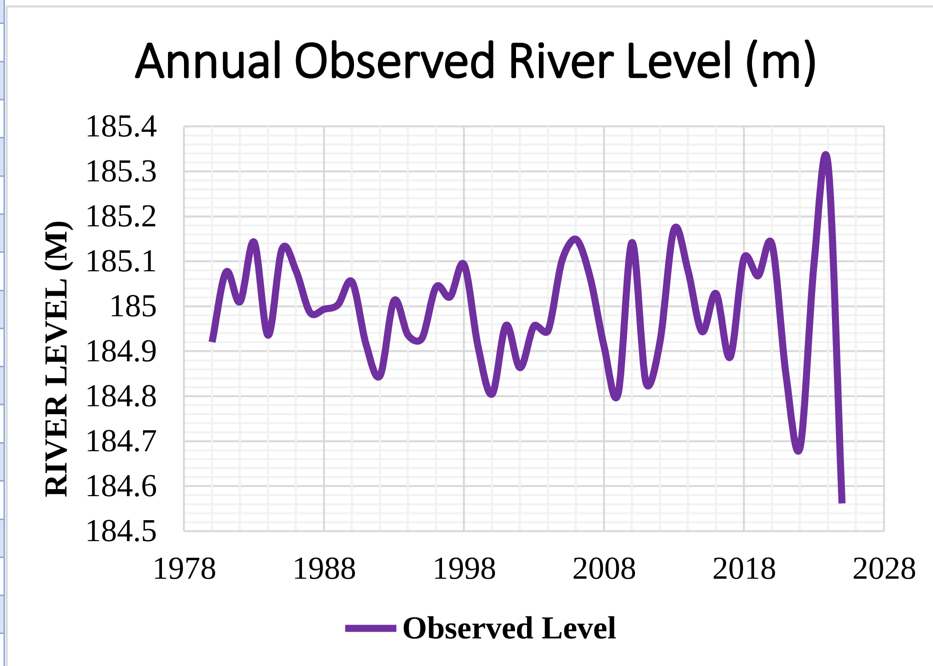

Appendix C-3: Detailed dataset of 1D model calibration iterations, comparing observed water levels against simulated values for varying Manning's roughness coefficients

Daytime	Iteration 1	Iteration 2	Iteration 3	Iteration 4	Iteration 5	Observed (m)
2019-10-01	185.04	185.21	185.33	185.38	185.42	**185.66**
2019-10-02	184.99	185.14	185.26	185.30	185.34	**185.63**
2019-10-03	184.95	185.10	185.21	185.25	185.29	**185.59**

2019-10-04	184.96	185.12	185.22	185.27	185.30	**185.6**
2019-10-05	185.02	185.18	185.30	185.34	185.38	**185.64**
2019-10-06	185.10	185.28	185.42	185.48	185.53	**185.7**
2019-10-07	185.16	185.37	185.54	185.60	185.66	**185.76**
2019-10-08	185.21	185.43	185.61	185.68	185.74	**185.82**
2019-10-09	185.26	185.51	185.70	185.78	185.85	**185.87**
2019-10-10	185.31	185.57	185.78	185.87	185.94	**185.91**
2019-10-11	185.32	185.59	185.81	185.90	185.98	**185.93**
2019-10-12	185.30	185.56	185.78	185.86	185.94	**185.91**
2019-10-13	185.28	185.54	185.74	185.83	185.90	**185.89**
2019-10-14	185.33	185.59	185.81	185.90	185.98	**185.93**
2019-10-15	185.39	185.68	185.92	186.02	186.10	**185.99**
2019-10-16	185.43	185.74	186.00	186.10	186.19	**186.03**
2019-10-17	185.39	185.69	185.94	186.04	186.13	**186.01**
2019-10-18	185.35	185.63	185.86	185.95	186.04	**185.97**
2019-10-19	185.33	185.60	185.83	185.92	186.00	**185.95**
2019-10-20	185.34	185.61	185.84	185.93	186.00	**185.95**
2019-10-21	185.35	185.62	185.85	185.95	186.03	**185.96**
2019-10-22	185.35	185.62	185.86	185.95	186.03	**185.96**
2019-10-23	185.31	185.58	185.80	185.89	185.97	**185.94**
2019-10-24	185.26	185.51	185.71	185.80	185.87	**185.89**
2019-10-25	185.20	185.43	185.61	185.68	185.75	**185.82**
2019-10-26	185.13	185.33	185.49	185.55	185.61	**185.76**
2019-10-27	185.04	185.21	185.34	185.40	185.44	**185.67**
2019-10-28	184.94	185.09	185.20	185.24	185.28	**185.59**
2019-10-29	184.88	185.02	185.12	185.15	185.18	**185.52**
2019-10-30	184.85	184.99	185.08	185.11	185.14	**185.49**
2019-10-31	185.12	185.31	185.44	185.49	185.53	**185.69**
2019-11-01	185.63	186.00	186.30	186.42	186.52	**186.14**
2019-11-02	185.69	186.10	186.45	186.59	186.71	**186.22**
2019-11-03	185.61	185.99	186.33	186.46	186.57	**186.18**
2019-11-04	185.51	185.86	186.15	186.27	186.38	**186.07**
2019-11-05	185.37	185.67	185.93	186.03	186.12	**185.93**
2019-11-06	185.21	185.44	185.63	185.71	185.78	**185.8**
2019-11-07	185.08	185.27	185.42	185.48	185.53	**185.71**
2019-11-08	184.99	185.15	185.27	185.32	185.36	**185.64**
2019-11-09	184.96	185.11	185.22	185.26	185.30	**185.61**
2019-11-10	185.07	185.25	185.38	185.42	185.47	**185.68**

2019-11-11	185.26	185.50	185.69	185.76	185.82	**185.82**
2019-11-12	185.32	185.58	185.80	185.89	185.97	**185.89**
2019-11-13	185.24	185.49	185.69	185.77	185.84	**185.84**
2019-11-14	185.09	185.28	185.43	185.49	185.55	**185.71**
2019-11-15	184.98	185.14	185.26	185.31	185.35	**185.59**

Appendix C-4: Comparative dataset for 2D model calibration, detailing the observed water surface elevations versus the simulated results from the HEC-RAS 2D unsteady flow analysis

Daytime	Iteration 1	Iteration 2	Iteration 3	Iteration 4	Observed (m)
2019-10-01	185.44	185.52	185.52	185.63	**185.66**
2019-10-02	185.50	185.59	185.60	185.74	**185.63**
2019-10-03	185.48	185.58	185.58	185.71	**185.59**
2019-10-04	185.49	185.58	185.58	185.72	**185.6**
2019-10-05	185.52	185.61	185.61	185.75	**185.64**
2019-10-06	185.57	185.66	185.66	185.80	**185.7**
2019-10-07	185.60	185.69	185.70	185.84	**185.76**
2019-10-08	185.62	185.72	185.72	185.86	**185.82**
2019-10-09	185.65	185.74	185.75	185.90	**185.87**
2019-10-10	185.67	185.76	185.77	185.93	**185.91**
2019-10-11	185.67	185.77	185.78	185.95	**185.93**
2019-10-12	185.66	185.76	185.77	185.94	**185.91**
2019-10-13	185.66	185.75	185.76	185.93	**185.89**
2019-10-14	185.67	185.77	185.78	185.95	**185.93**
2019-10-15	185.70	185.79	185.81	186.00	**185.99**
2019-10-16	185.71	185.81	185.83	186.04	**186.03**
2019-10-17	185.70	185.79	185.82	186.03	**186.01**
2019-10-18	185.68	185.78	185.80	186.00	**185.97**
2019-10-19	185.68	185.77	185.79	185.98	**185.95**
2019-10-20	185.68	185.77	185.79	185.98	**185.95**
2019-10-21	185.68	185.78	185.79	185.98	**185.96**
2019-10-22	185.68	185.78	185.79	185.98	**185.96**
2019-10-23	185.67	185.76	185.78	185.97	**185.94**
2019-10-24	185.65	185.74	185.75	185.93	**185.89**
2019-10-25	185.62	185.72	185.72	185.88	**185.82**
2019-10-26	185.59	185.68	185.68	185.83	**185.76**
2019-10-27	185.54	185.63	185.63	185.77	**185.67**
2019-10-28	185.48	185.57	185.57	185.71	**185.59**
2019-10-29	185.44	185.53	185.53	185.67	**185.52**
2019-10-30	185.42	185.51	185.52	185.65	**185.49**

2019-10-31	185.56	185.65	185.65	185.78	**185.69**
2019-11-01	185.78	185.87	185.88	186.07	**186.14**
2019-11-02	185.79	185.90	185.95	186.19	**186.22**
2019-11-03	185.77	185.89	185.95	186.24	**186.18**
2019-11-04	185.74	185.85	185.91	186.20	**186.07**
2019-11-05	185.69	185.79	185.84	186.10	**185.93**
2019-11-06	185.62	185.72	185.74	185.94	**185.8**
2019-11-07	185.56	185.65	185.66	185.82	**185.71**
2019-11-08	185.51	185.60	185.60	185.74	**185.64**
2019-11-09	185.49	185.58	185.58	185.72	**185.61**
2019-11-10	185.55	185.64	185.64	185.78	**185.68**
2019-11-11	185.64	185.74	185.74	185.88	**185.82**
2019-11-12	185.67	185.77	185.77	185.93	**185.89**
2019-11-13	185.64	185.73	185.74	185.90	**185.84**
2019-11-14	185.57	185.66	185.66	185.81	**185.71**
2019-11-15	185.51	185.60	185.60	185.75	**185.59**